PULSED GAS METAL ARC WELDING OF THICK-SECTION STEELS FOR LOW TEMPERATURE APPLICATIONS

Final Report By:

D. V. Dorling
R. M. Huntley
J. Geerligs
A. B. Rothwell

Work on this project was jointly funded by NOVA, AN ALBERTA CORPORATION and the Physical Metallurgy Research Laboratories, Canada Centre for Mineral and Energy Technology, Energy Mines and Resources Canada.

DSS FILE NUMBER: 14SQ.23440-4-9065
DSS CONTRACT SERIAL NUMBER: 0SQ84-00042
CANMET SCIENTIFIC AUTHORITY: Dr. J. E. M. Braid

September 1986

188 pp

MICROMEDIA

ABSTRACT

For the economical construction of offshore structures and pipelines and of Arctic vessels, a clear need exists for welding processes which are capable of depositing weld metal of high integrity and toughness, and which offer significantly improved productivity, relative to the conventional, shielded metal arc process. A previous study has examined the viability of the mechanized and automated flux-cored arc welding process for this application. The present report examines the potential of mechanized, pulsed gas metal arc welding (GMAW). Traditionally, fixed-position GMAW has been limited to the short-circuiting mode, with its attendant productivity limitations and susceptibility to fusion defects. The pulsed mode, by extending controlled open-arc conditions to lower mean currents, can circumvent these difficulties, and in addition allows the use of shielding gases having very low oxygen potential. This report describes studies of metal transfer, burn-off and fusion characteristics, using a range of wire and shielding gas combinations, which have led to the establishment of optimum pulse structure and synergic logic. Power source characteristics have been modified so that excellent arc stability and metal transfer characteristics are maintained for all-position groove welds. Pulsed GMAW procedures have been established which present considerable productivity advantages, relative to SMAW; further improvements could be achieved in modified groove geometries. Test panels produced in 30 mm thick Lloyds LT60 plate, using similar procedures, indicated the excellent capability of the process for control of weld metal composition in low oxygen-potential gases. Exceptional Charpy toughness was achieved in the best of the deposits (up to 99 J at -60°C), but CTOD

toughness at -45°C was unsatisfactory for all but one of the wires examined. Fracture initiation appeared to be controlled by the behaviour of the root region, however, and it is likely that this problem can be overcome by the use of alternative methods of deposition and/or fixturing. It is thus believed that further, systematic optimization of welding consumables and procedure will allow the full potential of pulsed GMAW as a high productivity process giving excellent low temperature toughness to be exploited.

TABLE OF CONTENTS

Page

1.0 INTRODUCTION 1

2.0 EXPERIMENTAL APPROACH 7

3.0 EQUIPMENT AND MATERIALS 8

- 3.1 Pulsed GMAW Power Source 8
- 3.2 Mechanized Welding System 10
- 3.3 Parent Material 11
- 3.4 Welding Consumables 11
- 3.5 Instrumentation 14

4.0 EXPERIMENTAL PROCEDURE 15

- 4.1 Process Characteristics 15
  - 4.1.1 Arc Stability and Metal Transfer 16
  - 4.1.2 Burn-off Characteristics 18
  - 4.1.3 Fusion Characteristics 19
- 4.2 Procedure Development 20
- 4.3 Metallurgical Evaluation 25
  - 4.3.1 Welding Procedure 25
  - 4.3.2 Chemical Analysis 26
  - 4.3.3 Mechanical Testing 26
  - 4.3.4 Metallographic Examination 27

5.0 RESULTS 28

- 5.1 Process Characteristics 28
  - 5.1.1 Arc Stability and Metal Transfer 28
  - 5.1.2 Burn-Off Characteristics 32
  - 5.1.3 Fusion Characteristics 33
- 5.2 Procedure Development 35
- 5.3 Metallurgical Evaluation 37
  - 5.3.1 Welding Procedure 37
  - 5.3.2 Chemical Composition 38
  - 5.3.3 Mechanical Properties 40
    - 5.3.3.1 Hardness Test Results 40
    - 5.3.3.2 Tensile Test Results 40
    - 5.3.3.3 Charpy Impact Test Results 42
    - 5.3.3.4 CTOD Test Results 44
  - 5.3.4 Metallographic Observations 45

6.0 DISCUSSION 48

7.0 CONCLUSIONS 67

ACKNOWLEDGEMENTS 72

REFERENCES 73

1.0 INTRODUCTION

The construction of offshore structures, either fixed production platforms or mobile exploration units, follows, in many respects, standard shipyard practice, in that it involves fabrication of sub-assemblies in a shop environment and subsequent launch-site or berth erection. The stringency of the requirements for offshore oil and gas installations and the conditions in which welding has to be carried out have essentially limited the choice of welding process to mechanized submerged arc welding (SAW) and shielded metal arc welding (SMAW) for fabrication of sub-assemblies and SMAW for site erection (1). The application of high quality, high productivity submerged arc welding is limited to joints of simple geometry in the flat position, such as the welding of stiffened shell panels, the axial welds of large structural cans and tubulars and circumferential or girth welds when the workpiece can be rotated beneath the welding head. For out-of-position welding, both in the shop and on site, the most widely used process is still the basic, low-hydrogen shielded metal arc welding process.

The physical scale and cost of these installations, together with the greater demands for positive assurance of the technical integrity of structures and vessels for Arctic service, has led to considerable interest in the development of welding processes and procedures which offer better productivity and improved reproducibility and control, relative to traditional, shielded metal arc welding techniques.

The attainment of adequate weld-metal notch toughness (to at least -60°C for Arctic service) and the prevention of hydrogen-assisted cracking are the main considerations when selecting a welding process and developing welding procedures for high-integrity fabrications. The necessity of using the SMAW process to meet these requirements in welded connections in all positions other than flat is very costly. Process deposition rate and duty cycle are the most influential factors affecting productivity and hence welding costs (2). In a continued effort to improve productivity, fabricators are giving consideration to the replacement of the traditional, manual welding techniques by processes using continuous wire electrodes. There has been increasing interest in the use of flux-cored arc welding for high-integrity fabrication, and a program of work carried out at NOVA, and partially funded by the Federal Government, has evaluated mechanized and automatic FCAW for the welding of offshore structures and Arctic vessels (3). It was found that only electrodes of rutile flux formulation had true all-position capability. While some of the most-recently developed rutile wires showed reasonable Charpy toughness down to -60°C, CTOD results in 25 mm plate at -45°C were marginal. For the most exacting service, further improvements would be required. Since the minimum oxygen content achievable with flux-cored wires of rutile-based formulation is in the range 400-500 ppm, regardless of shielding gas, there is an inherent limitation in the toughness levels which can be achieved, even under fully-ductile conditions.

The potential technical and economic advantages of the GMAW process over SMAW have been widely discussed and recognized (4,5). The continuous nature of the electrode makes the process amenable to mechanization and automation; the weld deposit is low in hydrogen, essentially eliminating the danger of cold cracking, and there is a potential for the achievement of excellent mechanical properties by judicious selection of wire and shielding gas. However, to date, welding in all positions has only been achieved by using the short-circuiting technique and, as a result, the process is inherently one of low heat input, due to the limited current range and intermittent nature of the arc. This technique not only imposes limitations on productivity, but also can be prone to the occurrence of inter-run and sidewall fusion defects, which are not always easily detected by radiography (6). For these reasons, the GMAW process has not been widely used in the construction industry for fixed position welding in critical applications.

Mechanized, solid-wire GMAW has been extensively used by NOVA and its affiliates for the construction of cross-country pipelines. Following a program of consumable evaluation, together with extensive refinement of on-site procedures for its application, it has become the standard technique for the construction of major, large-diameter pipelines in Canada (4,7). In addition, of course, it has been widely used in the construction of offshore pipelines, where its productivity and the relatively compact nature of the equipment makes its use highly advantageous. As mentioned above, the systems used all achieve positional capability by the use of the short-circuiting mode of metal transfer, with its attendant limitations in heat input and tendency towards fusion defects which can only be avoided by a high level of operator attention. Because of the shielding gases which must be used, minimum oxygen levels in the deposit are limited to the range 400-500 ppm, comparable to those typical of FCAW with rutile wires.

The development of more-advanced power sources has provided the opportunity to solve these problems (5). The control of metal transfer through current pulsation enables the GMAW process to be used in the spray transfer mode, in all welding positions, over a wide range of mean currents. A feasibility study on the application of advanced GMAW techniques to the mechanized welding of cross-country pipelines (8) has shown that the pulsed GMAW process offers the potential for reduced incidence of lack-of-fusion defects, through improved metal transfer characteristics, and better CTOD toughness properties (0.45 mm CTOD at -5°C with pulsed GMAW compared to 0.20 mm CTOD at -5°C with short circuiting GMAW, using 1.2 Ni-Ti consumables) through the use of lower oxygen potential gas mixtures.

The application of advanced power sources and welding control systems to the gas metal arc welding of thick section structural steel would have considerable cost and quality benefits during the fabrication of offshore structures and Arctic vessels. Using recently-developed solid-state power control technology, a nominally square-wave current output is easily produced in which the pulse parameters of peak current, peak duration, background current and background duration can be infinitely and independently varied and accurately reproduced. In principle, therefore, it should be feasible to select suitable pulse parameters to give stable open-arc metal transfer over a wide range of mean current values. In practice this is not easily accomplished, especially by 'trial-and-error' experimentation, because of the large number of welding variables (including wire-feed speed, travel speed, electrical stickout, wire composition, shielding gas composition) and the possible interactions between them. The work of Amin (9) and Allum, both alone (5) and in concert with Quintino (10), has done much to further an understanding of the process. Nevertheless, the choice of parameters, and of pulse parameters especially, can affect a wide range of arc and deposition characteristics, and must be precisely determined for each intended production application if the potential of the pulsed gas metal arc welding process is to be fully realized.

Clearly, in production, it is desirable for the number of variables which must be set up individually to be minimized; the so-called 'synergic' approach (11) allows wire-feed speed or mean current to be selected to meet the application requirements, with other parameters being automatically adjusted to maintain the required welding characteristics. In pulsed GMAW, the internal logic of synergic systems must be such that all pulse parameters remain within the envelope determined for optimum metal transfer and fusion characteristics, throughout the available range of mean current. While general guidelines have been established for this purpose, they have not been explored for a wide range of real welding situations. The present work aims to establish appropriate pulse structure and synergic logic for mechanized, positional, groove welding with a wide range of consumables, and to assess the practical applicability of the resulting system by procedure development and by metallurgical evaluation of welds made with a number of wire and shielding gas combinations.

2.0 EXPERIMENTAL APPROACH

The principal objective of this investigation was to evaluate the potential of the pulsed gas metal arc welding process for the all-position, mechanized and automated welding of offshore oil and gas installations and Arctic vessels. The experimental program was divided into three parts. The first part involved an evaluation of pulsed gas metal arc welding process characteristics in order to determine the optimum welding parameters, including pulse amplitude and duration and background amplitude and duration, for the specific application under consideration. This consisted of investigations, using a number of wire and shielding gas combinations, into:

arc stability and metal transfer;
wire burn-off characteristics;
weld bead profiles.

In the second part of the program, welding procedures were developed in the mechanized mode and with vertical up progression, with selected consumables, in 30 mm mild steel plate in the flat, vertical and 45^{0} overhead positions and, finally, in 1067 mm O.D., 30 mm W.T. pipe in the fixed, 5G, position. The procedures were evaluated in terms of welding process characteristics and productivity. The third part of the program involved the completion of test panels in 30 mm Lloyds LT60 steel, with selected combinations from eight wires and three shielding gas mixtures, for metallurgical evaluation, especially as regards low-temperature toughness.

3.0 EQUIPMENT AND MATERIALS

3.1 Pulsed GMAW Power Source

All welding was carried out using a GEC M450PS pulsed GMAW power source manufactured by GEC Industrial Controls Limited of the United Kingdom. The M450PS was selected because of its high degree of flexibility and repeatability, and this may best be illustrated by a brief description of its operation.

The M450PS can be divided into two main sections, power control section and pulse logic section, as shown in the block diagram in Fig. 1. The pulse logic section can be considered as the outer control loop which sets the mean current, wire-feed rate and, as will be discussed in more detail later in the text, any automatic stability compensation required. The power control section, which is the inner control loop, is a high-performance, feedback control system that maintains the correct arc current as well as controlling special conditions such as arc starting and short circuiting. It also has safety shutdown features to prevent destruction of expensive, high-current control devices.

The M450PS has two modes of operation; programmable and synergic. These are selected by front-panel, push-button switch. In the programmable mode, the pulse parameters, (peak current, Ip, peak time, Tp, background current, Ib and background time, Tb), are selected by thumbwheel switches and the wire-feed rate is set by the main, front-panel, potentiometer control. In this mode, the mean current is determined solely by the programmed pulse parameters and the power supply operates as a current control. Changes in wire-feed rate result only in changes in arc voltage. In the synergic mode, the power source can be programmed with one set of pulse parameters through four internal potentiometers, one each for Ip, Tp, Ib and Tb. Wire-feed speed can then be varied by the main front-panel control and the pulse parameters will track according to the factory-programmed synergic logic to give the required average current to match burn-off with the selected wire-feed speed. The synergic waveform programmed into the M450PS is as illustrated in Fig. 2; Ip, Ib and Tb vary with wire-feed speed, with only Tp remaining constant.

In the programmable mode the pulse parameters can be independently varied in small increments over a wide range:

Ip: 0-450 A in 1 A steps
Ib: 0-450 A in 1 A steps
Tp: 0.1-99.9 ms in 0.1 ms steps
Tb: 0.1-99.9 ms in 0.1 ms steps

In this mode, optimum pulse parameters can be precisely determined for specific applications. With the power source in the synergic mode, these optimum pulse parameters can be programmed into the unit and further procedure development and production applications carried out with one-knob, synergic control.

3.2 Mechanized Welding System

The mechanized system selected for the investigation was the CRC Model M-200. This system had already been successfully used in production by NOVA for the site welding of large-diameter, heavy-wall pipe and piping components (12). The M-200 (Fig. 3) is, essentially, an orbital welding machine which travels on a 120 mm wide, spring-steel band. The unit has three sections; a carriage section, control-box section, and welding section. The carriage section consists of a hinged base that can be adjusted for diameters from 254 mm to flat plate, a 24 V drive motor and gear box, and a cam mechanism used to latch the machine onto the band. There are also three grooved guide wheels and a knurled drive wheel that ride on the edges of the band. The control box contains three printed circuit boards that control travel speed, wire-feed speed, oscillation frequency and dwell time, and wire and gas shut-off delay. There are check buttons for each function of the unit and on and off control buttons to energize and de-energize all control circuits. A power switch applies 24 V d.c. to the circuit. A thumb-wheel control sets oscillation width and single-turn potentiometers set left and right dwell and oscillation rate. Ten-turn potentiometers control travel and wire-feed speeds. The welding section consists of a wire drive motor, oscillation motor, welding head, and capacity for a 4.5 kg spool of wire.

To make full use of the synergic control capability of the M450PS power source, the M200 wire-feed control was replaced by a remote wire-feed control circuit using constant EMF motor control, with compensation for motor load changes. This provided stable and linear speed control over the range 2 m/min to 10 m/min and could be set by an external, calibrated, ten-turn potentiometer dial indicator. A remote input is provided via an internal/external switch. When the switch is set to external, the ten-turn potentiometer dial indicator is used to match the wire feed of the M200 to that of the external source command. The wire-feed speed will then track the external source command, i.e. adjusting the front-panel potentiometer control on the M450PS power source will change the wire feed to track the change in mean current.

3.3 Parent Material

Process evaluation and procedure development were carried out on 12.7 and 30 mm thick mild steel plate and one length of 1067 mm O.D., 30 mm W.T., CSA Z245.1 Grade 414 MPa pipe. Test panels for metallurgical evaluation were prepared from 30 mm thick Lloyds LT60 steel plate supplied by Algoma Steel, the composition of which is given in Table 1.

3.4 Welding Consumables

Eight 1.2 mm diameter GMAW welding wires with varying alloying and microalloying additions were evaluated:

Carbon-manganese-silicon (C-Mn-Si)

Low carbon-manganese-silicon (LowC-Mn-Si)

Carbon-manganese-silicon-titanium (C-Mn-Si-Ti)

Carbon-manganese-titanium-boron (C-Mn-Ti-B)

Carbon-manganese-nickel (C-Mn-Ni)

Carbon-manganese-nickel-titanium (C-Mn-Ni-Ti)

Carbon-manganese-molybdenum (C-Mn-Mo)

Carbon-manganese-molybdenum-titanium (C-Mn-Mo-Ti)

The chemical compositions of the wires are given in Table 2.

Shielding gases evaluated consisted of two commercially available mixtures:

95% argon - 5% carbon dioxide ($95Ar-5CO_2$)

80% argon - 20% carbon dioxide ($80Ar-20CO_2$)

and two experimental gas mixtures:

88% argon - 10% helium - 2% carbon dioxide ($88Ar-10He-2CO_2$)

87.5% argon - 10% helium - 2% carbon dioxide - 0.5% hydrogen ($87.5Ar-10He-2CO_2-0.5H_2$).

The reasons for the selection of these shielding gas mixtures are as follows:

Of the commercially-available gas mixtures, 95Ar-5CO_2 has featured in several reported investigations (9,10,13); on the other hand, the exclusive use of 80Ar-20CO_2 is recommended by the suppliers of a number of pulsed GMAW power sources with preprogrammed pulse parameters.

The two experimental shielding gas mixtures were arrived at from a consideration of the results of an investigation of the effects of shielding gas composition on fusion characteristics in pulsed gas metal arc welds by Bicknell and Patchett (14). Included in the study was a 97.5Ar-2CO_2-0.5H_2 mixture previously developed for the mechanized short-arc welding of rare-earth-treated pipeline steels. When used with the pulsed mode of metal transfer, this hydrogen-bearing gas mixture improved the lateral stability of the arc and reduced the amount of uneven or preferential penetration to one side observed with Ar-CO_2 mixtures. The addition of 10% He to the Ar-2CO_2-0.5H_2 mixture resulted in a less-pronounced finger penetration profile. The 88Ar-10He-2CO_2 shielding gas mixture was included to assess the influence, if any, of hydrogen on process characteristics other than fusion and to ensure that the small hydrogen addition had no detrimental effect on metallurgical properties.

The experimental gas mixtures were produced in the laboratory using a Matheson four tube Rotameter flowmeter. A flowrate of 16.5 l/min was used throughout.

3.5 Instrumentation

Pulse parameters were continuously monitored and, in the case of synergic operation of the GEC M450PS power source, were programmed using a Gould OS4000 digital storage oscilloscope. Average current and voltage was monitored on digital meters built into the front panel of the M450PS.

For the work on arc stability and metal transfer, arc voltage was measured using a resistive divider to reduce the signal to a 0-10 V range and then isolated with an Analog Devices AD293 isolation amplifier. Arc current was measured using a Hall-effect-type current transducer. Both signals were optimized for gain and frequency bandwidth by a Krohn-Hite 3342R filter and then recorded on a Thorn EMI SE7000 FM tape recorder. The signals were played back and examined using a Hewlett Packard HP 5423A digital signal analyser and typical examples plotted using a HP 9872C digital plotter.

Metal transfer was recorded on video tape using a Kodak SP 2000 motion picture analysis system, with a Xenon backing lamp, at a framing speed of 2000 fps.

4.0 EXPERIMENTAL PROCEDURE

4.1 Process Characteristics

Pulsed GMAW adds further complication to the selection of welding parameters for a given application in that there are four additional variables to contend with; peak current (Ip), peak duration (Tp), background current (Tb) and background duration (Tb). It is generally accepted that, for optimum arc stability, the pulse parameters must be adjusted in order to detach one drop with each pulse. In addition, the mean current determined by the pulse parameters, i.e.:

$$\bar{I} = F(IpTp + IbTb)$$

where F is the pulse frequency

must give a burn-off rate to match the wire-feed speed in order to maintain a constant arc length. For the particular application under investigation, the welding of thick-section structural steels, fusion characteristics are also of prime importance if the potential of the pulsed GMAW process, with respect to avoiding the lack-of-fusion defects to which conventional short-circuiting GMAW is particularly prone, is to be fully realized.

For the above reasons, the investigation into process characteristics was divided into three separate, but sequential, exercises, as follows:

Arc stability and metal transfer studies to establish the pulse parameters for one-drop-per-pulse detachment, for the wire and shielding gas combinations under investigation;

Wire burn-off rate studies to determine the burn-off characteristics of the various wires, together with the influence of shielding gas composition and electrical stickout;

Weld bead shape studies to determine the effect of welding parameters on fusion characteristics.

4.1.1 Arc Stability and Metal Transfer

A considerable amount of work to determine the influence of pulse structure on arc stability and metal transfer has been carried out by Allum (5,10), and his work provides an appropriate background for this investigation. For steel wires, Allum found that, with a constant peak condition, background conditions and hence mean current had little influence on droplet detachment. Further experiments conducted to investigate the influence of peak parameters on metal transfer showed that, for a given peak current, there was a critical peak duration Tpc, which had to be reached before a droplet was detached consistently in the peak. When this duration was reached, droplet detachment occurred at the trailing edge of the pulse peak. The detachment remained at the trailing edge even when the pulse duration was increased by 1 to 2 ms; however, with further increases in pulse duration, detachment occurred earlier within the peak. This behavior is shown in Fig.4. When peak current was varied, it was observed that one droplet per pulse was detached if

$$Ip^nTp = \text{const.}$$

Similar results had previously been reported by Amin (9) and, more recently, by Smati (13). All three present results for "mild steel" wire in Ar-5CO$_2$, however, and there is no reason to believe that the Ip-Tp relationship or "zone" for one drop per pulse transfer will be unaffected by changes in either wire or shielding gas composition.

The object of this first stage of the present investigation was to determine the zones for stable metal transfer for all combinations of the eight wires and four shielding gases under investigation.
Over 1200 bead-on-plate runs were deposited in the flat position on individual 100 mm by 50 mm pieces of 12.7 mm thick, surface-ground, mild steel plate. Peak current was varied in 50 A increments from 250 A to 400 A and, at each peak current value, peak duration was varied from 2 ms to up to 10 ms in 0.1 to 1.0 ms increments. As with Allum's work, background conditions were maintained constant at 50 A and 10 ms. Both Allum and Smati had adopted a constant 20 mm contact-tip-to-work distance with a 5 mm arc. This was considered to be excessive for practical application with respect to both arc length and electrical stickout and, for the present investigation, arc length was a maximum of 4 mm and contact-tip-to-work distance remained constant at 13 mm; a preliminary investigation had shown

that metal transfer characteristics were insensitive to electrical stickout. Droplet detachments were detected from current and voltage traces measured and recorded as detailed earlier. The reason for processing the signals in the manner described was the fact that the GEC M450PS power source operates in the switch mode, controlling the current by very rapid switching of the output. This causes noise on the traces which can mask the voltage spike that indicates droplet detachment unless the signal is properly filtered. Arc stability was evaluated through the subjective assessment of the welding operator and from the current and voltage traces; the observations were correlated with droplet detachment phenomena.

The tests were repeated for two wires and two shielding gases and metal transfer recorded on video tape using the Kodak SP2000 motion picture analysis system. This enabled droplet detachment to be precisely defined and facilitated accurate interpretation of current and voltage traces. For one wire and shielding gas combination, the high-speed video technique was also used to investigate the influence of background conditions on metal transfer, at constant Ip and Tp.

4.1.2 Burn-off Characteristics

The stable relationship between wire-feed speed and mean current was determined for all combinations of the eight wires and four shielding gases. Arc length was maintained at 4 mm maximum and contact-tip-to-work distance varied from 13 mm to 24 mm for one wire and maintained at 13 mm for the remaining seven. Pulse parameters were programmed to give the required mean current; peak conditions were taken from the results of the previous experiments and background conditions were determined using a 50 Hz/100 A frequency/mean current relationship, as suggested by Quintino and Allum for 1.2 mm wire (10). The background to this relationship will be discussed in a later section. Wire-feed speed was adjusted until the correct arc length was achieved and measured manually on completion of the weld run.

4.1.3 Fusion Characteristics

The influence of process parameters on fusion characteristics in pulsed GMAW has been covered extensively by Quintino and Allum (10), Allum and Quintino (15) and Smati (13) and it was the general conclusion that the parameters affecting key weld bead dimensions, such as the bead to plate (wetting) angle and the ratio of plate melted to total melted area (dilution), are restricted to average current and travel speed. It was felt, therefore, that only a limited study was required in the present program to investigate the effect on fusion characteristics of those variables not fully covered in previous investigations, such as wire chemistry and shielding gas composition. In addition, the study could be limited to values of mean current of interest in the context of an all-positional welding capability.

The influence of wire chemistry on fusion characteristics was evaluated from bead-on-plate welds at a mean current of 150 A with all eight wires in 95Ar-5CO_2 shielding gas mixture. Any competing or compounding effect of mean current was examined with four of the wires (low C-Mn-Si, C-Mn-Si-Ti, C-Mn-Ni and C-Mn-Mo) in 95Ar-5CO_2 at mean current values of 100, 150 and 200 A. Ip and Tp remained constant as previously determined and background conditions were derived from the 50 Hz/100 A rule. Contact tip-to-work distance was 13 mm. Travel speed was adjusted to give a nominal heat input of 1.5 kJ/mm for all weld deposits. The influence of shielding gas composition was assessed through additional tests with C-Mn-Mo wire in all four shielding gas mixtures at 150 A mean current. Beads were deposited in the flat position on 100 mm by 50 mm by 12.7 mm thick, surface ground, mild steel plate. The welds were sectioned in two places; the sections were prepared by mounting in bakelite, wet grinding on graded silicon carbide papers and polishing on a rotating cloth pad, using 6 μm diamond dust paste. The weld bead shape parameters measured were depth of penetration, reinforcement height, bead width, wetting angle, plate fusion area and weld reinforcement area.

4.2 Procedure Development

Based on the results of the previous experiments, only three of the four shielding gas mixtures were selected for further evaluation. It was also determined that a single pulse peak condition would meet the requirement of one drop per pulse metal transfer in all combinations of the eight wires and three remaining shielding gases and, therefore, further procedure development could be adequately carried out with only one wire and shielding gas combination. Procedures were developed in 600 mm wide, 1000 mm long, 30 mm thick mild steel test panels with a 60° included angle, single vee preparation, in the vertical up, 45° overhead and flat positions.

However, before this phase of the investigation could begin, it was necessary to modify the pulse logic section of the M450PS power source in order to be able to operate the unit in its synergic mode while maintaining optimum pulse parameters, as determined from the results of the previous experiments, over the required range of average current values. Fig. 5 shows the original pulse logic circuit. The mean current is set by the main control potentiometer on the front panel. This signal is conditioned by gain and offset and then converted to frequency by a relationship of approximately 50 Hz/100 A. A timer, set by the internal potentiometer Tp, is triggered by the frequency signal and generates the switching signals used to add in the peak current signal. The time at peak is a constant so that only the time at background varies with frequency, as a result of changes in mean current setpoint. Peak current is set by another internal potentiometer Ip. The output is conditioned by gain and offset and then goes to the switch controlled by the time at peak signal. The background current signal is derived from a portion of the mean current control and thus varies with mean current. After being conditioned by gain and offset the background current signal then goes to the summing amplifier. The output of the peak current switch also goes to the summing amplifier and is added to the background current signal. After passing through the final gain calibration circuits, this signal is used as the current setpoint into the power control section. This means that, as mean current is changed, Ip, Ib and Tb will vary, only Tp remaining constant (Fig. 2).

As suggested by Allum (5), and confirmed from the results of the present investigation, for one drop per pulse transfer over a range of current values, both Ip and Tp must remain constant. The pulse logic circuit was thus modified by adding a switch so that both the peak and background current levels could be switched in independently as shown in Fig. 6. The background current signal now goes to the switch controlled by the time-at-background signal. The output of the switch controlled by the time-at-peak signal and the output of the switch controlled by the time-at-background signal are connected together, since only one switch at a time can be on. This output, after passing through the final gain calibration circuits, is used as the current setpoint into the power control section. In this way, Ip and Tp remain constant and only Ib and Tb vary with changes in mean current, as illustrated in Fig. 7.

The M450PS has constant current power characteristics and GEC has foresaken self-adjustment in favour of keeping what is considered the most important arc variable, arc current, well defined. Thus, the arc behaves quite differently when compared with conventional GMAW, in that, as the welding torch is withdrawn from the work, the electrical stickout remains fixed and the arc length increases. The power source worked well in this mode for the bead-on-plate studies and may be perfectly adequate for manual welding in a groove, where the welder can control arc length as in the SMAW process. However, when mechanized welding in a groove was attempted at the start of procedure development, process instabilities arose as the arc impinged on the sidewalls; the arc length was reduced leading to short circuiting, spatter and the potential for sidewall fusion defects.

Arc length may be controlled under conditions of constant current by modulating the wire feed in response to a voltage error signal. This method was investigated first, but proved incapable of providing a reliable and stable response to arc length changes. The arc voltage feedback signal must be filtered because of the presence of the low frequency pulsing, normally in the range 50 to 100 Hz. Filtering adds time delay to the feedback and this time constant, plus the wire-feeder response time constant, causes the voltage compensation loop to be only marginally stable. Even with the low gain in the compensation loop it was not possible to maintain stability in the event of an arc disturbance.

The alternative was to modulate mean current in response to a voltage error signal. The simplest method was to vary the pulse frequency in proportion to the arc voltage feedback error signal. As shown in Fig. 8, the arc voltage error signal, switched with the arc-on signal, is added to the frequency control signal. A frequency limiter was inserted between the resulting control signal and the voltage-to-frequency converter. This is to prevent large errors from increasing or decreasing the frequency too much. The limits are set at 40 and 200 Hz. The gain in the compensation loop is 25 Hz per arc volt of error and the filtering time constant is approximately 20 ms. The arc voltage reference is set by a remote control potentiometer. A digital voltmeter was added to the M450PS front panel to aid in the setting of the reference voltage and the monitoring of arc voltage, once the arc is established.

Based on the results obtained from the welding of the mild steel test panels, a welding procedure was developed in 1067 mm O.D., 30 mm W.T., Gr. 414 MPa pipe in order to generate productivity data which, in combination with production data from field experience with both mechanized FCAW and SMAW in this diameter and wall thickness, would provide a basis for economic comparison. The machined pipe preparation was a 60° included angle with a 3.2 mm land and 3.2 mm gap. The root pass was made using E55010-G SMAW electrodes. Mechanized pulsed GMAW procedures were chosen to maximize productivity with mean current set as high as possible, consistent with the formation of a weld bead of flat to slightly concave profile, with even fusion into the sidewalls. Travel speeds were based on maintaining the arc at the leading edge of the weld pool, and oscillation rate and dwell times were selected to optimize fusion characteristics and overall bead appearance.

4.3 Metallurgical Evaluation

4.3.1 Welding Procedure

Twelve test panels, 1 m long by 0.75 m wide, were prepared in 30 mm thick Lloyds LT60 plate. The edge preparation, illustrated in Fig. 9, was produced by flame cutting and grinding and the plates were assembled as shown in Fig. 10. Restraint bars 150 mm x 750 mm, of the same LT60 material, were welded at either end of test panels to prevent rotation about the weld. The test panels were welded in the vertical position, using the CRC M-200 mechanized welding system, with power supplied by the modified GEC M450PS. The welding procedures adopted were essentially the same as those developed for the 1067 mm O.D., 30 mm W.T. pipe, with the exception that a backwelding technique was adopted for the root, in place of the SMAW root pass; the 60° included angle bevel was filled and capped, the test panel turned, the root ground to sound metal and the backweld completed in one pass with the M-200. No preheat was applied and the interpass temperature was $200^{\circ}C$ maximum, as measured 25 mm from the weld preparation. Eight test panels were completed using $95Ar$-$5CO_2$ shielding gas, two with $88Ar$-$10He$-$2CO_2$ and two with $87.5Ar$-$10He$-$2CO_2$-$0.5H_2$. The latter four panels were made with the C-Mn-Si and C-Mn-Ti-B wires, which were considered to represent the extremes of alloy design for this application. All twelve test panels were subjected to radiography according to the requirements of DnV Rules for the Design, Construction and Inspection of Offshore Structures, Section 6.5.

A further three test panels, this time of only 0.33 m in length, were completed with the most promising wire/shielding gas combination (C-Mn-Ti-B in 95Ar-5CO_2). The test panels were prepared as shown in Figure 10 and were welded from one side only with full penetration root beads, the first with E41010 SMAW electrodes, the second and third with the mechanized pulsed GMAW process. The first and second panels were filled and capped as before, while for the third, a lower heat input was maintained. These additional panels were made to assess the influence of bead deposition sequence, root bead welding process and weld-metal strength, and fill and cap pass heat input on CTOD toughness.

4.3.2 Chemical Analysis

Broken tensile testpieces were used to supply weld metal for chemical analysis, and wire samples were taken directly. Non-gaseous elements were analyzed spectrographically and gaseous elements by the high temperature, inert-gas fusion technique.

4.3.3 Mechanical Testing

Each of the first twelve welded test panels was sectioned for mechanical testing as shown in Fig. 11. Two all-weld-metal tensile testpieces of 12 mm diameter, to ASTM A370, were extracted from 2 mm below the plate surface and tested at room temperature. Yield strength, tensile strength, percent elongation, and percent reduction of area were measured. Eighteen Charpy V-notch specimens were prepared according to ASTM E23 with the notch positioned at the centre of the weld and the notch plane parallel to the weld direction and perpendicular to the plate surface. Fifteen Cv specimens were selected from 2 mm below the top surface of the test panels and three were selected from 2 mm above the bottom surface of the test panel. The subsurface Cv specimens were broken at various temperatures to obtain transition curves for each test panel evaluated; the root Cv testpieces were tested at -45°C. Three B x 2B CTOD specimens were prepared, with the notch at the weld centreline and in the through-thickness direction, and tested in accordance with BS 5762 at a test temperature of -45°C. Local pre-compression was carried out on each specimen prior to fatigue cracking: a 13 mm diameter platen was used to produce an indent depth equivalent to 0.5% of the specimen thickness on each side, and thereby provide a sufficient amount of mechanical stress relief to ensure uniform fatigue crack growth. Three B x 2B CTOD specimens only were extracted from the remaining three test panels and tested at -45°C. Macrosections were prepared for examination of bead profiles, potential for defects and weld run sequence, and a hardness survey was conducted at a load of 0.5 kgf.

4.3.4 Metallographic Examination

Charpy specimens broken at -45°C were selected from the cap and root of each test panel. The notched surfaces were then ground flush to the notch root, mounted in bakelite, polished, etched in 2% nital, and examined for identification of the microstructural features adjacent to the fracture surface.

5.0 RESULTS

5.1 Process Characteristics

5.1.1 Arc Stability and Metal Transfer

Typical current and voltage traces from the bead-on-plate weld runs are shown in Fig. 12. These particular traces are for the C-Mn-Mo wire in 95Ar-5CO_2 at a pulse peak current of 350 A. Drop detachment was determined from the occurrence of spikes on the voltage traces, while an indication of arc and process stability was obtained from the regularity of both current and voltage traces. At 2 ms peak duration the voltage trace shows irregular metal transfer, with more than one pulse required to transfer one drop; detachment occurs primarily in the background. Arc instability is indicated by inconsistencies in the level of background current attained after each current pulse and, although none appear in this particular trace, a number of short circuits were recorded. At 3 ms peak duration the arc appears to be very stable and the voltage trace shows regular drop detachment occurring at the trailing edge of the pulse peak. The 4 ms trace continues to show regular drop detachment at the trailing edge of each pulse peak, whereas the voltage trace at 350 A and 6 ms shows detachment within the peak and away from the trailing edge. In point of fact, for this consumable combination, the minimum peak duration for one drop per pulse metal transfer at a peak current of 350 A was determined to be 3.0 ms; drop detachment remained on the trailing edge of the pulse peak until a peak duration of 4.8 ms was reached, after which detachment occurred within the peak. From the observations of the welding operator, the irregular metal transfer at short peak durations resulted in short circuiting and considerable spatter, while regular drop detachment at the trailing edge of each current pulse gave very stable and "smooth" arcing conditions; "within-the-peak" detachments coincided with the onset of fine spatter with a number of wire/gas combinations, although the arc remained essentially stable.

In this manner, voltage and current traces were used to determine the relationship between ip and Tp for the "ideal" one drop per pulse metal transfer for all combinations of the eight wires and four shielding gases; the results are shown in Figs. 13 to 16. There was little difference in behaviour between the various wire/shielding gas combinations with 95Ar-5CO_2, 88Ar-10He-2CO_2 and 87.5Ar-10He-2CO_2-0.5H_2 gas mixtures. In 80Ar-20CO_2, however, there was a tendency to fine spatter even when drop detachment at the trailing edge was indicated; in addition, the curves shifted to higher peak durations for the majority of the eight wires investigated. The results at peak current values of less than 300 A have been omitted from the figures since, at the long peak durations required to achieve stable metal transfer, the arc appeared to the operator as "soft" and less obviously penetrating than at the higher peak current values. These characteristics would be less suitable for normal groove-welding applications, although there may be fields in which they would be desirable.

There was little difference, in terms of arc characteristics, between values of peak current within the 300 to 400 A range, and the mid-range value of 350 A was selected for further examination of drop detachment phenomena using the high-speed video, motion picture analysis system. Access to this equipment was limited, and high-speed video recordings were made at 2, 3 and 4 ms peak duration only, in order to assess the validity of interpretation of the current and voltage traces as regards droplet detachment. Complete details of pulse parameters are given in Table 3. Metal transfer with C-Mn-Mo wire in 95Ar-5CO_2 was filmed first; the video recording, played back at speeds of 60 and 4 frames/s, revealed a number of important considerations with respect to controlled metal transfer which had hitherto gone unrecognized. As had been inferred from the traces, more than one current pulse was seen to be required to detach a droplet at a peak duration of 2 ms and, as illustrated in the still photographs in Fig. 17a, a droplet would grow, on occasions, to a diameter much greater than that of the wire. At 3 ms peak duration the video recording showed one droplet, of approximately the same size as the wire diameter, being detached, consistently, at the trailing edge of the pulse peak; transfer across the arc took place during the quiet, background period (Fig. 17 b). At 4 ms, a droplet of similar diameter was detached at the trailing edge of the pulse peak, but this was immediately followed by a stream of fine droplets (Fig. 17c). The exercise was repeated with C-Mn-Mo-Ti wire in 95Ar-5CO_2 and C-Mn-Mo wire in 87.5Ar-10He-2CO_2-0.5H_2 shielding gas mixture, and the results were identical; multiple drop transfer of the dual nature described above was recorded, in both cases, at 4 ms peak duration.

It would seem, therefore, that while current and voltage traces are useful for determining the critical peak duration, Tpc, for the onset of stable, one drop per pulse metal transfer, they give no indication of the initial breakdown of this condition. Although no further attempt was made to define the precise range of peak duration for the "ideal" one drop per pulse metal transfer, it appears to be limited to less than 1 ms.

The results of brief experiments, carried out with the motion picture analysis system and using C-Mn-Mo wire in 95Ar-5CO_2, to examine the influence of background conditions on drop size, are shown in Tables 4 and 5. Increasing the frequency-to-mean-current relationship from 50 Hz/100 A to 60 Hz/100 A had no measurable effect. Decreasing the background current resulted in a corresponding decrease in drop diameter. Metal transfer remained unaffected.

For the remainder of the investigation, a pulse peak of 350 A for 3 ms was selected for all experiments. As can be seen from Figs. 13, 15, and 16, this particular point falls on or within +0.3 ms of Tpc for all combinations of the eight wires and 95A-5CO_2, 88Ar-10He-2CO_2 and 87.5Ar-10He-2CO_2-0.5H_2 shielding gas mixtures. Fig. 14 shows that these pulse parameters are not ideal for all eight wires in 80Ar-2CO_2; one drop per pulse metal transfer would only be consistently obtained with the C-Mn-Mo wire. As mentioned earlier, arc characteristics in $80Ar-20CO_2$ were inferior when compared with the other three gas mixtures and it was, therefore, the least likely candidate for procedure development. For these reasons, detailed analysis of burn-off characteristics and weld bead profiles in $80Ar-20CO_2$ was limited to the one C-Mn-Mo wire.

5.1.2 Burn-off Characteristics

The relationship between wire feed speed and mean current at a 13 mm contact tip-to-work distance varied little from one wire/shielding gas combination to another for all eight wires and four shielding gas mixtures. The results for the eight wires in $95Ar-5CO_2$ are shown in Fig. 18. There would appear to be a linear relationship, through the origin, at low values of mean current (less than 150 A), with deviation from linearity toward higher wire feed speeds as mean current is increased. Burn off characteristics were then determined for one wire, C-Mn-Mo, in all four shielding gas mixtures at electrical stickouts of 9, 12, 16 and 20 mm (corresponding to contact-tip-to-work distance of 13, 16, 20 and 24 mm) and the results are shown in Fig 19. Similar results were obtained in all four shielding gases; they show that the deviation from linearity of the relationship between wire feed speed and average current begins at progressively lower values of mean current as electrical stickout is increased.

5.1.3 Fusion Characteristics

The weld bead shape characteristics for the selected wire and shielding gas combinations investigated are detailed in Tables 6 and 7.

In the present study, one of the main objectives is to overcome the susceptibility to fusion defects, inherent in the GMAW process, through the use of pulsed current. With this end in mind, key weld bead shape parameters are penetration, bead-to-plate angle or "wetting" angle and dilution, defined as the fraction or percentage of the total fusion zone originating from the plate. Dilution, especially, may be used as a rough measure of the susceptibility to fusion defects and as a means of comparing the fusion characteristics of different processes. For example, dilution with all-positional, conventional GMAW is typically 20% or less, whereas for SMAW the corresponding figure is 40%.

Figure 20 summarizes the fusion characteristics for all eight wires in 95Ar-5CO_2 at 150 A. There was little variation in penetration, wetting angle or dilution that could be attributed to wire chemistry. Fig. 21 shows the dominant effect of mean current on fusion characteristics when four of the wires were examined in 95Ar-5CO_2 at mean current values of 100, 150 and 200 A. (Strictly speaking, the figure shows the combined effect of mean current and travel speed; travel speed was increased with mean current to maintain a constant heat input.) Penetration and dilution increased with average current for all four wires, accompanied by a corresponding decrease in wetting angle. The macrophotographs in Fig. 22 provide further illustration of the influence of mean current.

With regard to the influence of shielding gas composition, there appears from Fig. 23 to be a distinct improvement in depth of penetration and, more importantly, dilution with 95Ar-5CO_2 and the two helium containing gas mixtures, when compared with 80Ar-20CO_2. However, the major influence of shielding gas composition is on plate fusion or penetration shape and this is best illustrated by the macrophotographs in Fig. 24. In general, pulsed gas metal arc welds in argon-rich shielding gas mixtures exhibit finger penetration, with weak secondary fusion extending towards the bead edges. Similar penetration profiles are produced with conventional GMAW operating in the spray mode of metal transfer, and carbon dioxide and/or helium are added to enhance secondary fusion and thereby avoid fusion defects. Indeed, the 80Ar-20CO_2 produced the more-rounded penetration profile, while the other three gas mixtures showed a more-pronounced finger penetration, (though not to the extent where the reduced secondary fusion would result in overall fusion characteristics being considered suspect). Lateral displacement of the finger penetration was observed in the 80Ar-20CO_2, 95Ar-5CO_2 and 88Ar-10He-2CO_2 shielding gas, but was absent in the Ar-He-CO_2-H_2 gas mixture. This confirms the findings of a previous investigation (14) and has important connotations with respect to reduced susceptibility of the pulsed GMAW process to lack of fusion defects.

5.2 Procedure Development

Three shielding gas mixtures, $95Ar-5CO_2$, $88Ar-10He-2CO_2$ and $87.5Ar-10He-2CO_2-0.5H_2$, were selected for further investigation, $80Ar-20CO_2$ being excluded due to inferior metal transfer characteristics. In addition, a single peak condition, 350 A at 3 ms, would meet the requirement of one drop per pulse metal transfer for all eight wires in the three remaining shielding gases, thereby simplifying further procedure development and metallurgical property evaluation.

The procedures developed for welding in the vertical up, 45^0 overhead and flat positions in the 30 mm thick mild steel test panels are included in Tables 8 to 10. C-Mn-Mo wire with $95Ar-5CO_2$ shielding gas was used and peak parameters were, as mentioned above, 350 A for 3 ms, with background conditions selected based on the 50 Hz/100 A rule. Other welding parameters were chosen to maximize productivity, although not at the expense of fusion characteristics.

The major variable affecting the formation and appearance of any particular weld pass was mean current. In the vertical and 45^0 overhead positions, excellent bead profiles were obtained at approximately 150 A, with travel speeds selected to ensure that the arc remained at the leading edge of the weld puddle. At low values of mean current (less than 110 A), weld pool fluidity decreased and sidewall fusion was impaired. At higher mean current, and especially in the 45^0 overhead position, crowning of the weld deposit would occur, leaving a less-than-ideal bead profile for application of subsequent passes. Oscillation rate was matched with travel speed to ensure good inter-run fusion; for sidewall fusion, oscillation width was carefully set and balanced with sidewall dwell time. Maintaining a contact-tip-to-work distance of 13 mm enhanced weld puddle control. Larger weld puddles can be carried in the flat position, and there is obviously less restriction on mean current than in the vertical and 45° overhead. However, the weld puddle still has to be controlled in the context of achieving optimum sidewall and inter-run fusion, and these considerations led to the selection of mean currents in the range 180 to 200 A for all weld passes.

Very smooth and stable arcing conditions were maintained throughout, with a total absence of spatter. Completed test panels were subjected to radiography and no discontinuities were detected.

The procedure for completing the girth weld in 1067 mm O.D., 30 mm W.T. pipe is given in Table 11. The root bead was completed with vertical up progression with E55010 SMAW electrodes. The pulsed GMAW fill and cap welding parameters were chosen to maximize productivity, while remaining suitable for completing the whole circumference in the 5G position without significant change. The joint completion time was then calculated based on a 70% operating factor, a figure arrived at through production experience with the mechanized FCAW process; this may be considered conservative for the mechanized pulsed GMAW process, as there is no inter-run slag removal required.

This calculated figure was then compared with the true joint completion time for a shielded metal arc weld in the same diameter and wall thickness, as measured in production, and the result is shown in Fig. 25. The procedure for completing the shielded metal arc weld is given in Table 12.

5.3 Metallurgical Evaluation

5.3.1 Welding Procedure

The welding procedures used to complete the test panels in the 30 mm thick Lloyds LT60 plate are given in Tables 13 to 27. In general, welding characteristics, in the vertical position, with the eight wires in 95Ar-5CO_2, were excellent. With the two wires in the 88Ar-10He-2CO_2 gas mixture, the weld pool appeared to be less fluid, and closer control of the positioning of the torch in the weld preparation and of weave parameters was necessary to ensure adequate sidewall fusion. The addition of 0.5% hydrogen improved sidewall wetting; little difference in process characteristics could be detected between the Ar-CO_2 and Ar-He-CO_2-H_2 shielding gas mixtures.

With two of the three additional test panels, a full penetration root bead was applied using the pulsed gas metal arc welding process. It should be stressed that the root welding parameters shown in Tables 26 and 27 were evaluated in the vertical position only, for the purpose of CTOD comparison, and may not be suitable for welding in all positions. Experience has indicated that the development of full penetration root welding procedures with the gas metal arc welding process requires systematic and time consuming investigation, beyond the scope of the present program of work, if lack of root fusion is to be avoided.

All test panels met the radiographic requirements of the DnV code.

5.3.2 Chemical Composition

The results of the all-weld-metal chemical analyses are shown in Table 28a for the eight test welds deposited under 95Ar-5CO_2, and in Tables 28b and 28c for the welds made under 88Ar-10He-2CO_2 and 87.5Ar-10He-2CO_2-0.5H_2, respectively. A general comparison with the wire chemical compositions in Table 2 shows that dilution levels are uniformly low, as would be anticipated from the results of the bead-on-plate studies reported above.

The essential features of the deposit compositions can be summarized as follows. Of the welds made under 95Ar-5CO_2 shielding, there is little difference between the two deposited with C-Mn-Si wires: both show relatively high levels of silicon and sulphur, reflecting the corresponding contents in the wires. The low carbon content of the second of these wires is carried over to the deposit, with no detectable increase arising from the higher-carbon parent plate. In the weld made with the C-Mn-Si-Ti wire, the chemical composition is very similar to those of the previous two welds, with the exception that fifty percent of the titanium content of the wire is recovered in the weld. In addition, the sulphur content reflects the significantly lower level in the wire. A similar level of titanium recovery is observed in the C-Mn-Ti-B deposit; most of the boron present in the wire is also recovered. This deposit also shows an extremely low sulphur content, as well as higher levels of manganese and residual chromium, copper and nickel.

The chemical compositions of the two nickel-containing deposits again reflect a low level of dilution, with the nickel contents of the welds being ninety percent or more of those in the wire. With the C-Mn-Ni-Ti wire, about fifty percent of the titanium is recovered; this deposit also shows a low sulphur content.

The C-Mn-Mo deposit shows generally high levels of residual nickel, chromium and copper, as well as a high sulphur content. In the C-Mn-Mo-Ti deposit, alloying, residual and impurity elements are generally at a lower level; the titanium content observed is consistent with the very high level in the wire, again with nearly fifty percent being recovered in the weld.

Features common to all eight welds are a low oxygen content (0.017-0.021%), reflecting the low oxygen potential of the shielding gas, and very limited pick-up of niobium or vanadium from the parent plate. Nitrogen contents fall in the range 0.012-0.017%. The four welds made under gases with lower oxygen potential have compositions which are essentially identical with those of the corresponding welds made under 95Ar-5CO_2, with the exception that the oxygen content is even lower (0.012-0.015%). Nitrogen contents also appear to be slightly reduced (0.010-0.011%).

5.3.3 Mechanical Properties

5.3.3.1 Hardness Test Results

The detailed results of hardness tests on the twelve original test panels are shown in Tables 29-40, and weld metal hardnesses are summarized in Table 41. The hardness in the root region was consistently higher than in the subsurface region, as would be expected from the lower heat input. In general, hardness was reasonably correlated with chemical composition, with the deposits containing alloying elements such as molybdenum, nickel or boron showing significantly higher levels of hardness than the C-Mn-Si deposits.

5.3.3.2 Tensile Test Results

The results of all-weld-metal tensile tests are shown in Table 42. Yield strengths lie in the range 480-775 MPa, and are, for the most part, higher than would be considered ideal for welding structural steels with yield strengths up to 355 MPa. To a large extent, this results from the alloying systems adopted in order to attain acceptable low-temperature toughness. In fact, the observed variations in yield strength can be approximately related to the chemical composition of the deposit, as Fig. 26 shows. The abscissa in this graph is Düren's CE_B, which was developed for the prediction of heat-affected zone hardness (16). There is no reason why weld-metal yield strength should correlate well with this particular expression of chemical composition, but its use does present the advantage, relative to the carbon equivalents used by previous workers (17,18), of allowing the effects of silicon as well as the principal alloying elements to be accounted for. Interesting features of this figure are that the yield strengths of all the deposits containing measurable amounts of titanium lie in a band significantly higher than that for the titanium-free welds, and that the presence of boron does not appear to have any significant additional effect.

As regards the tensile ductility of the deposits, there is a broad correlation with sulphur content, as is apparent in Fig. 27, though clearly other factors are involved. Since the titanium-bearing wires, generally speaking, are 'second-generation' products in which greater emphasis has been placed on steel cleanness, they also have lower sulphur contents and their tensile ductilities lie at the upper end of the range. One weld made under the hydrogen-containing shielding gas showed a low reduction of area, which was associated with 'fish-eyes' in the fracture surface. No hydrogen-reduction treatment had been carried out prior to testing.

5.3.3.3 Charpy Impact Test Results

The results of the Charpy V-notch tests on the twelve panels are shown in Tables 43 - 54 and Figs. 28 - 32. The principal features of these results can be summarized as follows.

The 0.1% C-Mn-Si weld showed average impact energies of 81 J and 19 J at + 20°C and -45°C, respectively. These figures improved significantly with the reduction of carbon content in the low C-Mn-Si weld (Fig. 28). A further improvement occurred with the addition of titanium; this may also have been partly due to the lower sulphur content in this deposit. The C-Mn-Ti-B deposit showed the best impact properties of all the welds tested, with an average absorbed energy of 99 J at -60°C. The extremely low sulphur content of this weld, in conjunction with the low oxygen content common to all the deposits, would account for the high shelf energy, while the low transition temperature is related to microstructural effects which are discussed in a later section.

The toughness of the root region in this series of welds was generally somewhat lower than that of the sub-surface region, as is normally observed in thick-section weldments. In the case of the 0.10% C-Mn-Si deposit, however, the root region toughness was slightly higher.

The C-Mn-Ni weld shows a transition curve intermediate between that of the two C-Mn-Si deposits. The addition of titanium to this composition, (Fig. 29) together with the associated reduction in sulphur content, led to a significant improvement in toughness. The root-region toughness at -45^{o}C fell significantly in the second of these two welds, but was unchanged, relative to the sub-surface region, in the first.

The C-Mn-Mo weld shows relatively poor impact toughness (Fig. 30), similar to that of the 0.1% C-Mn-Si weld; this is probably the result of the excessively high yield strength of this deposit. The addition of a high level of titanium, and the accompanying reduction of sulphur content, improved the shelf energy but led to a sharper transition behaviour, with essentially-brittle fractures being observed at -45^{o}C. Conceivably, the titanium level in this deposit is high enough, in conjunction with the low oxygen content, to lead to some degree of precipitation hardening. Root region toughness values in these welds are identical with those in the sub-surface region.

Fig. 31 shows that the use of less-oxidising shielding gases leads to only very slight improvements in the toughness of welds made with the 0.09% C-Mn-Si wire. The improvement is presumably related to the lower oxygen content of these deposits; its extent is limited, however, by the persistence of less-than-ideal microstructural features, as will be discussed in a later section.

Fig. 32 shows the influence of shielding gas composition on the toughness of welds made with the C-Mn-Ti-B wire. In this case, the transition temperature deteriorates as the oxygen potential of the gas decreases. This behaviour, also, can be related to microstructural effects which are discussed below.

5.3.3.4 CTOD Test Results

The results of the CTOD tests on the twelve original panels are shown in Table 55; results of tests on additional welds made to assess the effects of certain procedural variables appear in Table 56. As regards the welds made under 95Ar-5CO_2, while there are relatively minor variations in the observed values of CTOD at -45^{o}C in the other seven welds, only the C-Mn-Ti-B deposit shows levels of CTOD approaching acceptability for critical service. Even in this case, one low result was obtained. The change to shielding gases of lower oxygen potential led to a serious deterioration in the CTOD values of the C-Mn-Ti-B welds, as could have been anticipated from the Charpy results. The C-Mn-Si weld made under the hydrogen-containing shielding gas showed significantly improved CTOD results. This was unexpected, on the basis of the Charpy results discussed above, and no explanation of this observation could be found.

In most of the testpieces which showed low levels of CTOD (less than 0.1 mm), fracture initiation was controlled by the behaviour of the root region, as has also been reported in the literature for welds made with a double-V preparation (19). It was considered that this could have been related to the deposition sequence used, which involved back-gouging and welding the root as the final pass. As well as leaving the entire root region in the as-deposited condition, this also led to a highly asymmetrical distribution of residual stress, which would be unlikely to be wholly eliminated by any practical local pre-compression treatment. The first two welds whose CTOD results are listed in Table 56 were made with a view to assessing the effects of alternative root-pass techniques on the level and consistency of CTOD which could be obtained. Reasonably good CTOD values were obtained in both of these cases. A final additional weld was made to determine whether a limitation on heat input in fill and cap passes would lead to any improvement; for all practical purposes, the results obtained were very similar to those observed in the original test panel.

5.3.4 Metallographic Observations

Macrographs representative of the twelve test welds are shown in Fig. 33, and indicate the general geometry and the bead placement adopted, as well as illustrating the excellent fusion characteristics which have been referred to previously.

Representative micrographs of the test welds are shown in Figs 34 to 45. As-deposited and refined microstructures are shown, at a magnification of 500x, for both root and sub-surface regions for each weld. Table 57 indicates the percentage of refined microstructure observed in each weld, as measured on both the sub-surface and root-region Charpy testpieces. The general, qualitative aspects of the metallographic observations can be summarized as follows.*

In the as-deposited regions, the 0.1% C-Mn-Si deposits show relatively-coarse acicular ferrite; grain-boundary ferrite and some ferrite with aligned second phase (martensite, austenite or carbides) are also present. The ferrite grain size and second-phase particle sizes in the refined region are relatively coarse. The low C-Mn-Si deposit has considerably more primary ferrite, particularly in the sub-surface region, in keeping with the lower anticipated hardenability of this wire. The grain size in the refined region is somewhat finer. The C-Mn-Si-Ti deposit consists of very fine acicular ferrite, with small amounts of grain-boundary ferrite and ferrite with aligned second phase. The microstructure of the as-deposited regions in the C-Mn-Ti-B weld is entirely composed of acicular ferrite, reflecting an ideal balance between hardenability, cooling rate and inclusion content. Interestingly, some regions of ferrite with aligned second phase appear in the welds made with this wire under less oxidizing gases (Figs. 43 and 45), suggesting that impurity levels may now be too low for consistently-effective nucleation of acicular ferrite.

---

* Nomenclature adopted in describing weld-metal microstructures generally follows that proposed by Sub-Commission IXJ of the IIW.

The as-deposited regions of the C-Mn-Ni weld are essentially composed of acicular ferrite with some grain-boundary ferrite; there is a small amount of ferrite with aligned second phase. The C-Mn-Ni-Ti deposit has a similar microstructure, with somewhat less ferrite + second phase. The grain-size in the refined region also appears finer.

The C-Mn-Mo deposit shows a very fine acicular ferrite microstructure with no grain-boundary ferrite. Grain-boundary ferrite is also absent in the C-Mn-Mo-Ti weld; the acicular ferrite is a little coarser in this weld, and some fine ferrite with second phase is also present.

There are few consistent trends in the results presented in Table 57. The C-Mn-Mo deposit shows an extremely small proportion of refined microstructure; evidence of this can also be seen in Fig. 33g. This tendency had been observed previously with this wire, when welding at much lower heat inputs, in the short-circuiting mode (7). Interestingly, the other high manganese, molybdenum-alloyed weld showed a similar behaviour, despite the significant differences in other aspects of its chemical composition. Generally speaking, there was a smaller proportion of refined microstructure in the welds made under gases of lower oxygen potential, possibly reflecting differences in fusion behaviour and bead shape. In most welds, as expected, there was less refined microstructure in the root region, where only one pass per layer was required.

6.0 DISCUSSION

The detachment of one droplet per pulse has been identified by many workers as an important criterion for controlled metal transfer in pulsed GMAW (5,9,13). From the present work, it would appear that the range of pulse peak parameters (to be more precise, the range of values of peak duration, Tp, at any given peak current, Ip) with which one drop per pulse metal transfer can be achieved is considerably narrower than previously indicated in the literature. Admittedly, the study of drop detachment phenomena, using the motion picture analysis system, was limited to only two wires and two shielding gases, but the observations are extremely valuable in assisting the interpretation of current and voltage traces. As a result of the comparison of video recordings of droplet detachment phenomena with the corresponding current and voltage traces, it can be concluded that the latter are a reliable means of detecting the critical peak duration, Tpc, for the onset of one drop per pulse metal transfer; the range of peak time over which this condition is maintained cannot be determined, however. Additional correlation for the determination of critical peak duration at constant Ip was obtained from the observations of the welding operator. The change in arc characteristics as Tp was increased through Tpc was quite dramatic; an audible change from the 'crackle' of short-circuit transfer to the 'hiss' of spray, coupled with the elimination of spatter, coincided with the onset of one drop per pulse metal transfer, as indicated by the current and voltage traces.

As a consequence of the above, only conditions close to the leading edge of the acceptable operating zones shown in Figs. 13 to 16 are considered to express valid relationships between pulse peak parameters for one drop per pulse metal transfer. The relationship

$$I^n pTp = \text{const.}$$

has been widely cited as defining the pulse structure necessary for the condition of one drop per pulse. The present work provided further experimental confirmation of the general form of this relationship. Analysis of the curves defining the leading edge of the acceptable operating zones in Figs. 13 to 16 did not lead to the determination of a unique exponent of Ip, though most values lay in the range 2.0 - 2.7. This can be compared with the work of Amin (9), who found this exponent to be 2.3, of Allum (5) and of Smati (13). Interestingly, despite Smati's use, for analytical purposes, of an $I^2 pTp$ relationship, the experimental results published in Ref. (13) are more consistent with an exponent of 2.5. The present work agrees precisely with Smati's numerical criteria for one drop per pulse (e.g. Ip = 350 A, Tp = 3 ms), but suggests that, under these conditions, droplet detachment takes place in coincidence with the trailing edge of the peak, rather than, as he states, during the background. (In reality, this difference may be purely semantic, since transfer does occur during the background.)

The mode of multiple drop transfer observed as Tp is increased within the range Tpc + 1 ms, whereby subsequent detachments during the same current pulse are in the form of a stream of fine droplets, has also been observed by Ma and Apps (20). However, in their work, with a

1.2 mm diameter mild steel wire in 95Ar-5CO_2 at 380 A peak current, there was a distinct time lapse, some 3 ms, between the first drop and subsequent stream spray detachments. In the present work, there was no measurable time delay between detachments, the first drop, of equivalent size to the wire diameter and detaching at the trailing edge of the pulse peak, being followed immediately by a stream of several fine droplets. In agreement with the work of Ma and Apps, the high speed video recordings showed that the most quiescent metal transfer mode in pulsed GMAW was with one drop per pulse.

Comparing the curves defining the leading edge of the acceptable operating zones for the various wire/gas combinations investigated, similar results were obtained with all eight wires in 95Ar-5CO_2 and both experimental shielding gas mixtures; this was not the case however, with 80Ar-20CO_2. (Interestingly, many preprogrammed pulsed GMAW power source manufacturers recommend the exclusive use of 80Ar-20CO_2). It is clear, therefore, that there is no single combination of Ip and Tp that will result in one drop per pulse metal transfer for all 1.2 mm diameter 'carbon steel' wires; both wire composition and shielding gas mixture can influence the values of Ip and Tp required. The main practical implication is that, to take full advantage of the controlled metal transfer offered by the pulsed gas metal arc welding process, with the flexibility to select any combination of wire and shielding gas for a specific production application, there is no quick alternative to the experimental determination of optimum pulse peak parameters. Hence, power sources with factory-programmed pulse parameters will be restricted as to the range of wire and shielding gas combinations that will give optimum metal transfer characteristics unless the program can be accessed and modified. Similarly, synergic logics that involve variations in peak current and/or peak duration with changes in mean current may significantly alter the mode of metal transfer and, as a result, have only a limited range of stable operation.

The situation as regards background conditions is less onerous. Both Allum (5) and Smati (13) concluded that, whereas peak parameters control metal transfer, the size of droplet transferred is influenced by background conditions. Furthermore, Quintino and Allum (10) proposed a simple 'rule of thumb' (the background of which is discussed later) whereby a pulse frequency corresponding to 0.5 Hz/A of mean current will result in a droplet size equivalent to the wire diameter, for a 1.2 mm diameter wire; other ratios were proposed for different wire sizes. From the few measurements taken from the video recordings and presented in Tables 4 and 5, there was no evidence to dispute these findings. Once Ip and Tp have been determined experimentally, then background parameters can be calculated essentially as suggested in Ref. (10), as follows:

Select the mean current appropriate to the particular production application;
Calculate the frequency, F, from the $F/\bar{I}$ relationship;
Calculate background time, Tb, from $F^{-1} = Tp + Tb$;
Calculate background current, Ib, from
$\bar{I} = F\,(IpTp + IbTb)$.

With this approach precise control of metal transfer over a wide range of mean current values can be achieved. Accordingly the pulse control logic of the GEC M450PS power source was modified to maintain Ip and Tp constant and allow Ib and Tb to vary with mean current, as dictated by the solutions to the above equations, and pulse parameters were determined in this way for the remainder of the investigation.

For stable arcing, the burn-off rate established by the selected pulse parameters must now be matched to the wire-feed speed. Halmoy (21) proposed an experimental relationship between burn-off rate, W, arc current, I, and electrical stick-out, L, in steady dc welding, which can be written as

$$W = \alpha I + \beta L I^2$$

where α is a factor accounting for localized arc heating at the wire tip and β is a factor describing the distributed resistance heating along the wire length. Allum (5) and Quintino and Allum (10) adapted this approach to pulsed current situations as follows.

If W(t) is the instantaneous burn-off rate, then the average burn-off rate W can be expressed as

$$W = \int_{\text{cycle}} W(t)dt$$

For a square-wave current, this can be written as

$$W = (W_pT_p + W_bT_b)F \tag{1}$$

where W_p and W_b are the wire melting rates for peak and background conditions, respectively.

From Halmoy's relationship, the two melting rates can be expressed as

$$W_p = \alpha I_p + \beta L I^2_p$$

and

$$W_b = \alpha I_b + \beta L I^2_b$$

Substituting in (1) and rearranging

$$W = [(I_pT_p + I_bT_b)\alpha + (I^2_pT_p + I^2_bT_b)\beta L]F \tag{2}$$

Now $\bar{I} = (I_pT_p + I_bT_b)F$ (3)

where $\bar{I}$ is the mean current.

Substituting (3) in (2)

$$W = \alpha\bar{I} + \beta LF(I^2_pT_p + I^2_bT_b) \tag{4}$$

At this point, Allum makes the approximation that Ohmic heating during the background period is negligible compared with that during the peak

$$\text{i.e.} \quad I_p^2 T_p \gg I_b^2 T_b$$

Equation (4) then becomes

$$W = \alpha \bar{I} + \beta L I_p^2 T_p F \qquad (5)$$

Using this equation, for 1.2 mm wire, Allum found mean values for α and β of 0.27 mm $A^{-1}s^{-1}$ and 5.93×10^{-5} $A^{-2}s^{-1}$, respectively. The approximation does not appear justified for the present work, however, since $I_b^2 T_b$ is a significant fraction of $I_p^2 T_p$ at the higher mean currents. The burn-off results presented in Fig. 19 have been replotted as a function of electrode extension, L, in Fig. 46. α and β values were then calculated using equation (4); the results are shown in Table 58. While α values were reasonably constant, in the range of 0.34 - 0.44 mm $A^{-1}s^{-1}$ for all four gases, β appeared to show a systematic increase with increasing mean current. An explanation of this observation may be sought in the work of Halmoy, who showed that, for direct current welding, the burn-off relationships deviated from linearity at low values of electrical extension, and that this deviation began at progressively longer stick-out as the current decreased (Fig. 47). While one of the probable causes cited for the breakdown in linearity (a change in metal transfer mode) is clearly not operative in the present case, it does seem likely that some of the burn-off data from which slopes were empirically determined (Fig. 46) lay below the true linear region; this effect would increase with decreasing mean current. This suggestion is consistent with the fact that Halmoy's results, for 1.2 mm diameter C-Mn-Si wire under Ar-2O_2, lead to a value for β of $6.64 \times 10^{-5}\ A^{-2}s^{-1}$, somewhat above the range determined in the present work for the highest currents. The main practical outcome of these observations is to suggest caution in the use of analytical relationships for burn-off rate which assume constant values of α and β for a given wire diameter; the direct use of experimental burn-off relationships is to be preferred.

Returning to equation (4), it is clear that, in general, W is not a linear function of $\bar{I}$ at constant stick-out even when F is made proportional to $\bar{I}$ since, with I^2pTp constant, Ib and Tb must change to accommodate the desired value of $\bar{I}$; in practice, I^2bTb will be a significant fraction of the total Ohmic heating term at all but the lowest mean currents. The resulting non-linearity will be accentuated by the observed dependence of β on mean current within the range studied, and will increase with increasing stick-out. Some of these trends are apparent in the curves of Figs. 18 and 19, and again emphasize the advisability of using experimental burn-off relationships for the establishment of welding parameters.

Allum has pointed out the desirability of maintaining a constant nominal droplet volume, ϕ, such that the droplet diameter is close to that of the wire; for one droplet per pulse

$$\phi = WA/F \qquad (6)$$

where A is the wire cross-sectional area.

By substituting this expression in the simplified equation (5), he demonstrates that droplet volume will remain constant, for a given wire-size, stick-out and I^2pTp, if frequency is made proportional to $\bar{I}$. In reality, as Smati points out (13), and as can be seen by substituting (6) in (4) rather than in (5), droplet size will still be a function of background parameters. Nevertheless, the use of a fixed ratio of frequency to mean current will minimize variations in droplet size, since, with Ip and Tp fixed, Ib is itself a function of $\bar{I}/F$. The optimum value of this ratio was originally arrived at on an experimental basis (10); as an example, Tables 4 and 5 illustrate that when $\bar{I}/F$ is close to 2, the droplet and wire diameter are coincident. This provides a rationale for the $\bar{I}/F$ relationship which has been employed throughout the present work, though the extent of variations in droplet size which can be tolerated is not known in detail. This factor may need to be pursued further, since a number of commercial pulsed GMAW power supplies, especially those that modulate mean current through frequency in response to a voltage error signal, maintain constant values not only of Ip and Tp but also of Ib; only Tb varies with mean current. With such machines, droplet detachment can be controlled over a range of mean current as long as Ip and Tp can be accurately programmed to meet the relationships which have been discussed. However, the background current is typically fixed between 30 and 60 A. A consideration of the frequency/mean current relationship for such a power source, together with Equation (6), reveals that droplet sizes smaller than any observed in the present work will be reached as the mean current is increased, within a practical range. Though the video recordings corresponding to Table 5, where droplet diameter varied from 0.9 to 1.3 mm, did not reveal any differences in metal transfer characteristics, it would be necessary to investigate further before concluding that power sources with fixed levels of background current will perform satisfactorily over a wide range of mean current.

Equations (4) or (5) should be used with caution for the calculation of deposition rates, since, for a significant range of practical welding conditions, β may not be constant. If appropriate values for α and β are available, the deposition rate $\dot{m}$ can be calculated by substituting from equation (4) or (5) into

$$\dot{m} = WA\rho$$

where ρ is the density of the wire (7.9×10^{-6} kg/mm^2 for steel).

Except for the influence of mean current/travel speed, which has already been well documented by Allum and Quintino (15), the only variable to have a pronounced effect on fusion characteristics was shielding gas. The few results obtained gave only an indication of what might be achieved through manipulation of shielding gas composition. Additions of helium to Ar-CO_2 mixtures allow the CO_2 content, and therefore, the oxygen potential of the shielding gas, to be reduced without detriment to fusion characteristics. A small addition of hydrogen reduces the tendency for asymmetrical finger penetration, observed in this and other investigations (14) with the pulsed GMAW process. A more detailed and systematic study is required to identify argon-helium-carbon dioxide (and, possibly, oxygen) -hydrogen shielding gas mixtures, for specific production applications, which optimize both metal transfer and fusion characteristics, and thereby reduce the tendency for lack-of-fusion defects.

Up to this point in the program, only bead-on-plate welds had been attempted with the GEC M450PS, with the constant current power source providing a high degree of stability and reproducibility for such a series of controlled experiments. However, for the development of practical welding procedures in groove geometries, some form of arc voltage compensation proved essential to avoid process instabilities as the arc impinged on the sidewalls. As mentioned earlier, it is possible to control arc length under conditions of constant current by modulating wire feed in response to a voltage error signal, but this method could not be made to provide a stable response to arc length changes for the all-positional welding application under investigation. The method adopted, whereby mean current was modulated by varying pulse frequency in response to a voltage error signal, represents not only a compromise in constant current/constant voltage power output characteristics but also in terms of arc stability and metal transfer; drop size is no longer tightly controlled, as a result of the concomitant fluctuations in background time. In point of fact, frequency variations with arc voltage compensation, monitored during vertical welding at 150 A nominal mean current, did not exceed 15 Hz (ranging from 75 Hz at the centre of the weld preparation to 90 Hz at the sidewall); the small change which this represents in background time (10.3 ms to 8.1 ms) would not, from the results presented in Table 4, be expected to influence drop size to any measurable extent. This method of arc voltage compensation has the added benefit that mean current is somewhat increased (from 150 A to 162 A) as the arc hits the sidewall, with the potential for improved fusion characteristics.

The compensation loop worked well, in conjunction with the pulse parameters selected, to aid procedure development and facilitate production of the 1067 mm O.D., 30 mm W.T. girth weld and the 30 mm thick Lloyds LT60 test panels for metallurgical evaluation. It is significant to note that, from the results of radiography of all butt welds and from multiple sectioning for metallurgical evaluation of the LT60 test panels, no evidence of lack of fusion at the sidewall or between passes was detected.

The procedures developed for the various welding positions were designed to maximize productivity, while controlling sidewall and inter-run fusion, by adopting wire feed speeds at the high end of the parameter envelope and travel speeds to maintain the arc at the leading edge of the weld pool. No attempt was made either to limit heat input or maintain a constant heat input through the thickness of the joint. In addition, welding parameters for the girth weld were chosen to maximize productivity while remaining suitable for completing the whole circumference in the 5G position.

As expected, mechanized pulsed GMAW showed a significant productivity advantage when compared with the SMAW process. The joint completion time for the girth weld in 1067 mm O.D., 30 mm W.T. pipe was approximately 50% less than that for a comparable shielded metal arc weld using basic electrodes. This worthwhile increase in productivity could be further improved by the adoption of reduced-gap joint designs. This would entail an alternative to the SMAW process for the root bead. Although it is beyond the scope of the present investigation, the development of procedures and techniques for the deposition of full penetration root beads in all positions with the pulsed GMAW process would make a further, very significant contribution to improved productivity in practical applications.

The results of the metallurgical evaluation are of interest in making an initial assessment of the potential of the pulsed GMAW process for applications requiring good low-temperature toughness. Examination of the chemical analyses for wire and weld deposits, particularly as regards the less-oxidizable elements such as nickel, suggests an overall level of dilution of ten percent or less. Even the highly oxidisable elements such as titanium and boron appear to be recovered at high (∿ 50%) and reasonably predictable levels. It can be concluded, in general, that pulsed GMAW under gases with low oxygen potential represents a process giving excellent control of weld metal chemical composition, even at heat inputs more typical of high-dilution processes such as SAW. In effect, it should be possible to design weld metal essentially on the basis of wire composition alone, an appropriate inclusion population to balance the transformation behaviour being achieved by a judicious choice of shielding gas.

The anticipated low levels of oxygen were achieved in all the welds, with the gases containing only 2% CO_2 producing a further reduction relative to $95Ar-5CO_2$. At such low oxygen contents, sulphur content can be expected to assume a greater significance in the determination of the overall inclusion population, and in related effects on microstructure and mechanical properties; certainly, there were indications of such effects in the ductility and toughness results observed in the present work. In this context, the balance between chemical composition and heat input will generally need to be re-examined. As an example, a wire which is correctly formulated to give a high percentage of acicular ferrite in the presence of 400-500 ppm oxygen, as might be found in welds made under $80Ar-20CO_2$, might have too high a hardenability when applied at the same heat input, but with a weld metal oxygen content of less than 200 ppm.

A final observation on chemical composition concerns the hydrogen content of the welds made under $87.5Ar-10He-2CO_2-0.5H_2$. No hydrogen determinations were carried out in the present work. Bicknell and Patchett (22), however, found hydrogen contents between 3 and 7 ppm in GMA welds made under short-circuiting conditions with a similar shielding gas containing 1% H_2; this is well within the range normally considered 'low hydrogen'. There was no indication of any tendency towards cracking in any of the welds made under the hydrogen-containing gas in the present work; the only evidence of any potential problem was the occurrence of 'fish-eyes' in tensile testpieces from one weld. Any such tendency may be accentuated by the very low inclusion contents; however, if no other hydrogen-related problems exist, this can be legitimately solved by a hydrogen-removal treatment (23). Certainly, because of the time involved in testpiece preparation, it is not believed that hydrogen had any adverse effect on CTOD results. Thus, if wire composition can be appropriately balanced for the very low inclusion contents of welds made under this gas, there is no reason why its potential benefits as regards fusion characteristics cannot be exploited.

There is relatively little published information with which the tensile properties presented in Table 42 can be compared. Widgery (17,24) considered the effect of chemical composition on the strength and toughness of mild steel welds deposited in the spray mode, at a heat input of 1.6 kJ/mm, under 100% CO_2. The corresponding cooling time from 800-500^{o}C (t(800-500)) would be around 6 s, while in the present work, it would range from 15 to 30 s for the fill region. Widgery found a linear relationship between yield strength and a carbon equivalent expressed as C + Mn/5 + Si/7 + 2Ti. Clearly, neither this carbon equivalent nor the IIW formula used by other investigators as a measure of the yield strength of SAW deposits (18) is appropriate to express the chemical composition of welds in which the levels of both alloying elements and silicon vary quite widely. However, if Widgery's results for Ti-containing welds are plotted in terms of CE_B, they are clearly consistent with those of the present study (Fig. 26). While there are insufficient results to isolate any specific factor for titanium, there is agreement between the present work and that of Widgery regarding its substantial strengthening effect. The essential continuity between Widgery's work and the present results suggests that the faster cooling rate in the former is counterbalanced, in terms of transformation behaviour, by the lower inclusion content in the latter (oxygen contents in the earlier work ranged from 0.029 to 0.067%). This interpretation is also supported by comparison with earlier work by the present authors, on dip-transfer GMAW welds made with heat inputs of $\sim$0.8 kJ/mm (t(800-500) $\sim$4 s) under 100% CO_2. Generally speaking, where direct comparisons are possible for the same wire, the yield strengths observed in the present work were little lower than those observed previously; the oxygen contents in the earlier work ranged from 0.030 - 0.065%.

At oxygen contents typical of welds made under gases containing 20% or more CO_2, little effect of sulphur content is discernible, since overall cleanness is dominated by oxide inclusions. As was mentioned previously, and as Fig. 27 shows, this is no longer the case at oxygen contents below 200 ppm, and the use of low-sulphur wires can lead to worthwhile improvements in tensile ductility. These effects also appear to be reflected in Charpy shelf energy. Even though 100% shear fracture was measured in very few Charpy testpieces, the overall shape of the curves in Figs. 28 to 32, coupled with the shear area figures in Tables 43 - 54, can be used to infer a significant influence of sulphur content on shelf energy.

Overall, it is interesting to compare the Charpy results in Figs. 28 - 32 with those obtained by George et al. (25), who produced welds at 2 kJ/mm under 80Ar-20CO$_2$; t(800-500) would have been approximately 8 s. Impact energies at -45°C ranged from about 25 J, for a titanium-bearing manganese-silicon wire, to almost 80 J, for a 0.54% molybdenum wire. With the exception of the molybdenum-containing deposit, all the remaining welds had impact energies at -45°C between 25 and 40 J. Clearly, the best of the welds in the current study have significantly better toughness, despite the considerably slower cooling conditions. For the most part, this arises from the higher shelf energy associated with the much cleaner welds (oxygen contents in George's work ranged from 0.039 to 0.048%). When the balance of alloying is optimized to produce ideal microstructures, as in the C-Mn-Ti-B deposit, which consists entirely of acicular ferrite, extremely good low-temperature toughness results. On the other hand, some of the current wires are clearly over-alloyed, even for the relatively slow cooling rate associated with this work. An example is the C-Mn-Mo wire, which is quite similar to the one which gave the best toughness in George's work. At the low oxygen level of the present work, the resulting deposit had a very high yield strength, and it can be inferred that this was detrimental to the impact transition temperature. Some regions having a martensitic appearance are visible in the root region of this weld.

As Fig. 31 shows, reducing oxygen content still further has little beneficial effect on the toughness of C-Mn-Si welds. In fact, as can be seen from Figs. 34, 42, and 44, the presence of ferrite with aligned second phase is, if anything, accentuated in these welds. In the case of the C-Mn-Ti-B welds made under the less-oxidizing gases, it is clear that the ideal transformation characteristics observed in 95Ar-5CO_2 have been disturbed. Specifically, regions of ferrite with aligned second phase appear in both these welds (Figs. 43 and 45), suggesting that the overall inclusion population is no longer adequate for the consistent nucleation of acicular ferrite. This microstructural change is reflected in the significant deterioration in Charpy transition temperature which is seen in Fig. 32.

As a whole, the Charpy results, taken together with the metallographic observations, emphasize both the opportunity and the need to optimize wire and gas compositions in pulsed GMAW, so as to produce ideal microstructures at very high levels of weld-metal purity. Only a limited, qualitative microstructural analysis was possible within the scope of the present program; a more exhaustive optimization of consumable compositions should take as its starting point a detailed consideration of the balance between weld-metal inclusion content, chemical composition and transformation behaviour.

The CTOD results obtained in the present work can be compared with those presented in a previous report on flux-cored arc welding for Arctic and offshore service (3). The values observed can be measured against the same general criterion (0.20-0.25 mm at service temperature). In the few instances in which failures occurred close to maximum load, it was apparent that the resistance to ductile tearing was much higher than in the previous work, reflecting the much-improved weld metal cleanness. With few exceptions, however, the overall CTOD transition temperatures were high, resulting in essentially-brittle behaviour at -45°C. As has been mentioned earlier, fracture initiation was usually controlled by the behaviour of the root region. While the limited number of welds made with alternative root pass techniques did not show any consistent improvement in CTOD, by systematic optimization of weld metal microstructure and welding procedure it should be possible to obtain reliably CTOD values over 0.2 mm at -45°C using the pulsed GMAW process. The C-Mn-Ti-B and C-Mn-Si-Ti wires would appear to represent the most suitable starting point for such an exercise.

7.0 CONCLUSIONS

A detailed investigation into the process characteristics of the pulsed GMAW process has been carried out. All-position, mechanized welding procedures have been developed, and the metallurgical characteristics of pulsed gas metal arc welds made with eight 1.2 mm diameter wires and three shielding gases of low oxygen potential have been evaluated. The following are the principal conclusions.

1. Pulse peak parameters governing the onset of one drop per pulse metal transfer essentially followed the hyperbolic relationship Ip^nTp = const. proposed by previous workers. Detailed analysis of metal transfer using a high-speed video system showed that the range of Tp over which these conditions were maintained was narrower than had previously been supposed, less than 1 ms at a peak current of 350 A.

2. Pulse peak parameters for one drop per pulse metal transfer can vary with wire and gas composition, so that power sources with a fixed pulse structure for a given diameter and general category of wire may not allow a full range of consumables to be exploited.

3. The relationship betwen burn-off rate and mean current is not strictly linear, since the Ohmic heating effect of the background current is not negligible. This non-linearity is accentuated as electrical stick-out is increased.

4. Changes in droplet size in the range 0.9 - 1.3 mm, brought about by changes in background conditions, had no discernible effect on metal transfer. However, it is not clear that changes outside this range would be acceptable, and this may impose limitations on the application of power sources with fixed background current.

5. Fusion characteristics were somewhat affected by gas composition, but the effect of mean current was dominant. Depth of penetration and dilution were increased when welding under $95Ar-5CO_2$, $88Ar-10He-2CO_2$ and $87.5Ar-10He-2CO_2-0.5H_2$, relative to $80Ar-20CO_2$. The hydrogen-containing shielding gas appeared to eliminate lateral 'wandering' of the central, finger penetration. All groove welds were made with the first three shielding gases, and no indication of fusion defects at the sidewall or between runs was detected.

6. In order to maintain stable arcing in a groove, it was necessary to modify the constant-current characteristics of the GEC M450PS power source using a frequency-modulated arc voltage control system. In this way, very stable arc behaviour and excellent sidewall fusion was obtained. The resulting, small change in pulse structure and mean current had no detrimental effect on metal transfer.

7. Procedures were developed for welding plate in the vertical up, flat and 45-degree overhead positions, and for completing pipe girth welds in the fixed, 5G position. Mean currents as high as 200 A could be used in the flat position, but mean current was limited to 150-160 A in other positions. Heat inputs were in the range 2-5 kJ/mm, allowing a girth weld in 30 mm wall thickness pipe with a 60^o included angle, single-Vee preparation, to be completed in nine passes. Very significant productivity improvements were achieved, relative to the SMAW process; these could be enhanced by the use of a reduced gap joint design, to which the pulsed GMAW process lends itself.

8. Welds were completed in 30 mm LT60 plate for metallurgical evaluation using eight wires under $95Ar-5CO_2$ and two wires under $88Ar-10He-2CO_2$ and $87.5Ar-10He-2CO_2-0.5H_2$. Oxygen contents were uniformly low (200 ppm or less) under $95Ar-5CO_2$ shielding, and were further reduced by the use of the other two gases. Presumably as a result of the effect of the low inclusion content on transformation characteristics, yield strengths were relatively high despite heat inputs reaching 5 kJ/mm. The titanium-containing deposits had higher strength than did the titanium-free deposits; in general, their ductility was also better, though this could be largely related to the fact that they also, in general, had lower sulphur contents. Excellent Charpy toughness was obtained in the best of these welds. In particular, a C-Mn-Ti-B wire welded under $95Ar-5CO_2$ gave a mean Charpy energy of 99 J at -60^oC.

Metallographic examination confirmed that this weld had an ideal microstructure, consisting entirely of fine, acicular ferrite. Most of the other welds showed greater or lesser amounts of ferrite with aligned second phase and/or of primary ferrite, which are both detrimental to low-temperature toughness. The less-oxidizing gases produced little improvement in the toughness of welds made with a C-Mn-Si wire, and a serious deterioration in that of welds made with the C-Mn-Ti-B wire. Overall, the Charpy and metallographic results confirmed the need for a careful balance between chemical composition and inclusion population when using gases of low oxygen potential. On the other hand, the low dilution and consistent recovery of even the easily oxidized elements considerably simplifies the precise design of weld metal chemical composition.

9. Generally speaking, the CTOD toughness achieved in the LT60 test panels at -45°C was poor, with only the best of the wires in 95Ar-5CO_2 giving encouraging values. Fracture initiation was invariably from the root region, suggesting that the root completion procedure initially adopted was compromising the overall CTOD values. A limited trial of alternative root-pass techniques produced encouraging CTOD results, though in no case were they consistently above the 0.2 mm level which is the minimum that would be needed for service in the as-welded condition. Nevertheless, it is

believed that a careful optimization of welding procedure, based on the most promising consumables, would allow this goal to be reached.

10. As an overall conclusion, mechanized, pulsed GMAW, with appropriately chosen pulse parameters, represents a high-quality, high-productivity process with unusually broad scope for metallurgical optimization through the judicious choice of wire and shielding gas. It is considered that this approach currently constitutes the most promising avenue for the development of a high-productivity welding technique for exacting, low-temperature service.

ACKNOWLEDGEMENTS

This work was partially funded by the Physical Metallurgy Research Laboratories, CANMET, Energy Mines and Resources Canada, under Supply and Services Canada Contract OSQ84-00042. Lloyds LT60 material, also produced under a CANMET program, was supplied by the Algoma Steel Corporation. Thanks are due to CRC-Evans Automatic Welding for the loan of the M-200 welding machine.

Any data presented, opinions, findings, conclusions or recommendations expressed in this report are those of the authors, and do not necessarily reflect the views of CANMET.

Crown copyright of this report is reserved.

REFERENCES

1. H. C. Cotton: Welded Steel for Offshore Construction. Proc. Inst. Mech. E., 1979, 193(26).

2. J. M. Cameron: An Overview of Welding Cost Factors in Shipbuilding. Conference on Welding in Shipbuilding, 1984, Norfolk, VA.

3. D. V. Dorling, R. M. Huntley and A. B. Rothwell: Development of All-Position, Mechanized and Automatic FCAW Systems for the Fabrication of Offshore Structures and Arctic Vessels. Final Report to CANMET on Jointly-Funded Project under DSS Contract OSQ82-00250, July 1984.

4. A. B. Rothwell and D. V. Dorling: The Toughness Properties of Girth Welds in Modern Pipeline Steels. In "HSLA Steels; Technology and Applications", p. 943. American Society for Metals, Metals Park, OH, 1984.

5. C. J. Allum: MIG Welding - Time for Reassessment. Metal Construction, 1983, 15 No 6, 347.

6. R. I. Coote and M. P. Fingerhut: Ultrasonic Inspection of Girth Welds. Proc. Int. Conf. on Pipeline Inspection, p. 263. CANMET, Ottawa, 1983.

7. D. V. Dorling and A. B. Rothwell: The Toughness of Mechanized Gas Metal Arc Welds. Proc. Conf. "Welding in Energy-Related Projects", p. 379. Pergamon, Toronto, 1984.

8. A. Ditschun, B. Zajaczkowski and D. V. Dorling: Pulsed FM-GMA Welding. Proc. WIC/ASM Conf. "Welding for Challenging Environments", p. 21. Pergamon, Toronto, 1986.

9. M. Amin: Pulse Current Parameters for Arc Stability and Controlled Metal Transfer. Metal Construction, 1983, 15 No 5, 272.

10. L. Quintino and C. J. Allum: Pulsed GMAW: Interactions Between Process Parameters, Parts 1 and 2. Welding and Metal Fabrication, 1984, 52 Nos 2 and 3, 85 and 126.

11. M. Amin: Synergic Pulse MIG Welding. Metal Construction, 1981, 13 No 6, 349.

12. R. M. Huntley, D. V. Dorling and A. B. Rothwell: Pipeline Girth Welding Using the Flux-Cored Arc Welding Process. Proc. Conf. "Welding in Energy-Related Projects", p. 85. Pergamon, Toronto, 1984.

13. Z. Smati: Automatic Pulsed MIG Welding. Metal Construction, 1986, 18 No 1, 38R.

14. A. C. Bicknell and B. M. Patchett: Pulsed GMA Welding: Shielding Gas Effects on Fusion Characteristics. University of Alberta, Department of Mineral Engineering. Unpublished Report, 1984.

15. C. J. Allum and L. Quintino: Control of Fusion Characteristics in Pulsed Current MIG Welding. Metal Construction, 1985, 17 Nos 4 & 5, 242R and 314R.

16. K. Lorenz and C. Düren: Evaluation of Large-Diameter Pipe Steel Weldability by Means of the Carbon Equivalent. Proc. Conf. "Steels for Line-Pipe and Pipeline Fittings", p. 322. The Metals Society, London, 1983.

17. D. J. Widgery: Deoxidation Practice and Toughness of Mild Steel Weld Metal. The Welding Institute, Research Report M/76/73, 1973.

18. N. Bailey: The Influence of Flux Type on the Strength and Toughness of Submerged-Arc Weld Metal. The Welding Institute, Research Report 152, 1981.

19. R. E. Dolby: Charpy-V and COD - Correlations Between Test Data for Ferritic Weld Metals. Metal Construction, 1981, 13 No 1, 43.

20. Jilong Ma and R. L. Apps: MIG Transfer Discovery of Importance to Industry. Welding and Metal Fabrication, 1982, 50 No 9, 307.

21. E. Halmoy: Wire Melting Rate, Droplet Temperature, and Effective Anode Melting Potential. Proc. Conf. "Arc Physics and Weld Pool Behaviour", p. 49. The Welding Institute, Abington, 1979.

22. A. C. Bicknell and B. M. Patchett: Field Welding Procedures for Welding RE-Treated Linepipe with the GMAW-S Process. Report L51485, American Gas Association, Arlington VA, 1984.

23. R. B. G. Yeo and J. Clark: Fisheyes in Procedure Tension Tests. Metal Construction, 1986, 18 No 6, 377.

24. D. J. Widgery: Deoxidation Practice and Toughness of Mild Steel Weld Metal - Report 2. The Welding Institute, Report M/78/74, 1974.

25. M. J. George, J. R. Still and P. Terry: Gas Metal Arc Welds for High Toughness Applications - Microstructural and Other Factors. Metal Construction, 1981, 13 No 12, 730.

TABLE 1

CHEMICAL COMPOSITION OF LT60 STEEL USED FOR TEST PANELS

C	Mn	P	S	Si	Ni	Cr	Mo	Cu	Al	V	Nb
.07	1.33	.005	.005	.28	.25	.28	.01	.02	.043	.062	.019

TABLE 2

CHEMICAL COMPOSITION OF ELECTRODE WIRES

Electrode	C	Mn	P	S	Si	Ni	Cr	Mo	Cu	Ti	Al	V	Nb	B	Zr
C-Mn-Si	.09	1.58	.010	.015	.77	.02	.02	.01	.15	<.005	<.005	<.005	<.005	<.0005	<.005
LowC-Mn-Si	.05	1.52	.016	.020	.76	.03	.04	.01	.07	<.005	<.005	<.005	.006	<.0005	<.005
C-Mn-Si-Ti	.08	1.59	.010	.009	.74	.02	.06	.01	.06	.034	<.005	<.005	<.005	<.0005	<.005
C-Mn-Ti-B	.07	1.82	.010	.005	.39	.06	.14	.01	.20	.078	<.005	.005	<.005	.0056	<.005
C-Mn-Ni	.10	1.25	.008	.008	.58	1.45	.12	.01	.07	<.005	.005	<.005	.006	<.0005	<.005
C-Mn-Ni-Ti	.11	1.19	.005	.007	.53	1.31	.05	<.01	.07	.092	<.005	<.005	<.005	<.0005	<.005
C-Mn-Mo	.12	1.91	.016	.022	.60	.14	.12	.55	.43	.010	<.005	.009	.005	<.0005	<.005
C-Mn-Mo-Ti	.06	1.92	.008	.012	.58	.03	.13	.16	.25	.19	<.005	.008	.007	<.0005	<.005

TABLE 3

WELDING PARAMETERS CORRESPONDING TO FIGURE 17

Ip A	Tp ms	Ib A	Tb ms	F Hz	$\bar{I}$ A	Wire Feed m/min
350	2	115	11.3	75	150	4.0
350	3	92	10.3	75	150	4.2
350	4	65	9.3	75	150	4.3

TABLE 4

EFFECT OF F/$\bar{I}$ RELATIONSHIP ON DROP DIAMETER

Ip A	Tp ms	Ib A	Tb ms	F Hz	$\bar{I}$ A	Wire Feed m/min	Drop Diameter mm
350	3	92	10.3	75	150	4.2	1.2
350	3	76	8.1	90	150	4.4	1.2

TABLE 5

EFFECT OF BACKGROUND CURRENT ON DROP DIAMETER

Ip A	Tp ms	Ib A	Tb ms	F Hz	$\bar{I}$ A	Wire Feed m/min	Drop Diameter mm
350	3	120	10.3	75	171	5.0	1.3
350	3	80	10.3	75	141	4.1	1.2
350	3	60	10.3	75	125	3.8	1.1
350	3	40	10.3	75	110	3.3	0.9

TABLE 6

WELD BEAD PROFILE MEASUREMENTS FOR BEAD-ON-PLATE DEPOSITS IN 95Ar-5CO_2 SHIELDING GAS

Electrode	Mean Current A	Bead Height mm	Bead Width mm	Penetration mm	Wetting Angle o	Dilution %
C-Mn-Si	150	3.6	9.8	2.5	71	30
LowC-Mn-Si	100	3.8	9.3	1.4	81	12
	150	3.7	10.5	2.2	62	28
	200	3.1	11.5	2.7	50	29
C-Mn-Si-Ti	100	3.2	9.4	1.5	69	19
	150	3.2	10.7	2.3	64	29
	200	2.8	11.2	3.0	44	39
C-Mn-Ti-B	150	2.9	10.4	2.1	46	29
C-Mn-Ni	100	3.3	7.7	1.4	75	13
	150	3.5	10.9	2.7	57	26
	200	3.0	12.9	2.8	37	30
C-Mn-Ni-Ti	150	3.1	9.0	2.5	73	33
C-Mn-Mo	100	3.5	9.7	1.2	68	15
	150	3.4	9.9	2.3	63	31
	200	2.9	11.8	2.6	49	35
C-Mn-Mo-Ti	150	2.9	10.4	1.8	52	30

TABLE 7

WELD BEAD PROFILE MEASUREMENTS FOR BEAD-ON-PLATE DEPOSITS WITH C-Mn-Mo WIRE

Shielding Gas	Mean Current A	Bead Height mm	Bead Width mm	Penetration mm	Wetting Angle o	Dilution %
95Ar-5CO_2	150	3.4	9.9	2.3	63	31
80Ar-5CO_2	150	3.4	11.3	1.6	53	24
88Ar-10He-2CO_2	150	3.2	8.7	2.0	55	33
87.5Ar-10He-2CO_2-0.5H_2	150	3.4	9.0	2.3	68	32

TABLE 8

TEST PANEL WELDING PROCEDURE IN THE VERTICAL UP (3G) POSITION

Wire Diameter and Type:	1.2 mm Linde HI-84
Shielding Gas:	95Ar-5CO$_2$
Power Source:	GEC M450 PS
Plate Thickness and Type:	30 mm Mild Steel

Joint/Preparation Details

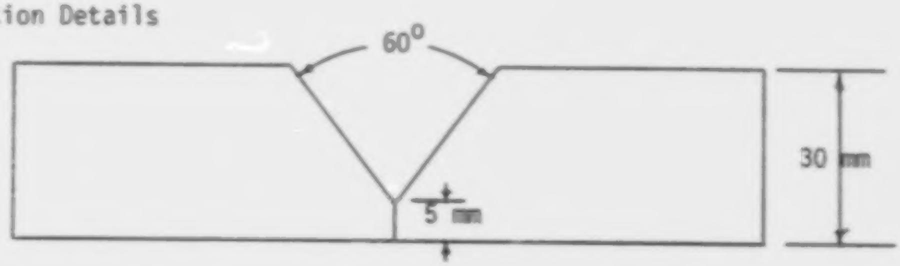

Welding Parameters

Pass	Wire Feed Speed (mm/min)	Travel (mm/min)	Oscillation Width (mm)	Oscillation Velocity (mm/s)	Stickout (mm)	Dwell L (s)	Dwell R (s)	Arc Voltage (V)	Mean Current (A)
1	4267	38	8	112	12.7	0.2	0.2	21.7	160
2	4013	38	13	81	12.7	0.6	0.6	21.6	150
3	4013	76	11	91	12.7	0.9	0.0	21.6	150
4	4013	64	11	81	12.7	0.4	0.8	21.6	150
5	4013	51	11	81	12.7	0.9	0.0	21.6	150
6	4013	38	14	81	12.7	0.4	0.8	21.6	150
7	4013	38	12	81	12.7	0.9	0.0	21.6	150
8	4013	38	12	81	12.7	0.9	0.9	21.6	150
9	4013	140	6	102	12.7	1.0	1.0	21.6	150

Pulse Parameters

Mean Current A	Peak Current A	Time at Peak ms	Background Current A	Frequency Hz
160	350	3	100	80
150	350	3	92	75

Bead Placement

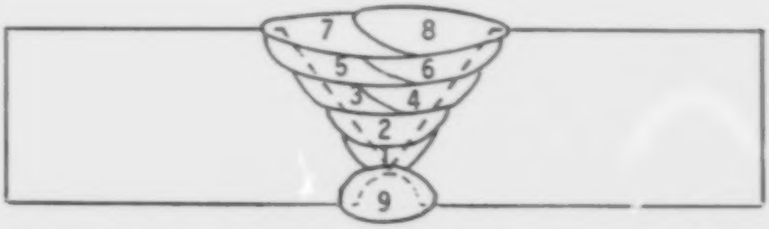

TABLE 9

TEST PANEL WELDING PROCEDURE IN THE 45° OVERHEAD (4G) POSITION

Wire Diameter and Type:	1.2 mm Linde HI-84
Shielding Gas:	95Ar-5CO$_2$
Power Source:	GEC M450 PS
Plate Thickness and Type:	30 mm Mild Steel

Joint/Preparation Details

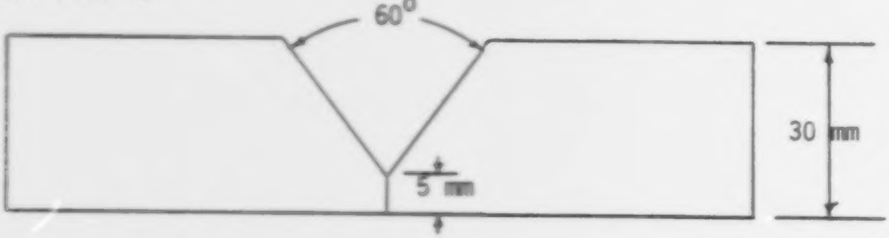

Welding Parameters

Pass	Wire Feed Speed (mm/min)	Travel (mm/min)	Oscillation Width (mm)	Oscillation Velocity (mm/s)	Stickout (mm)	Dwell L (s)	Dwell R (s)	Arc Voltage (V)	Mean Current (A)
1	4267	38	8	112	12.7	0.2	0.2	21.7	160
2	4013	38	13	81	12.7	0.6	0.6	21.6	150
3	4013	76	11	91	12.7	0.9	0.0	21.6	150
4	4013	64	11	81	12.7	0.4	0.8	21.6	150
5	4013	51	11	81	12.7	0.9	0.0	21.6	150
6	4013	38	14	81	12.7	0.4	0.8	21.6	150
7	4013	38	12	81	12.7	0.9	0.0	21.6	150
8	4013	38	12	81	12.7	0.9	0.9	21.6	150
9	4013	140	6	102	12.7	1.0	1.0	21.6	150

Pulse Parameters

Mean Current A	Peak Current A	Time at Peak ms	Background Current A	Frequency Hz
160	350	3	100	80
150	350	3	92	75

Bead Placement

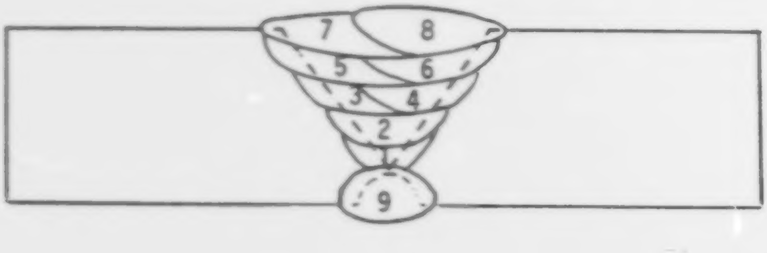

TABLE 10

TEST PANEL WELDING PROCEDURE IN THE FLAT (1G) POSITION

Wire Diameter and Type:	1.2 mm Linde HI-84
Shielding Gas:	95Ar-5CO_2
Power Source:	GEC M450 PS
Pipe Material:	30 mm Lloyds LT60

Joint/Preparation Details

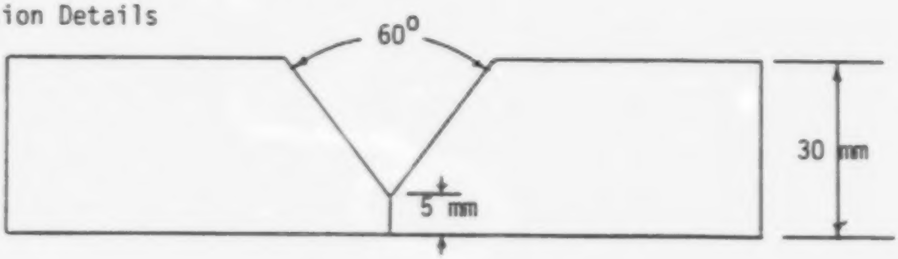

Welding Parameters

Pass	Wire Feed Speed (mm/min)	Travel (mm/min)	Oscillation Width (mm)	Oscillation Velocity (mm/s)	Stickout (mm)	Dwell L (s)	Dwell R (s)	Arc Voltage (V)	Mean Current (A)
1	5334	64	0	0	12.7	0		21.0	200
2	5334	64	8	112	12.7	0.1	0.1	21.0	200
3	5334	51	11	112	12.7	0.2	0.2	21.0	200
4	5334	51	16	102	12.7	0.2	0.2	21.0	200
5	4800	64	11	112	12.7	1.0	0.0	21.5	180
6	4800	76	11	112	12.7	0.2	1.0	21.5	180
7	4800	140	0	0	12.7	0.2	0.2	21.0	180

Pulse Parameters

Mean Current A	Peak Current A	Time at Peak ms	Background Current A	Frequency Hz
200	350	3	136	100
180	350	3	117	90

Bead Placement

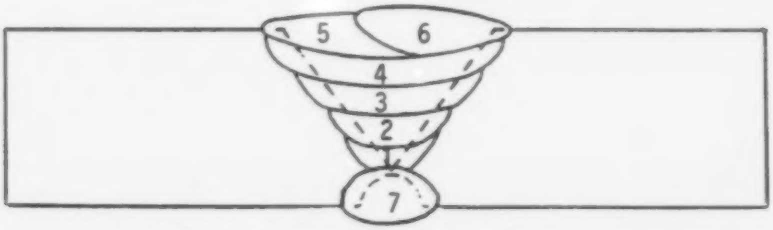

TABLE 11

GIRTH WELDING PROCEDURE

Wire Diameter and Type: 3.2 mm Lincoln 70+/1.2 mm LINDE HI-84
Shielding Gas: 95Ar-5CO$_2$
Power Source: GEC M450 PS
Pipe Material: 1067 mm O.D., 30 mmm W.T., CSA Z245.2, Gr. 414 MPa

Joint/Preparation Details

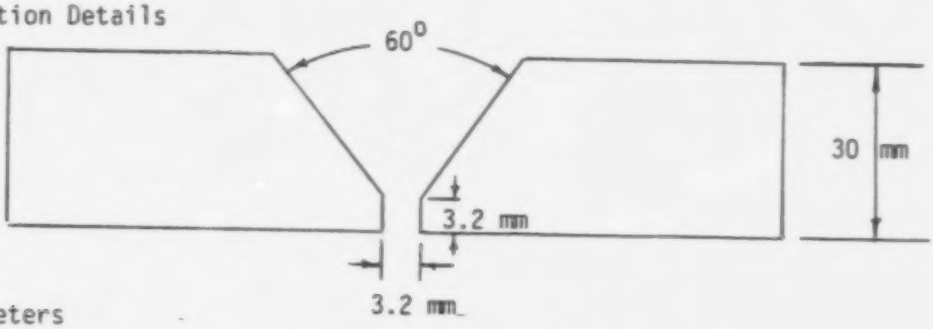

Welding Parameters

Pass	Wire Feed Speed (mm/min)	Travel (mm/min)	Oscillation Width (mm)	Oscillation Velocity (mm/s)	Stickout (mm)	Dwell L (s)	Dwell R (s)	Arc Voltage (V)	Mean Current (A)
1	N/A	76	N/A	N/A	N/A	N/A		24.0	85
2	4724	102	8	121	12.7	0.6	0.6	21.7	160
3	4572	64	13	81	12.7	0.6	0.6	21.6	150
4	4572	76	11	91	12.7	0.9	0.0	21.6	150
5	4572	76	11	81	12.7	0.4	0.8	21.6	150
6	4394	64-76	13	81	12.7	1.0	1.0	20.4	150
7	4318	38	12	81	12.7	0.4	0.4	20.0	150
8	4318	38-64	12	81	12.7	1.0	1.0	20.0	150
9	4318	38	15	81	12.7	1.0	1.0	20.0	150

Pulse Parameters

Mean Current A	Peak Current A	Time at Peak ms	Background Current A	Frequency Hz
160	350	3	100	80
150	350	3	92	75

Bead Placement

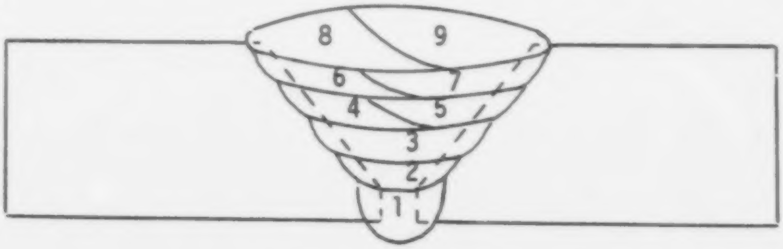

TABLE 12

GIRTH WELDING PROCEDURE WITH SMAW ELECTRODES

Wire Diameter and Type: 3.2 mm Lincoln 70+/3.2, 4.0 CLA Atom-Arc 8018N
Power Source: Miller Trailblazer 550
Pipe Material: 1067 mm O.D., 30 mmm W.T., CSA Z245.2, Gr. 414 MPa

Joint/Preparation Details

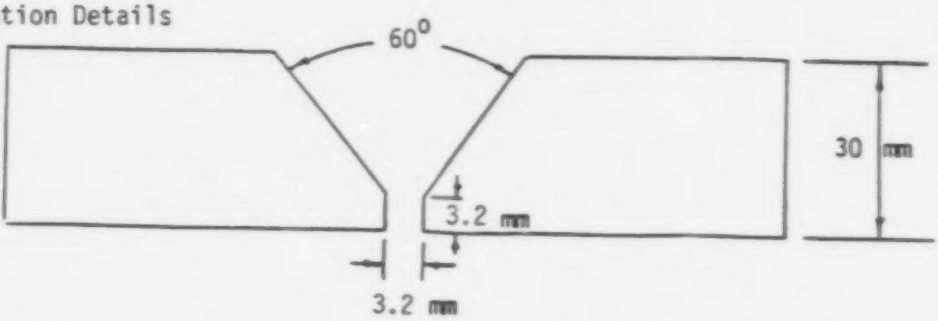

Welding Parameters

Pass	Electrode Size & Classification	Current (A)	Voltage (V)	Travel Speed (mm/min)
1-2	3.2 mm E55010G	85	24.0	76
3	3.2 mm E55018C2	120	24.5	66
4-11	4.0 mm E55018C2	135	26.0	85

Electrode Positive Polarity

Bead Placement

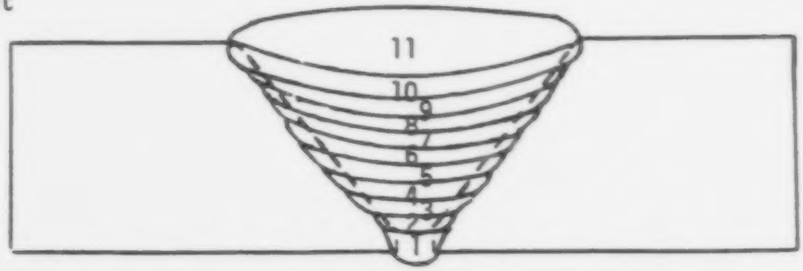

TABLE 13

TEST PANEL WELDING PROCEDURE WITH C-Mn-Si/95Ar-5CO_2

Wire Diameter and Type:	1.2 mm LINCOLN L-56
Shielding Gas:	95Ar-5CO_2
Power Source:	GEC M450 PS
Plate Thickness and Type:	30 mm Lloyds LT-60

Joint/Preparation Details

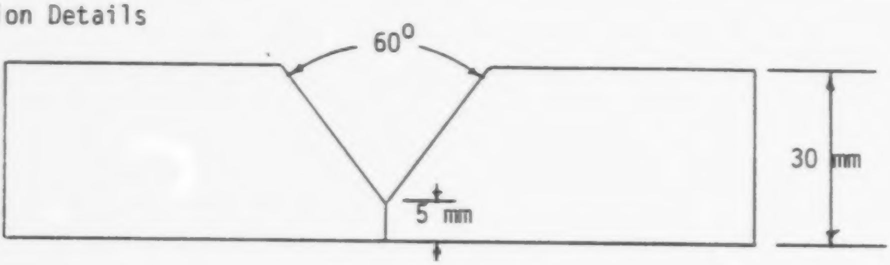

Welding Parameters

Pass	Wire Feed Speed (mm/min)	Travel (mm/min)	Oscillation Width (mm)	Oscillation Velocity (mm/s)	Stickout (mm)	Dwell L (s)	Dwell R (s)	Arc Voltage (V)	Mean Current (A)
1	3937	38	8	112	12.7	0.2	0.2	20.8	160
2	3810	38	13	91	12.7	1.0	1.0	20.4	150
3	3810	76	11	81	12.7	1.0	0.2	20.4	150
4	3810	64	11	91	12.7	1.0	1.0	20.4	150
5	3810	51	12	91	12.7	1.0	1.0	20.4	150
6	3810	51	12	102	12.7	1.0	1.0	20.4	150
7	3810	38	14	91	12.7	1.0	0.6	20.4	150
8	3810	38	16	81	12.7	1.0	1.0	20.4	150
9	3810	102	6	102	12.7	1.0	1.0	20.4	150

Pulse Parameters

Mean Current A	Peak Current A	Time at Peak ms	Background Current A	Frequency Hz
160	350	3	100	80
150	350	3	92	75

Bead Placement

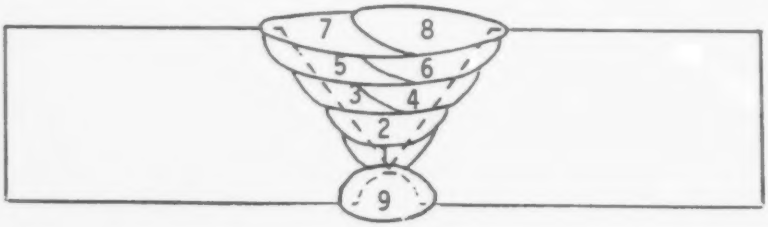

TABLE 14

TEST PANEL WELDING PROCEDURE WITH LOWC-Mn-Si/95Ar-5CO$_2$

Wire Diameter and Type:	1.2 mm Thyssen K-52
Shielding Gas:	95Ar-5CO$_2$
Power Source:	GEC M450 PS
Plate Thickness and Type:	30 mm Lloyds LT-60

Joint/Preparation Details

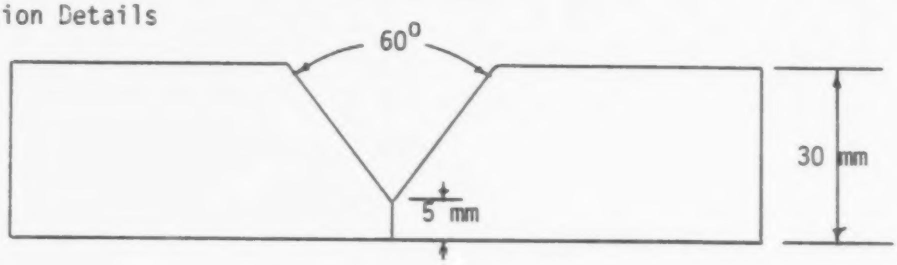

Welding Parameters

Pass	Wire Feed Speed (mm/min)	Travel (mm/min)	Oscillation Width (mm)	Oscillation Velocity (mm/s)	Stickout (mm)	Dwell L (s)	Dwell R (s)	Arc Voltage (V)	Mean Current (A)
1	4064	38	8	112	12.7	0.2	0.2	22.6	160
2	3810	38-64	13	91	12.7	0.6	0.6	22.5	150
3	3810	76	11	81	12.7	1.0	0.0	22.5	150
4	3810	64-76	9	81	12.7	1.0	1.0	22.5	150
5	3810	64	12	81	12.7	1.2	0.4	22.5	150
6	3810	38	12	81	12.7	1.0	1.0	22.5	150
7	3810	38	16	81	12.7	1.0	1.0	22.5	150
8	3810	38-64	12	81	12.7	1.4	0.6	22.5	150
9	3810	102	6	102	12.7	1.0	1.0	22.5	150

Pulse Parameters

Mean Current A	Peak Current A	Time at Peak ms	Background Current A	Frequency Hz
160	350	3	100	80
150	350	3	92	75

Bead Placement

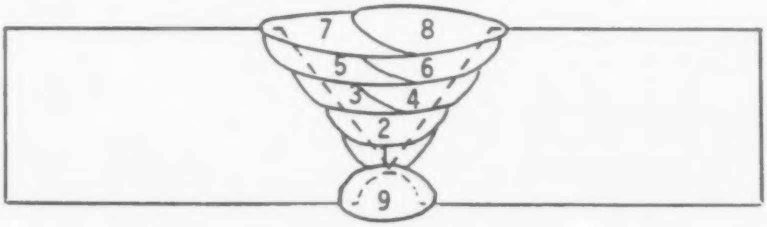

TABLE 15

TEST PANEL WELDING PROCEDURE WITH C-Mn-Si-Ti/95Ar-5CO_2

Wire Diameter and Type:	1.2 mm Thyssen K-NOVA
Shielding Gas:	95Ar-5CO_2
Power Source:	GEC M450 PS
Plate Thickness and Type:	30 mm Lloyds LT-60

Joint/Preparation Details

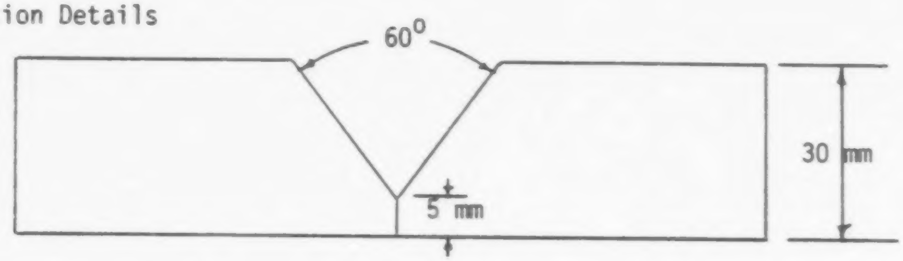

Welding Parameters

Pass	Wire Feed Speed (mm/min)	Travel (mm/min)	Oscillation Width (mm)	Oscillation Velocity (mm/s)	Stickout (mm)	Dwell L (s)	Dwell R (s)	Arc Voltage (V)	Mean Current (A)
1	4267	38	8	112	12.7	0.2	0.2	21.4	160
2	4013	38	13	81	12.7	0.6	0.6	21.2	150
3	4013	76	11	81	12.7	1.0	0.0	21.2	150
4	4013	64	11	81	12.7	1.0	1.0	21.2	150
5	4013	51	12	81	12.7	1.0	0.0	21.2	150
6	4013	38	12	81	12.7	1.0	1.0	21.2	150
7	4013	38	16	81	12.7	1.0	1.0	21.2	150
8	4013	38	16	81	12.7	1.0	1.0	21.2	150
9	4013	102	6	102	12.7	1.0	1.0	21.2	150

Pulse Parameters

Mean Current A	Peak Current A	Time at Peak ms	Background Current A	Frequency Hz
160	350	3	100	80
150	350	3	92	75

Bead Placement

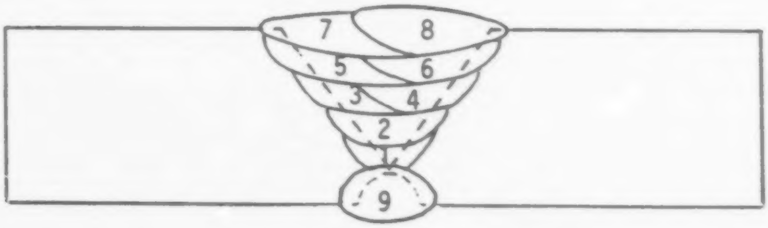

TABLE 16

TEST PANEL WELDING PROCEDURE WITH C-Mn-Ti-B/95Ar-5CO_2

Wire Diameter and Type:	1.2 mm Kobe MGS-50LT
Shielding Gas:	95Ar-5CO_2
Power Source:	GEC M450 PS
Plate Thickness and Type:	30 mm Lloyds LT-60

Joint/Preparation Details

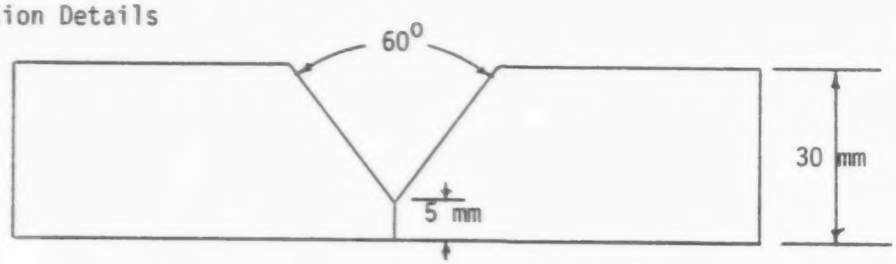

Welding Parameters

Pass	Wire Feed Speed (mm/min)	Travel (mm/min)	Oscillation Width (mm)	Oscillation Velocity (mm/s)	Stickout (mm)	Dwell L (s)	Dwell R (s)	Arc Voltage (V)	Mean Current (A)
1	4064	38	8	112	12.7	0.2	0.2	22.2	160
2	3759	38	13	81	12.7	0.6	0.6	21.6	150
3	3759	76	11	81	12.7	1.0	0.0	21.6	150
4	3759	64	11	81	12.7	0.0	1.0	21.6	150
5	3759	51	12	81	12.7	1.0	0.0	21.6	150
6	3759	51	12	81	12.7	0.8	0.8	21.6	150
7	3759	38	16	81	12.7	1.0	0.0	21.6	150
8	3759	38	16	81	12.7	1.0	1.0	21.6	150
9	3759	140	6	102	12.7	1.0	1.0	21.6	150

Pulse Parameters

Mean Current A	Peak Current A	Time at Peak ms	Background Current A	Frequency Hz
160	350	3	100	80
150	350	3	92	75

Bead Placement

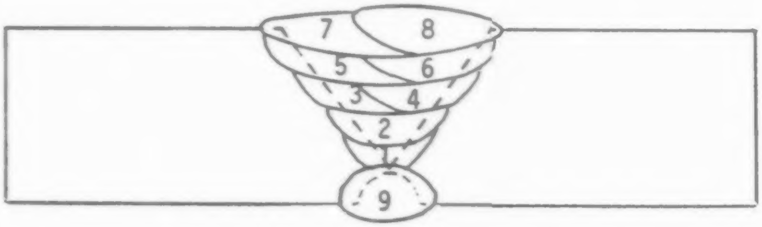

TABLE 17

TEST PANEL WELDING PROCEDURE WITH C-Mn-Ni/95Ar-5CO$_2$

Wire Diameter and Type: 1.2 mm Thyssen K5Ni
Shielding Gas: 95Ar-5CO$_2$
Power Source: GEC M450 PS
Plate Thickness and Type: 30 mm Lloyds LT-60

Joint/Preparation Details

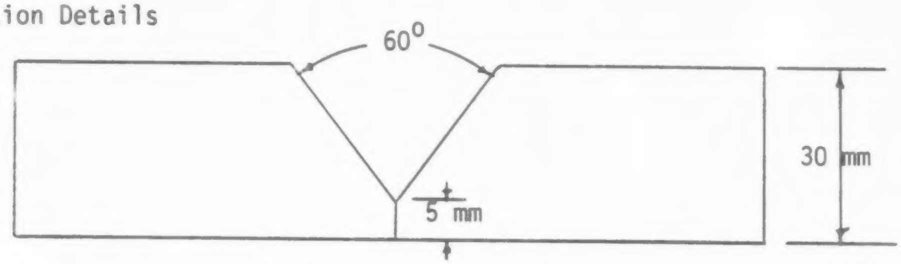

Welding Parameters

Pass	Wire Feed Speed (mm/min)	Travel (mm/min)	Oscillation		Stickout (mm)	Dwell (s)		Arc Voltage (V)	Mean Current (A)
			Width (mm)	Velocity (mm/s)		L	R		
1	4318	38	8	112	12.7	0.2	0.2	22.4	160
2	3861	38	13	81	12.7	0.6	0.6	21.7	150
3	3861	76	11	81	12.7	0.9	0.0	21.7	150
4	3861	64	11	81	12.7	0.4	1.0	21.7	150
5	3861	51	12	81	12.7	0.9	0.0	21.7	150
6	3861	38	14	81	12.7	0.4	0.8	21.7	150
7	3861	38	14	81	12.7	1.0	0.4	21.7	150
8	3861	38	19	81	12.7	1.0	1.0	21.7	150
9	3861	140	6	102	12.7	1.0	1.0	21.7	150

Pulse Parameters

Mean Current A	Peak Current A	Time at Peak ms	Background Current A	Frequency Hz
160	350	3	100	80
150	350	3	92	75

Bead Placement

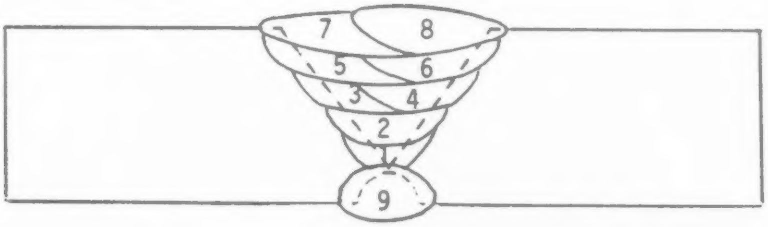

TABLE 18

TEST PANEL WELDING PROCEDURE WITH C-Mn-Ni-Ti/95Ar-5CO_2

Wire Diameter and Type:	1.2 mm Thyssen K5Ni (S)
Shielding Gas:	95Ar-5CO_2
Power Source:	GEC M450 PS
Plate Thickness and Type:	30 mm Lloyds LT-60

Joint/Preparation Details

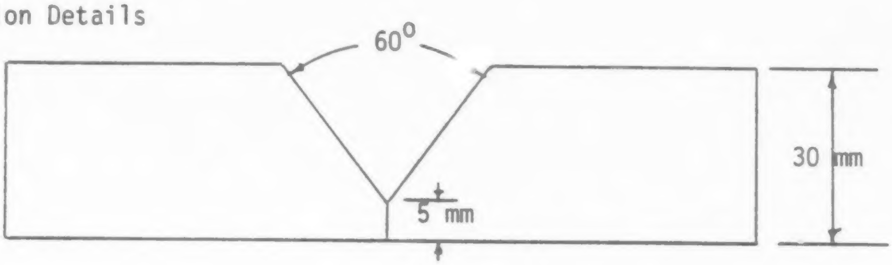

Welding Parameters

Pass	Wire Feed Speed (mm/min)	Travel (mm/min)	Oscillation Width (mm)	Oscillation Velocity (mm/s)	Stickout (mm)	Dwell L (s)	Dwell R (s)	Arc Voltage (V)	Mean Current (A)
1	4318	38	8	112	12.7	0.2	0.2	21.6	160
2	4064	38	13	81	12.7	0.6	0.6	21.0	150
3	4064	76	11	91	12.7	0.9	0.0	21.0	150
4	4064	64	11	81	12.7	0.4	0.8	21.0	150
5	4064	51	12	81	12.7	0.9	0.0	21.0	150
6	4064	38	12	81	12.7	0.4	0.8	21.0	150
7	4064	38	15	91	12.7	1.0	1.0	21.0	150
8	4064	38	16	91	12.7	1.0	1.0	21.0	150
9	4064	51	6	102	12.7	1.0	1.0	21.0	150

Pulse Parameters

Mean Current A	Peak Current A	Time at Peak ms	Background Current A	Frequency Hz
160	350	3	100	80
150	350	3	92	75

Bead Placement

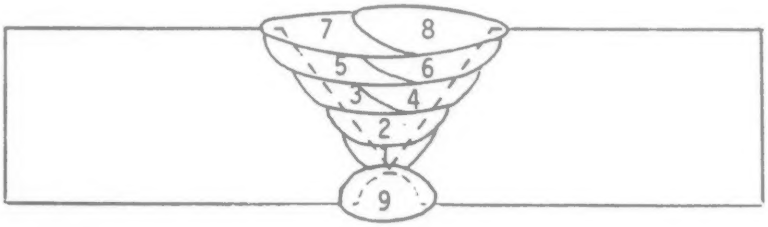

TABLE 19

TEST PANEL WELDING PROCEDURE WITH C-Mn-Mo/95Ar-5CO_2

Wire Diameter and Type:	1.2 mm Linde HI-84
Shielding Gas:	95Ar-5CO_2
Power Source:	GEC M450 PS
Plate Thickness and Type:	30 mm Lloyds LT-60

Joint/Preparation Details

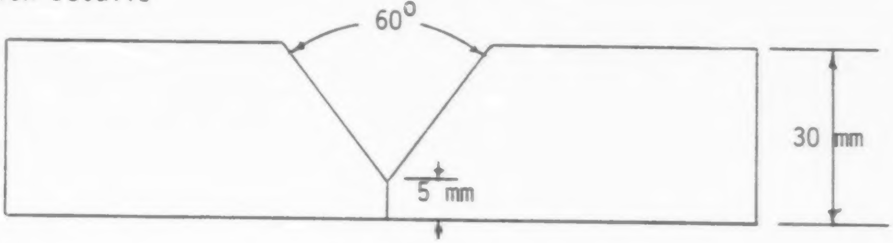

Welding Parameters

Pass	Wire Feed Speed (mm/min)	Travel (mm/min)	Oscillation Width (mm)	Oscillation Velocity (mm/s)	Stickout (mm)	Dwell L (s)	Dwell R (s)	Arc Voltage (V)	Mean Current (A)
1	4267	38	8	112	12.7	0.2	0.2	21.7	160
2	4013	38	13	81	12.7	0.6	0.6	21.6	150
3	4013	76	11	91	12.7	0.9	0.0	21.6	150
4	4013	64	11	81	12.7	0.4	0.8	21.6	150
5	4013	51	11	81	12.7	0.9	0.0	21.6	150
6	4013	38	14	81	12.7	0.4	0.8	21.6	150
7	4013	38	12	81	12.7	0.9	0.0	21.6	150
8	4013	38	12	81	12.7	0.9	0.9	21.6	150
9	4013	140	6	102	12.7	1.0	1.0	21.6	150

Pulse Parameters

Mean Current A	Peak Current A	Time at Peak ms	Background Current A	Frequency Hz
160	350	3	100	80
150	350	3	92	75

Bead Placement

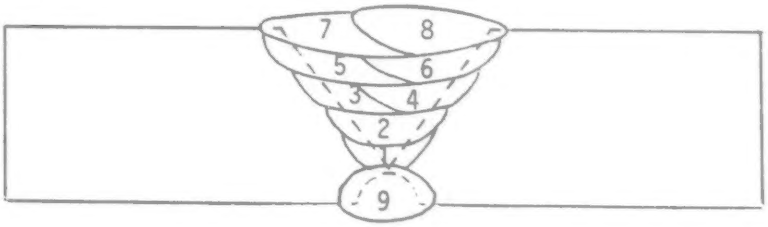

TABLE 20

TEST PANEL WELDING PROCEDURE WITH C-Mn-Mo-Ti/95Ar-5CO$_2$

Wire Diameter and Type:	1.2 mm Kobe MG-50D
Shielding Gas:	95Ar-5CO$_2$
Power Source:	GEC M450 PS
Plate Thickness and Type:	30 mm Lloyds LT-60

Joint/Preparation Details

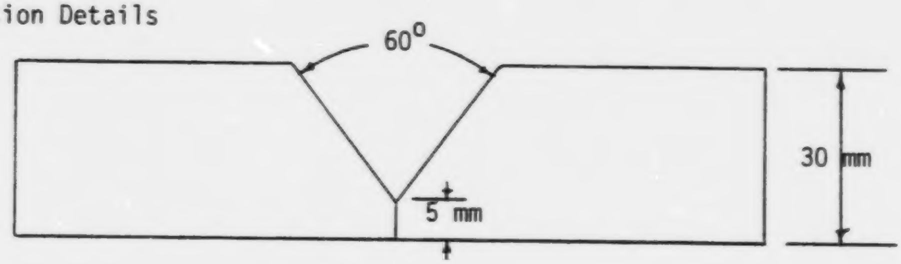

Welding Parameters

Pass	Wire Feed Speed (mm/min)	Travel (mm/min)	Oscillation Width (mm)	Oscillation Velocity (mm/s)	Stickout (mm)	Dwell L (s)	Dwell R (s)	Arc Voltage (V)	Mean Current (A)
1	4267	38	8	112	12.7	0.2	0.2	21.3	160
2	3937	38-64	13	91	12.7	0.8	0.8	21.4	150
3	3937	76	11	91	12.7	1.0	0.0	21.4	150
4	3937	64-76	9	81	12.7	1.0	1.0	21.4	150
5	3937	38-64	12	91	12.7	1.0	0.2	21.4	150
6	3937	38	12	81	12.7	1.0	1.0	21.4	150
7	3937	38	16	81	12.7	1.0	1.0	21.4	150
8	3937	38-64	15	81	12.7	1.0	1.0	21.4	150
9	3937	102	6	102	12.7	1.0	1.0	21.4	150

Pulse Parameters

Mean Current A	Peak Current A	Time at Peak ms	Background Current A	Frequency Hz
160	350	3	100	80
150	350	3	92	75

Bead Placement

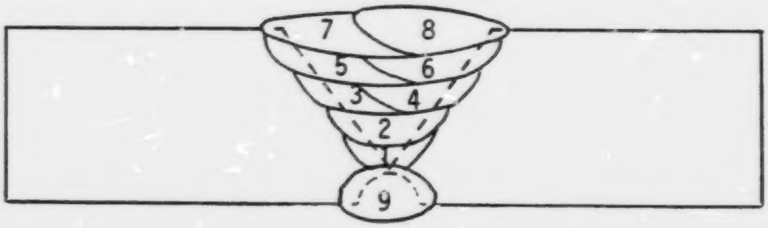

TABLE 21

TEST PANEL WELDING PROCEDURE WITH C-Mn-Si/88Ar-10He-2CO$_2$

Wire Diameter and Type:	1.2 mm LINCOLN L-56
Shielding Gas:	88Ar-10He-2CO$_2$
Power Source:	GEC M450 PS
Plate Thickness and Type:	30 mm Lloyds LT-60

Joint/Preparation Details

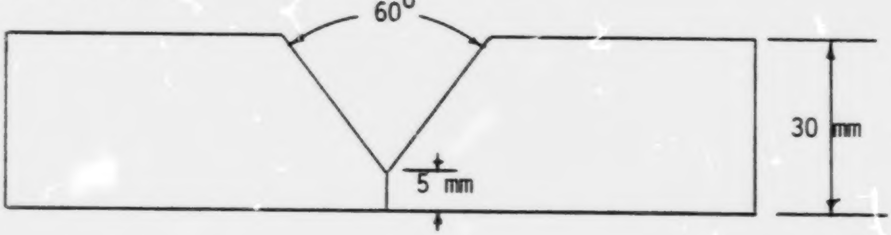

Welding Parameters

Pass	Wire Feed Speed (mm/min)	Travel (mm/min)	Oscillation Width (mm)	Oscillation Velocity (mm/s)	Stickout (mm)	Dwell L (s)	Dwell R (s)	Arc Voltage (V)	Mean Current (A)
1	4064	38	8	112	12.7	0.2	0.2	20.9	160
2	3912	38	13	91	12.7	0.6	0.6	20.7	150
3	3912	76	11	81	12.7	1.0	0.0	20.7	150
4	3912	76	9	91	12.7	1.0	1.0	20.7	150
5	3912	38	12	81	12.7	1.0	0.0	20.7	150
6	3912	38	12	81	12.7	1.0	1.0	20.7	150
7	3912	38	16	81	12.7	1.8	1.0	20.7	150
8	3912	38	16	81	12.7	1.0	1.0	20.7	150
9	3912	76	6	102	12.7	1.0	1.0	20.7	150

Pulse Parameters

Mean Current A	Peak Current A	Time at Peak ms	Background Current A	Frequency Hz
160	350	3	100	80
150	350	3	92	75

Bead Placement

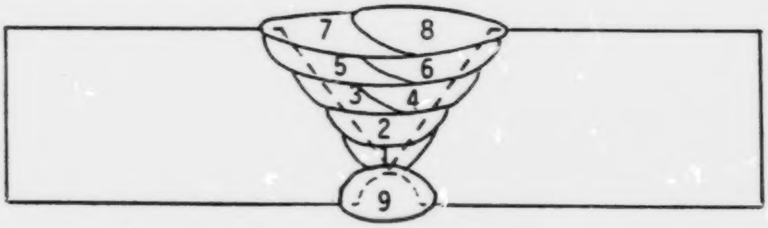

TABLE 22

TEST PANEL WELDING PROCEDURE WITH C-Mn-Ti-B/88Ar-10He-2CO_2

Wire Diameter and Type:	1.2 mm Kobe MGS-50LT
Shielding Gas:	88Ar-10He-2CO_2
Power Source:	GEC M450 PS
Plate Thickness and Type:	30 mm Lloyds LT-60

Joint/Preparation Details

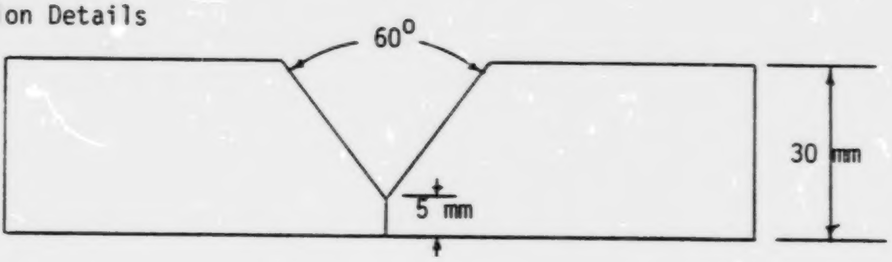

Welding Parameters

Pass	Wire Feed Speed (mm/min)	Travel (mm/min)	Oscillation Width (mm)	Oscillation Velocity (mm/s)	Stickout (mm)	Dwell L (s)	Dwell R (s)	Arc Voltage (V)	Mean Current (A)
1	3810	38	8	112	12.7	0.2	0.2	21.9	160
2	3785	38	13	81	12.7	1.0	1.0	21.7	150
3	3785	64	11	81	12.7	1.0	0.2	21.7	150
4	3785	38	11	81	12.7	1.0	1.0	21.7	150
5	3785	38	12	81	12.7	1.0	0.2	21.7	150
6	3785	38	12	81	12.7	1.0	1.0	21.7	150
7	3785	38	16	81	12.7	1.8	1.0	21.7	150
8	3785	38	16	81	12.7	1.0	1.0	21.7	150
9	3785	76	6	102	12.7	1.0	1.0	21.7	150

Pulse Parameters

Mean Current A	Peak Current A	Time at Peak ms	Background Current A	Frequency Hz
160	350	3	100	80
150	350	3	92	75

Bead Placement

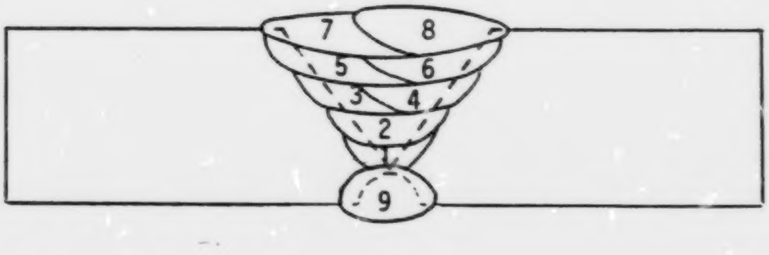

TABLE 23

TEST PANEL WELDING PROCEDURE WITH C-Mn-Si/87.5Ar-10He-2CO$_2$-0.5H$_2$

Wire Diameter and Type:	1.2 mm LINCOLN L-56
Shielding Gas:	87.5Ar-10He-2CO$_2$-0.5H$_2$
Power Source:	GEC M450 PS
Plate Thickness and Type:	30 mm Lloyds LT-60

Joint/Preparation Details

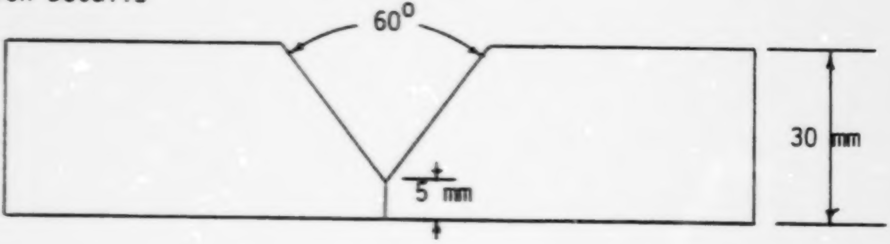

Welding Parameters

Pass	Wire Feed Speed (mm/min)	Travel (mm/min)	Oscillation		Stickout (mm)	Dwell		Arc Voltage (V)	Mean Current (A)
			Width (mm)	Velocity (mm/s)		L (s)	R (s)		
1	4039	38	8	112	12.7	0.2	0.2	22.7	160
2	3912	38	13	91	12.7	1.0	1.0	22.1	150
3	3912	64	11	81	12.7	1.0	0.2	22.1	150
4	3912	76	11	91	12.7	1.0	1.0	22.1	150
5	3912	51	12	91	12.7	1.0	1.0	22.1	150
6	3912	51-76	12	81	12.7	0.9	0.9	22.1	150
7	3912	38	16	91	12.7	1.0	0.6	22.1	150
8	3912	38	16	91	12.7	1.0	1.0	22.1	150
9	3912	102	6	102	12.7	1.0	1.0	22.1	150

Pulse Parameters

Mean Current A	Peak Current A	Time at Peak ms	Background Current A	Frequency Hz
160	350	3	100	80
150	350	3	92	75

Bead Placement

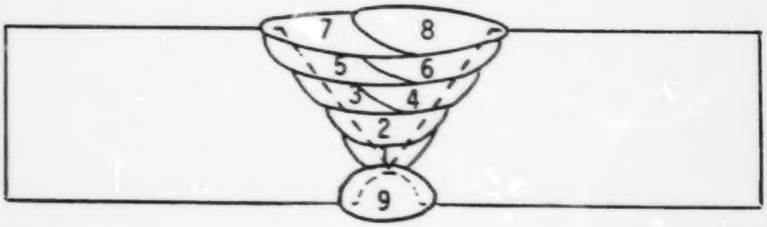

TABLE 24

TEST PANEL WELDING PROCEDURE WITH C-Mn-Ti-B/87.5Ar-10He-2CO_2-0.5H_2

Wire Diameter and Type: 1.2 mm Kobe MGS-50LT
Shielding Gas: 87.5Ar-10He-2CO_2-0.5H_2
Power Source: GEC M450 PS
Plate Thickness and Type: 30 mm Lloyds LT-60

Joint/Preparation Details

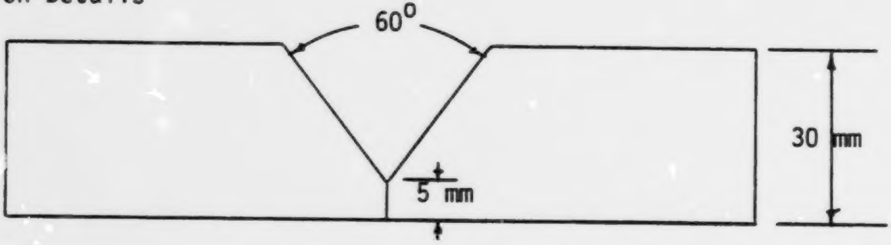

Welding Parameters

Pass	Wire Feed Speed (mm/min)	Travel (mm/min)	Oscillation		Stickout (mm)	Dwell		Arc Voltage (V)	Mean Current (A)
			Width (mm)	Velocity (mm/s)		L (s)	R (s)		
1	4140	38	8	112	12.7	0.2	0.2	22.9	160
2	3710	38	13	81	12.7	1.0	1.0	22.2	150
3	3710	64	11	81	12.7	1.0	0.2	22.2	150
4	3710	76	11	91	12.7	1.0	1.0	22.2	150
5	3710	51	12	91	12.7	1.0	1.0	22.2	150
6	3710	51-76	12	91	12.7	1.0	1.0	22.2	150
7	3710	38	16	91	12.7	1.0	0.6	22.2	150
8	3710	38	16	91	12.7	1.0	1.0	22.2	150
9	3710	102	6	102	12.7	1.0	1.0	22.2	150

Pulse Parameters

Mean Current A	Peak Current A	Time at Peak ms	Background Current A	Frequency Hz
160	350	3	100	80
150	350	3	92	75

Bead Placement

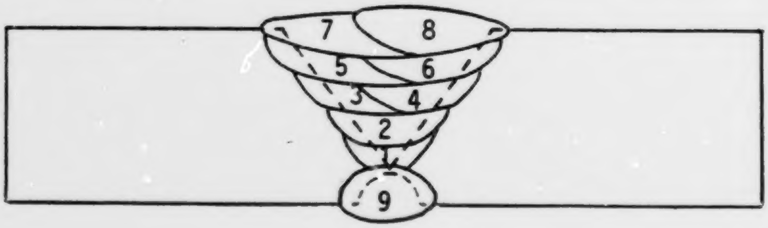

TABLE 25

TEST PANEL WELDING PROCEDURE WITH E41010 SMAW FULL PENETRATION ROOT AND C-Mn-Ti-B/95Ar-5CO_2 FILLS AND CAP

Wire Diameter and Type:	3.2 mm LINCOLN 5P+/1.2 mm KOBE MGS 50LT
Shielding Gas:	95Ar-5CO_2
Power Source:	GEC M450 PS
Pipe Material:	30 mm Lloyds LT60

Joint/Preparation Details

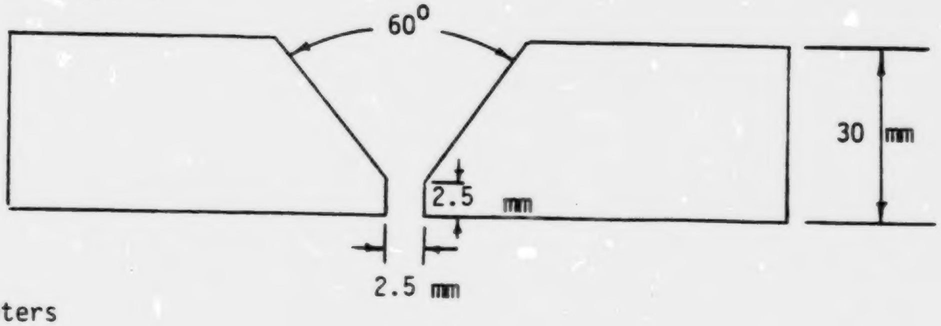

Welding Parameters

Pass	Wire Feed Speed (mm/min)	Travel (mm/min)	Oscillation Width (mm)	Oscillation Velocity (mm/s)	Stickout (mm)	Dwell L (s)	Dwell R (s)	Arc Voltage (V)	Mean Current (A)
1	N/A	76	N/A	N/A	N/A	N/A		24.0	85
2	3759	38	6	81	12.7	0.6	0.6	19.5	160
3	3759	45	12	81	12.7	1.0	1.0	20.5	150
4	3759	74	11	81	12.7	1.0	1.0	20.5	150
5	3759	64	11	81	12.7	0.0	1.0	20.5	150
6	3759	51	12	81	12.7	1.0	0.0	20.5	150
7	3759	51	12	81	12.7	0.0	1.0	20.5	150
8	3759	38	16	81	12.7	1.0	1.0	20.5	150
9	3759	38	16	81	12.7	1.0	1.0	20.5	150

Pulse Parameters

Mean Current A	Peak Current A	Time at Peak ms	Background Current A	Frequency Hz
150	350	3	92	75

Bead Placement

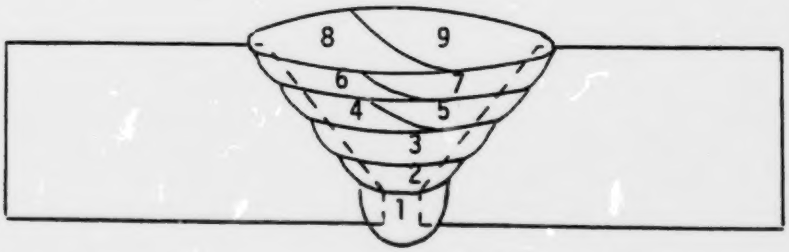

TABLE 26

TEST PANEL WELDING PROCEDURE C-Mn-Ti-B/95Ar-5CO_2 FULL PENETRATION ROOT, "HIGH" HEAT INPUT FILLS AND CAP

Wire Diameter and Type:	1.2 mm KOBE MGS 50LT
Shielding Gas:	95Ar-5CO_2
Power Source:	GEC M450 PS
Pipe Material:	30 mm Lloyds LT60

Joint/Preparation Details

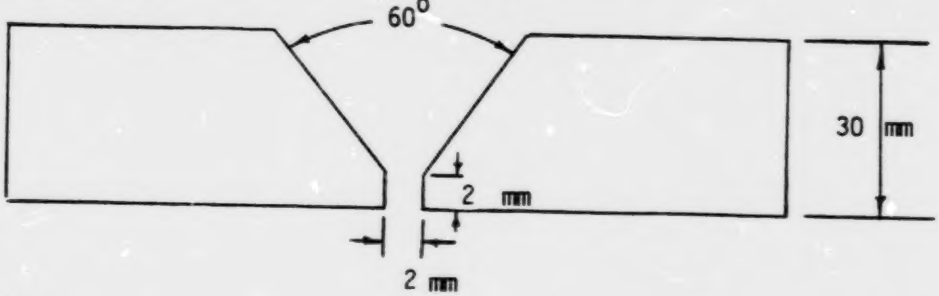

Welding Parameters

Pass	Wire Feed Speed (mm/min)	Travel (mm/min)	Oscillation Width (mm)	Oscillation Velocity (mm/s)	Stickout (mm)	Dwell L (s)	Dwell R (s)	Arc Voltage (V)	Mean Current (A)
1	4064	95	8	112	12.7	0.2	0.2	20.5	160
2	3759	42	6	81	12.7	0.6	0.6	20.5	150
3	3759	45	12	81	12.7	1.0	1.0	20.5	150
4	3759	74	11	81	12.7	1.0	1.0	20.5	150
5	3759	64	11	81	12.7	0.0	1.0	20.5	150
6	3759	51	12	81	12.7	1.0	0.0	20.5	150
7	3759	51	12	81	12.7	0.0	1.0	20.5	150
8	3759	38	16	81	12.7	1.0	1.0	20.5	150
9	3759	38	16	81	12.7	1.0	1.0	20.5	150

Pulse Parameters

Mean Current A	Peak Current A	Time at Peak ms	Background Current A	Frequency Hz
160	350	3	100	80
150	350	3	92	75

Bead Placement

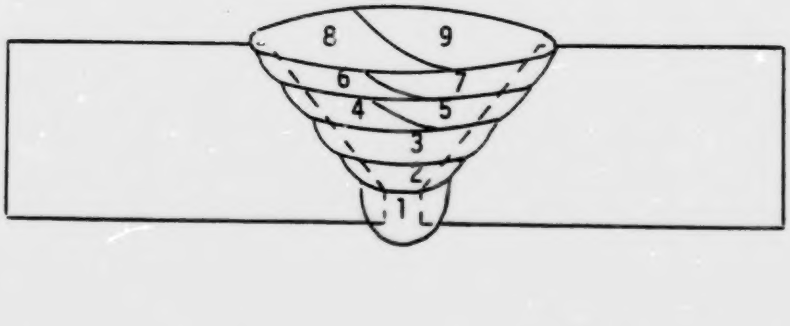

TABLE 27

TEST PANEL WELDING PROCEDURE C-Mn-Ti-B/95Ar-5CO_2 FULL PENETRATION ROOT, "LOW" HEAT INPUT FILLS AND CAP

Wire Diameter and Type:	1.2 mm KOBE MGS 50LT
Shielding Gas:	95Ar-5CO_2
Power Source:	GEC M450 PS
Pipe Material:	30 mm Lloyds LT60

Joint/Preparation Details

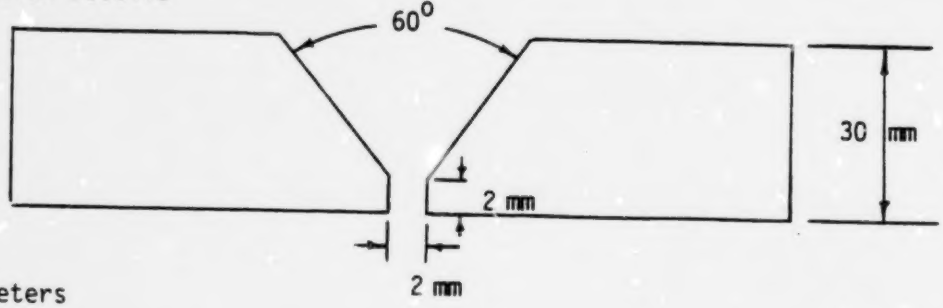

Welding Parameters

Pass	Wire Feed Speed (mm/min)	Travel (mm/min)	Oscillation Width (mm)	Oscillation Velocity (mm/s)	Stickout (mm)	Dwell L (s)	Dwell R (s)	Arc Voltage (V)	Mean Current (A)
1	4064	95	8	112	12.7	0.2	0.2	20.5	160
2	3759	127	7	112	12.7	1.0	1.0	20.0	150
3	3759	102	12	81	12.7	1.4.	1.4	20.0	150
4	3759	102	7	81	12.7	1.4	1.0	20.0	150
5	3759	89	10	81	12.7	1.4	1.0	20.0	150
6	3759	89	11	81	12.7	1.6	0.8	20.0	150
7	3759	76	12	81	12.7	0.6	1.4	20.0	150
8	3759	64	12	81	12.7	1.8	0.2	20.0	150
9	3759	64	12	81	12.7	2.0	0.0	20.0	150
10	3759	64	12	81	12.7	1.4	1.5	20.0	150

Pulse Parameters

Mean Current A	Peak Current A	Time at Peak ms	Background Current A	Frequency Hz
160	350	3	100	80
150	350	3	92	75

Bead Placement

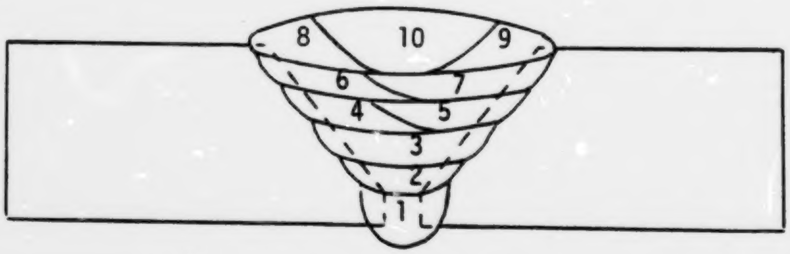

TABLE 28

WELD METAL CHEMICAL COMPOSITION

a) SHIELDING GAS: 95Ar-5CO_2

Electrode	C	Mn	P	S	Si	Ni	Cr	Mo	Cu	Ti	Al	V	Nb	B	O	N
C-Mn-Si	.10	1.47	.008	.014	.87	.02	.05	<.01	.08	<.005	<.005	.007	<.005	<.0005	.020	.013
LowC-Mn-Si	.05	1.31	.012	.015	.65	.04	.06	<.01	.05	<.005	.006	.007	<.005	<.0005	.017	.014
C-Mn-Si-Ti	.08	1.46	.009	.007	.69	.05	.08	.01	.05	.017	.007	.009	.006	<.0005	.018	.012
C-Mn-Ti-B	.07	1.66	.008	<.005	.34	.08	.16	.01	.15	.036	<.005	.014	.006	.0043	.021	.013
C-Mn-Ni	.11	1.18	.008	.010	.51	1.30	.14	.01	.06	<.005	.006	.010	.006	<.0005	.018	.014
C-Mn-Ni-Ti	.12	1.25	.007	.006	.61	1.27	.08	.01	.07	.048	.005	.011	.005	<.0005	.018	.012
C-Mn-Mo	.11	1.73	.013	.017	.53	.14	.13	.48	.33	.006	<.005	.014	.007	<.0005	.019	.017
C-Mn-Mo-Ti	.06	1.78	.007	.009	.54	.06	.15	.14	.21	.084	<.005	.012	.007	<.0005	.018	.014

TABLE 28 (cont)

b) SHIELDING GAS: 88Ar-10He-$2CO_2$

Electrode	C	Mn	P	S	Si	Ni	Cr	Mo	Cu	Ti	Al	V	Nb	B	O	N
C-Mn-Si	.11	1.40	.007	.013	.87	<.01	.03	<.01	.08	<.005	<.005	<.005	<.005	<.0005	.015	.011
C-Mn-Ti-B	.08	1.63	.007	<.005	.34	.05	.15	.01	.15	.034	<.005	.008	<.005	.0041	.012	.010

c) SHIELDING GAS: 87.5Ar-10He-$2CO_2$-$0.5H_2$

Electrode	C	Mn	P	S	Si	Ni	Cr	Mo	Cu	Ti	Al	V	Nb	B	O	N
C-Mn-Si	.09	1.43	.007	.013	.88	<.01	.03	<.01	.08	<.005	<.005	<.005	<.005	<.0005	.014	.011
C-Mn-Ti-B	.07	1.65	.006	<.005	.35	.04	.14	.01	.16	.036	<.005	.006	<.005	.0040	.012	.010

TABLE 29

HARDNESS TEST RESULTS FOR C-Mn-Si/95Ar-5CO_2

Type of Test: Vickers Microhardness (500 gram load, 15 sec. time)

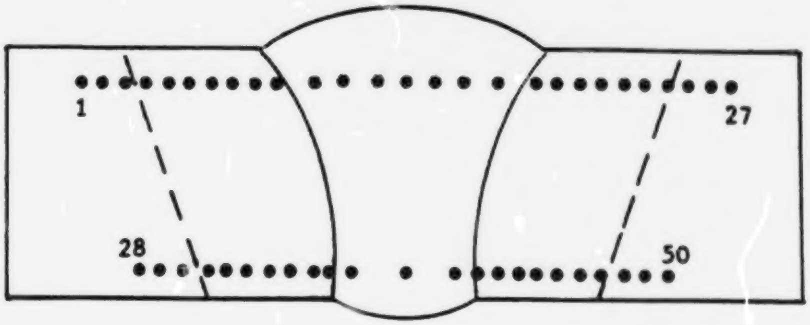

FG - Fine Grain
CG - Coarse Grain

	MICRO #				MICRO #		
	1	2	3		1	2	3
LOCATION	HVN	HVN	HVN	LOCATION	HVN	HVN	HVN
1. Parent Metal	168	161	170	26. Parent Metal	156	166	170
2. Parent Metal	158	174	168	27. Parent Metal	168	165	173
3. Parent Metal	168	167	184	28. Parent Metal	164	167	165
4. HAZ (FG)	175	174	201	29. Parent Metal	172	174	170
5. HAZ (FG)	179	182	189	30. Parent Metal	161	168	171
6. HAZ (FG)	174	162	184	31. HAZ (FG)	188	189	202
7. HAZ (FG)	183	214	201	32. HAZ (FG)	202	203	218
8. HAZ (CG)	186	219	223	33. HAZ (FG)	207	201	204
9. HAZ (CG)	195	205	210	34. HAZ (FG)	216	217	214
10. HAZ (CG)	182	214	207	35. HAZ (CG)	224	229	242
11. Weld Metal	199	217	233	36. HAZ (CG)	211	247	261
12. Weld Metal	209	199	236	37. HAZ (CG)	240	230	227
13. Weld Metal	217	226	225	38. Weld Metal	250	250	236
14. Weld Metal	197	232	195	39. Weld Metal	248	254	254
15. Weld Metal	268	216	222	40. Weld Metal	258	258	240
16. Weld Metal	208	217	224	41. HAZ (CG)	245	226	258
17. Weld Metal	212	228	232	42. HAZ (CG)	238	231	258
18. HAZ (CG)	205	211	224	43. HAZ (CG)	230	244	205
19. HAZ (CG)	208	214	231	44. HAZ (FG)	228	209	199
20. HAZ (CG)	202	220	214	45. HAZ (FG)	202	196	210
21. HAZ (FG)	187	178	202	46. HAZ (FG)	166	204	188
22. HAZ (FG)	197	188	188	47. HAZ (FG)	178	173	183
23. HAZ (FG)	186	210	177	48. Parent Metal	176	173	180
24. HAZ (FG)	177	191	189	49. Parent Metal	178	186	175
25. Parent Metal	182	173	188	50. Parent Metal	164	172	159

TABLE 30

HARDNESS TEST RESULTS FOR LowC-Mn-Si/95Ar-5CO_2

Type of Test: Vickers Microhardness (500 gram load, 15 sec. time)

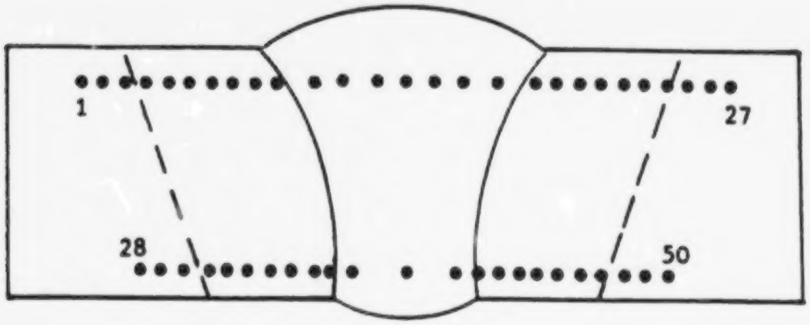

FG - Fine Grain
CG - Coarse Grain

LOCATION	MICRO # 1 HVN	MICRO # 2 HVN	MICRO # 3 HVN
1. Parent Metal	175	162	180
2. Parent Metal	180	163	172
3. Parent Metal	170	172	184
4. HAZ (FG)	177	182	186
5. HAZ (FG)	190	179	197
6. HAZ (FG)	175	178	207
7. HAZ (FG)	177	190	217
8. HAZ (CG)	222	214	231
9. HAZ (CG)	237	226	213
10. HAZ (CG)	190	229	220
11. Weld Metal	215	158	158
12. Weld Metal	202	171	173
13. Weld Metal	191	165	163
14. Weld Metal	191	179	173
15. Weld Metal	228	210	170
16. Weld Metal	219	206	161
17. Weld Metal	208	220	175
18. HAZ (CG)	224	221	204
19. HAZ (CG)	227	226	226
20. HAZ (CG)	205	207	229
21. HAZ (FG)	207	196	217
22. HAZ (FG)	205	191	203
23. HAZ (FG)	189	180	202
24. HAZ (FG)	181	183	196
25. Parent Metal	172	173	184
26. Parent Metal	182	184	175
27. Parent Metal	170	168	169
28. Parent Metal	176	184	171
29. Parent Metal	160	171	168
30. Parent Metal	167	169	173
31. HAZ (FG)	188	174	179
32. HAZ (FG)	186	176	181
33. HAZ (FG)	214	207	184
34. HAZ (FG)	202	201	195
35. HAZ (CG)	219	248	220
36. HAZ (CG)	261	243	234
37. HAZ (CG)	251	235	229
38. Weld Metal	231	220	240
39. Weld Metal	231	231	249
40. Weld Metal	229	227	245
41. HAZ (CG)	227	238	234
42. HAZ (CG)	258	244	235
43. HAZ (CG)	248	238	226
44. HAZ (FG)	252	258	229
45. HAZ (FG)	218	225	209
46. HAZ (FG)	231	190	184
47. HAZ (FG)	202	191	204
48. Parent Metal	164	168	167
49. Parent Metal	158	166	150
50. Parent Metal	168	159	158

TABLE 31

HARDNESS TEST RESULTS FOR C-Mn-Si-Ti/95Ar-5CO_2

Type of Test: Vickers Microhardness (500 gram load, 15 sec. time)

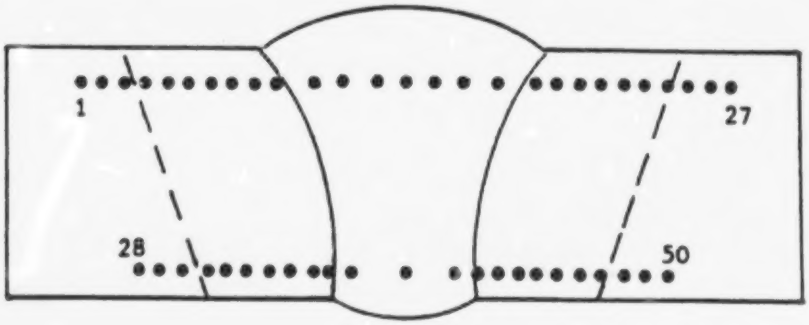

FG - Fine Grain
CG - Coarse Grain

		MICRO #	
LOCATION	1 HVN	2 HVN	3 HVN
1. Parent Metal	164	171	170
2. Parent Metal	170	173	170
3. Parent Metal	173	168	178
4. HAZ (FG)	175	169	180
5. HAZ (FG)	185	173	211
6. HAZ (FG)	187	197	214
7. HAZ (FG)	198	220	220
8. HAZ (CG)	219	217	211
9. HAZ (CG)	222	230	225
10. HAZ (CG)	205	207	246
11. Weld Metal	219	194	222
12. Weld Metal	207	202	214
13. Weld Metal	172	235	221
14. Weld Metal	214	216	215
15. Weld Metal	200	206	222
16. Weld Metal	192	210	217
17. Weld Metal	224	220	223
18. HAZ (CG)	218	216	216
19. HAZ (CG)	225	220	228
20. HAZ (CG)	209	205	228
21. HAZ (FG)	189	193	225
22. HAZ (FG)	193	207	203
23. HAZ (FG)	188	201	194
24. HAZ (FG)	188	183	208
25. Parent Metal	167	170	178
26. Parent Metal	161	174	172
27. Parent Metal	162	173	178
28. Parent Metal	173	180	176
29. Parent Metal	166	178	186
30. Parent Metal	177	181	188
31. HAZ (FG)	181	186	194
32. HAZ (FG)	208	210	186
33. HAZ (FG)	214	212	202
34. HAZ (FG)	211	230	202
35. HAZ (CG)	244	232	246
36. HAZ (CG)	250	236	238
37. HAZ (CG)	279	227	252
38. Weld Metal	245	222	282
39. Weld Metal	248	238	248
40. Weld Metal	253	240	259
41. HAZ (CG)	243	240	239
42. HAZ (CG)	236	237	247
43. HAZ (CG)	244	241	235
44. HAZ (FG)	240	230	227
45. HAZ (FG)	173	201	214
46. HAZ (FG)	201	212	193
47. HAZ (FG)	196	200	187
48. Parent Metal	174	152	182
49. Parent Metal	164	160	161
50. Parent Metal	163	163	170

TABLE 32

HARDNESS TEST RESULTS FOR C-Mn-Ti-B/95Ar-5CO$_2$

Type of Test: Vickers Microhardness (500 gram load, 15 sec. time)

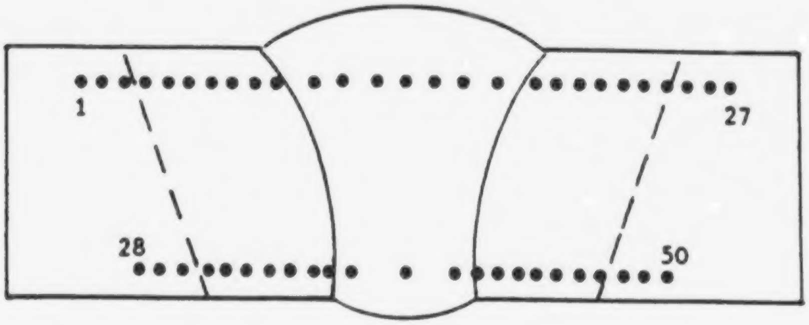

FG - Fine Grain
CG - Coarse Grain

	MICRO #				MICRO #		
LOCATION	1 HVN	2 HVN	3 HVN	LOCATION	1 HVN	2 HVN	3 HVN
1. Parent Metal	168	173	169	26. Parent Metal	171	171	186
2. Parent Metal	160	168	183	27. Parent Metal	178	176	165
3. Parent Metal	175	180	174	28. Parent Metal	165	156	156
4. HAZ (FG)	195	177	195	29. Parent Metal	175	168	177
5. HAZ (FG)	178	182	187	30. Parent Metal	165	173	166
6. HAZ (FG)	178	182	179	31. HAZ (FG)	199	205	189
7. HAZ (FG)	183	184	172	32. HAZ (FG)	202	217	178
8. HAZ (CG)	211	207	206	33. HAZ (FG)	186	244	201
9. HAZ (CG)	231	224	213	34. HAZ (FG)	218	258	203
10. HAZ (CG)	221	238	228	35. HAZ (CG)	250	253	226
11. Weld Metal	244	243	241	36. HAZ (CG)	258	263	258
12. Weld Metal	224	234	237	37. HAZ (CG)	244	279	232
13. Weld Metal	235	244	255	38. Weld Metal	278	291	280
14. Weld Metal	230	243	232	39. Weld Metal	278	287	282
15. Weld Metal	218	228	221	40. Weld Metal	281	294	278
16. Weld Metal	243	244	229	41. HAZ (CG)	238	248	273
17. Weld Metal	244	254	233	42. HAZ (CG)	246	265	244
18. HAZ (CG)	231	224	232	43. HAZ (CG)	242	214	258
19. HAZ (CG)	233	229	213	44. HAZ (FG)	225	186	241
20. HAZ (CG)	225	226	217	45. HAZ (FG)	214	175	212
21. HAZ (FG)	205	198	184	46. HAZ (FG)	200	184	189
22. HAZ (FG)	182	183	189	47. HAZ (FG)	175	163	192
23. HAZ (FG)	189	175	187	48. Parent Metal	158	177	178
24. HAZ (FG)	191	196	198	49. Parent Metal	172	169	175
25. Parent Metal	178	173	170	50. Parent Metal	163	183	180

TABLE 33

HARDNESS TEST RESULTS FOR C-Mn-Ni/95Ar-5CO_2

Type of Test: Vickers Microhardness (500 gram load, 15 sec. time)

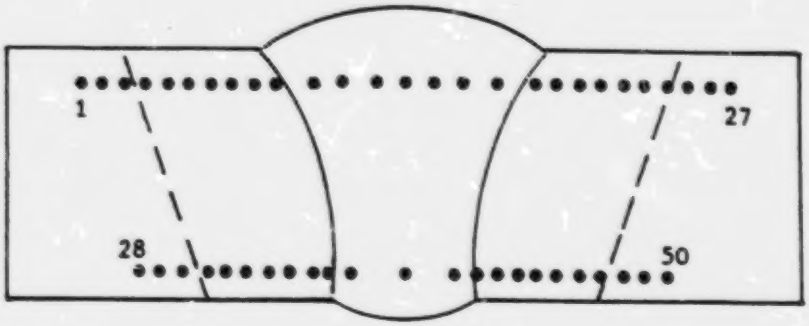

FG - Fine Grain
CG - Coarse Grain

LOCATION	MICRO #		
	1 HVN	2 HVN	3 HVN
1. Parent Metal	177	174	169
2. Parent Metal	168	173	164
3. Parent Metal	175	170	179
4. HAZ (FG)	189	178	185
5. HAZ (FG)	194	193	202
6. HAZ (FG)	181	178	195
7. HAZ (FG)	188	192	189
8. HAZ (CG)	225	226	220
9. HAZ (CG)	205	216	225
10. HAZ (CG)	214	218	202
11. Weld Metal	229	233	257
12. Weld Metal	218	240	229
13. Weld Metal	203	217	259
14. Weld Metal	235	232	226
15. Weld Metal	209	221	267
16. Weld Metal	219	231	234
17. Weld Metal	238	217	242
18. HAZ (CG)	228	226	222
19. HAZ (CG)	232	222	228
20. HAZ (CG)	229	224	241
21. HAZ (FG)	192	201	205
22. HAZ (FG)	194	197	168
23. HAZ (FG)	182	185	186
24. HAZ (FG)	175	178	177
25. Parent Metal	171	161	165
26. Parent Metal	180	175	167
27. Parent Metal	175	173	170
28. Parent Metal	166	188	163
29. Parent Metal	171	190	170
30. Parent Metal	174	178	181
31. HAZ (FG)	198	196	218
32. HAZ (FG)	200	191	224
33. HAZ (FG)	210	205	250
34. HAZ (FG)	198	227	217
35. HAZ (CG)	232	245	221
36. HAZ (CG)	236	266	266
37. HAZ (CG)	244	217	259
38. Weld Metal	279	253	281
39. Weld Metal	276	287	264
40. Weld Metal	264	265	288
41. HAZ (CG)	248	228	249
42. HAZ (CG)	255	261	241
43. HAZ (CG)	254	244	228
44. HAZ (FG)	184	241	216
45. HAZ (FG)	194	216	201
46. HAZ (FG)	192	215	220
47. HAZ (FG)	184	192	210
48. Parent Metal	166	180	167
49. Parent Metal	167	168	159
50. Parent Metal	175	179	161

TABLE 34

HARDNESS TEST RESULTS FOR C-Mn-Ni-Ti/95Ar-5CO$_2$

Type of Test: Vickers Microhardness (500 gram load, 15 sec. time)

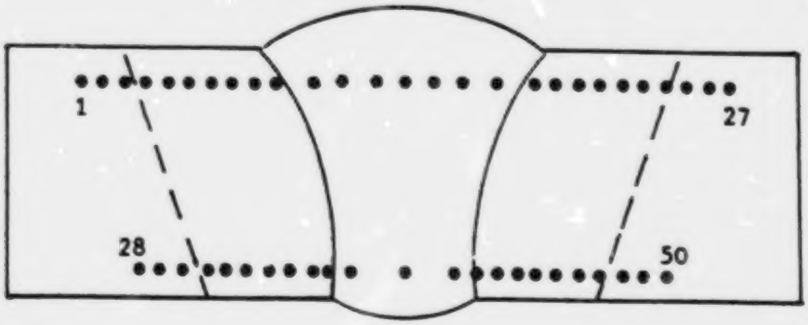

FG - Fine Grain
CG - Coarse Grain

LOCATION		MICRO #	
	1 HVN	2 HVN	3 HVN
1. Parent Metal	164	170	164
2. Parent Metal	171	159	165
3. Parent Metal	168	168	172
4. HAZ (FG)	184	189	188
5. HAZ (FG)	211	210	180
6. HAZ (FG)	204	200	198
7. HAZ (FG)	222	205	202
8. HAZ (CG)	221	230	221
9. HAZ (CG)	243	225	214
10. HAZ (CG)	221	244	223
11. Weld Metal	246	257	258
12. Weld Metal	236	253	230
13. Weld Metal	224	258	251
14. Weld Metal	194	256	232
15. Weld Metal	233	230	223
16. Weld Metal	247	244	233
17. Weld Metal	256	256	258
18. HAZ (CG)	224	216	227
19. HAZ (CG)	209	225	218
20. HAZ (CG)	202	214	199
21. HAZ (FG)	195	201	198
22. HAZ (FG)	187	203	194
23. HAZ (FG)	180	207	188
24. HAZ (FG)	188	194	184
25. Parent Metal	168	196	170
26. Parent Metal	177	166	175
27. Parent Metal	170	171	195
28. Parent Metal	166	156	168
29. Parent Metal	166	173	176
30. Parent Metal	172	176	175
31. HAZ (FG)	182	216	183
32. HAZ (FG)	193	221	273
33. HAZ (FG)	216	233	199
34. HAZ (FG)	214	242	231
35. HAZ (CG)	220	245	241
36. HAZ (CG)	228	251	230
37. HAZ (CG)	244	242	229
38. Weld Metal	266	258	219
39. Weld Metal	285	282	272
40. Weld Metal	283	309	280
41. HAZ (CG)	240	234	242
42. HAZ (CG)	246	191	220
43. HAZ (CG)	248	189	229
44. HAZ (FG)	217	201	194
45. HAZ (FG)	194	232	205
46. HAZ (FG)	186	207	178
47. HAZ (FG)	194	215	163
48. Parent Metal	164	212	161
49. Parent Metal	170	170	175
50. Parent Metal	166	164	174

TABLE 35

HARDNESS TEST RESULTS FOR C-Mn-Mo/95Ar-5CO$_2$

Type of Test: Vickers Microhardness (500 gram load, 15 sec. time)

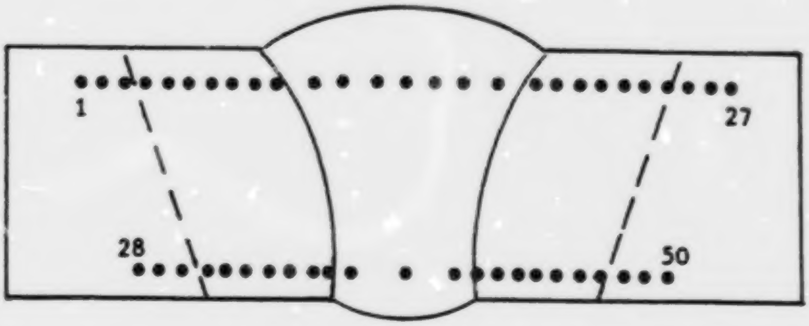

FG - Fine Grain
CG - Coarse Grain

LOCATION	MICRO # 1 HVN	MICRO # 2 HVN	MICRO # 3 HVN	LOCATION	MICRO # 1 HVN	MICRO # 2 HVN	MICRO # 3 HVN
1. Parent Metal	168	170	181	26. Parent Metal	178	167	177
2. Parent Metal	190	174	173	27. Parent Metal	168	168	194
3. Parent Metal	203	173	168	28. Parent Metal	152	158	182
4. HAZ (FG)	197	188	193	29. Parent Metal	161	164	169
5. HAZ (FG)	214	205	198	30. Parent Metal	149	176	175
6. HAZ (FG)	213	191	199	31. HAZ (FG)	189	199	211
7. HAZ (FG)	230	202	198	32. HAZ (FG)	211	177	193
8. HAZ (CG)	248	216	228	33. HAZ (FG)	195	214	200
9. HAZ (CG)	220	224	226	34. HAZ (FG)	223	220	205
10. HAZ (CG)	243	238	229	35. HAZ (CG)	256	246	220
11. Weld Metal	275	281	280	36. HAZ (CG)	240	239	241
12. Weld Metal	268	269	289	37. HAZ (CG)	245	257	261
13. Weld Metal	297	294	280	38. Weld Metal	262	304	298
14. Weld Metal	302	285	266	39. Weld Metal	313	302	310
15. Weld Metal	295	288	296	40. Weld Metal	282	300	303
16. Weld Metal	280	279	269	41. HAZ (CG)	258	246	266
17. Weld Metal	307	276	289	42. HAZ (CG)	241	251	286
18. HAZ (CG)	249	223	238	43. HAZ (CG)	248	283	267
19. HAZ (CG)	207	232	218	44. HAZ (FG)	212	246	277
20. HAZ (CG)	231	229	221	45. HAZ (FG)	220	204	238
21. HAZ (FG)	206	211	204	46. HAZ (FG)	206	203	218
22. HAZ (FG)	191	194	194	47. HAZ (FG)	207	202	210
23. HAZ (FG)	184	196	183	48. Parent Metal	180	189	186
24. HAZ (FG)	189	187	182	49. Parent Metal	164	172	178
25. Parent Metal	151	168	177	50. Parent Metal	172	177	173

TABLE 36

HARDNESS TEST RESULTS FOR C-Mn-Mo-Ti/95Ar-5CO$_2$

Type of Test: Vickers Microhardness (500 gram load, 15 sec. time)

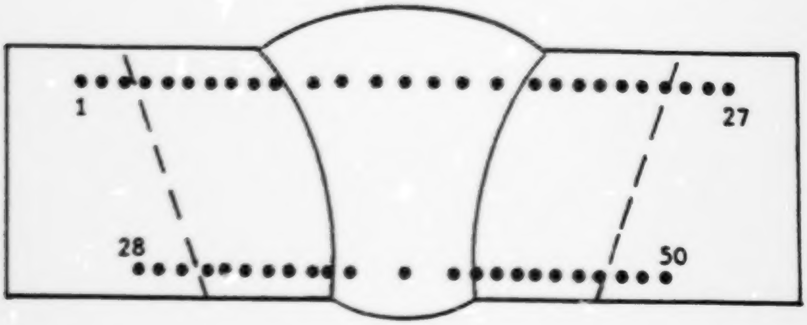

FG - Fine Grain
CG - Coarse Grain

		MICRO #	
LOCATION	1 HVN	2 HVN	3 HVN
1. Parent Metal	164	168	171
2. Parent Metal	173	170	175
3. Parent Metal	166	176	168
4. HAZ (FG)	194	190	162
5. HAZ (FG)	195	190	195
6. HAZ (FG)	203	201	186
7. HAZ (FG)	210	211	192
8. HAZ (CG)	244	217	217
9. HAZ (CG)	231	236	231
10. HAZ (CG)	236	229	238
11. Weld Metal	265	239	213
12. Weld Metal	251	231	256
13. Weld Metal	253	242	238
14. Weld Metal	253	232	240
15. Weld Metal	267	235	230
16. Weld Metal	258	258	241
17. Weld Metal	258	238	224
18. HAZ (CG)	231	231	220
19. HAZ (CG)	227	231	240
20. HAZ (CG)	232	214	219
21. HAZ (FG)	216	203	210
22. HAZ (FG)	187	194	195
23. HAZ (FG)	187	182	189
24. HAZ (FG)	186	196	174
25. Parent Metal	178	174	183

		MICRO #	
LOCATION	1 HVN	2 HVN	3 HVN
26. Parent Metal	172	177	200
27. Parent Metal	180	174	171
28. Parent Metal	158	158	166
29. Parent Metal	167	168	190
30. Parent Metal	164	183	188
31. HAZ (FG)	199	222	201
32. HAZ (FG)	205	208	220
33. HAZ (FG)	235	205	216
34. HAZ (FG)	221	220	200
35. HAZ (CG)	263	252	229
36. HAZ (CG)	243	235	219
37. HAZ (CG)	252	240	223
38. Weld Metal	278	282	240
39. Weld Metal	269	267	252
40. Weld Metal	277	266	258
41. HAZ (CG)	249	258	241
42. HAZ (CG)	252	234	220
43. HAZ (CG)	254	253	215
44. HAZ (FG)	216	216	216
45. HAZ (FG)	199	199	205
46. HAZ (FG)	177	197	197
47. HAZ (FG)	222	188	200
48. Parent Metal	175	180	217
49. Parent Metal	209	177	193
50. Parent Metal	172	172	182

TABLE 37

HARDNESS TEST RESULTS FOR C-Mn-Si/88Ar-10He-2CO_2

Type of Test: Vickers Microhardness (500 gram load, 15 sec. time)

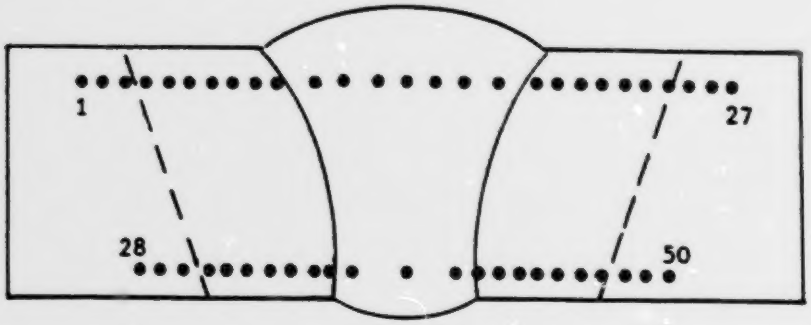

FG - Fine Grain
CG - Coarse Grain

	MICRO #				MICRO #		
LOCATION	1 HVN	2 HVN	3 HVN	LOCATION	1 HVN	2 HVN	3 HVN
1. Parent Metal	180	181	173	26. Parent Metal	176	170	177
2. Parent Metal	162	178	175	27. Parent Metal	168	161	180
3. Parent Metal	179	180	178	28. Parent Metal	166	165	162
4. HAZ (FG)	194	212	175	29. Parent Metal	166	180	179
5. HAZ (FG)	199	220	210	30. Parent Metal	164	173	161
6. HAZ (FG)	196	216	194	31. HAZ (FG)	198	190	182
7. HAZ (FG)	202	218	194	32. HAZ (FG)	196	184	201
8. HAZ (CG)	216	223	226	33. HAZ (FG)	199	197	211
9. HAZ (CG)	209	220	217	34. HAZ (FG)	229	203	226
10. HAZ (CG)	241	234	214	35. HAZ (CG)	236	206	224
11. Weld Metal	234	198	231	36. HAZ (CG)	235	228	240
12. Weld Metal	228	226	221	37. HAZ (CG)	216	226	222
13. Weld Metal	239	213	229	38. Weld Metal	286	240	241
14. Weld Metal	202	216	217	39. Weld Metal	258	256	237
15. Weld Metal	226	210	229	40. Weld Metal	259	251	251
16. Weld Metal	218	230	217	41. HAZ (CG)	251	212	241
17. Weld Metal	210	224	223	42. HAZ (CG)	241	194	231
18. HAZ (CG)	239	219	217	43. HAZ (CG)	224	220	226
19. HAZ (CG)	248	220	219	44. HAZ (FG)	204	218	198
20. HAZ (CG)	236	211	230	45. HAZ (FG)	212	209	192
21. HAZ (FG)	185	210	218	46. HAZ (FG)	175	217	177
22. HAZ (FG)	188	179	214	47. HAZ (FG)	199	200	177
23. HAZ (FG)	182	184	196	48. Parent Metal	175	156	168
24. HAZ (FG)	191	178	187	49. Parent Metal	178	167	171
25. Parent Metal	185	165	176	50. Parent Metal	169	160	168

TABLE 38

HARDNESS TEST RESULTS FOR C-Mn-Ti-B/88Ar-10He-$2CO_2$

Type of Test: Vickers Microhardness (500 gram load, 15 sec. time)

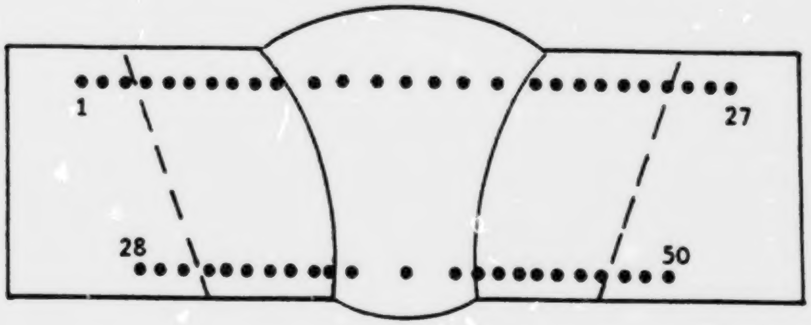

FG - Fine Grain
CG - Coarse Grain

	MICRO #				MICRO #		
LOCATION	1 HVN	2 HVN	3 HVN	LOCATION	1 HVN	2 HVN	3 HVN
1. Parent Metal	181	173	175	26. Parent Metal	188	182	186
2. Parent Metal	188	180	183	27. Parent Metal	179	191	172
3. Parent Metal	174	176	173	28. Parent Metal	170	184	171
4. HAZ (FG)	202	201	199	29. Parent Metal	164	189	178
5. HAZ (FG)	188	203	208	30. Parent Metal	178	190	180
6. HAZ (FG)	194	202	203	31. HAZ (FG)	189	201	186
7. HAZ (FG)	207	206	200	32. HAZ (FG)	188	196	201
8. HAZ (CG)	213	241	217	33. HAZ (FG)	235	208	211
9. HAZ (CG)	244	226	224	34. HAZ (FG)	196	227	208
10. HAZ (CG)	254	243	245	35. HAZ (CG)	218	224	229
11. Weld Metal	248	232	247	36. HAZ (CG)	238	235	238
12. Weld Metal	211	235	247	37. HAZ (CG)	223	230	226
13. Weld Metal	229	238	232	38. Weld Metal	282	269	278
14. Weld Metal	231	243	243	39. Weld Metal	285	272	258
15. Weld Metal	245	258	254	40. Weld Metal	287	273	258
16. Weld Metal	250	247	247	41. HAZ (CG)	268	247	231
17. Weld Metal	240	242	238	42. HAZ (CG)	252	246	224
18. HAZ (CG)	218	230	231	43. HAZ (CG)	247	242	230
19. HAZ (CG)	226	216	228	44. HAZ (FG)	230	205	214
20. HAZ (CG)	202	225	238	45. HAZ (FG)	208	211	211
21. HAZ (FG)	199	214	208	46. HAZ (FG)	220	214	222
22. HAZ (FG)	194	204	210	47. HAZ (FG)	196	207	215
23. HAZ (FG)	189	208	214	48. Parent Metal	184	186	177
24. HAZ (FG)	187	200	189	49. Parent Metal	173	178	173
25. Parent Metal	182	193	180	50. Parent Metal	188	171	186

TABLE 39

HARDNESS TEST RESULTS FOR C-Mn-Si/87.5Ar-10He-2CO_2-0.5H_2

Type of Test: Vickers Microhardness (500 gram load, 15 sec. time)

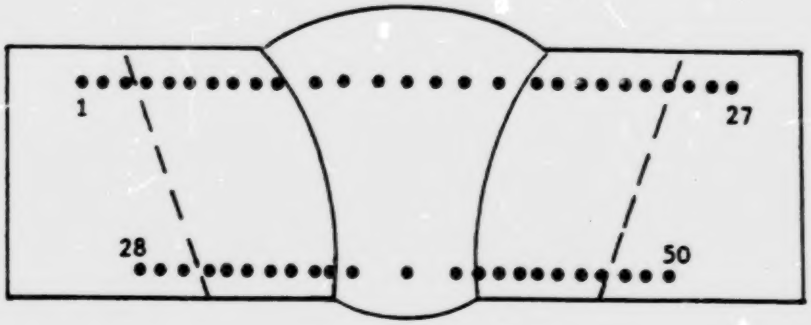

FG - Fine Grain
CG - Coarse Grain

	MICRO #				MICRO #		
	1	2	3		1	2	3
LOCATION	HVN	HVN	HVN	LOCATION	HVN	HVN	HVN
1. Parent Metal	162	167	179	26. Parent Metal	179	179	169
2. Parent Metal	163	162	178	27. Parent Metal	191	174	171
3. Parent Metal	164	169	186	28. Parent Metal	167	179	176
4. HAZ (FG)	190	182	189	29. Parent Metal	165	173	170
5. HAZ (FG)	187	188	191	30. Parent Metal	170	173	176
6. HAZ (FG)	203	199	195	31. HAZ (FG)	186	183	175
7. HAZ (FG)	214	199	198	32. HAZ (FG)	202	196	197
8. HAZ (CG)	211	214	223	33. HAZ (FG)	209	220	211
9. HAZ (CG)	226	180	230	34. HAZ (FG)	230	237	214
10. HAZ (CG)	220	208	232	35. HAZ (CG)	231	211	236
11. Weld Metal	255	229	230	36. HAZ (CG)	202	235	231
12. Weld Metal	237	225	227	37. HAZ (CG)	238	258	237
13. Weld Metal	239	224	216	38. Weld Metal	235	238	240
14. Weld Metal	242	208	219	39. Weld Metal	244	234	238
15. Weld Metal	200	226	235	40. Weld Metal	229	241	231
16. Weld Metal	224	223	232	41. HAZ (CG)	238	246	227
17. Weld Metal	222	224	237	42. HAZ (CG)	238	236	228
18. HAZ (CG)	222	220	229	43. HAZ (CG)	203	211	226
19. HAZ (CG)	197	211	216	44. HAZ (FG)	211	203	204
20. HAZ (CG)	213	223	229	45. HAZ (FG)	210	208	208
21. HAZ (FG)	204	195	208	46. HAZ (FG)	161	203	211
22. HAZ (FG)	207	189	199	47. HAZ (FG)	195	180	199
23. HAZ (FG)	203	195	193	48. Parent Metal	177	175	171
24. HAZ (FG)	196	214	198	49. Parent Metal	166	169	164
25. Parent Metal	186	180	179	50. Parent Metal	179	181	172

TABLE 40

HARDNESS TEST RESULTS FOR C-Mn-Ti-B/87.5Ar-10He-2CO_2-0.5H_2

Type of Test: Vickers Microhardness (500 gram load, 15 sec. time)

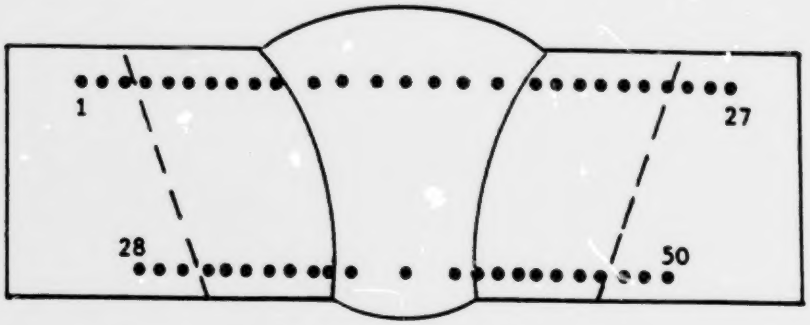

FG - Fine Grain
CG - Coarse Grain

	MICRO #		
LOCATION	1 HVN	2 HVN	3 HVN
1. Parent Metal	188	177	171
2. Parent Metal	186	179	178
3. Parent Metal	169	168	182
4. HAZ (FG)	181	187	199
5. HAZ (FG)	178	191	210
6. HAZ (FG)	180	201	190
7. HAZ (FG)	182	207	185
8. HAZ (CG)	224	224	223
9. HAZ (CG)	204	224	216
10. HAZ (CG)	217	238	220
11. Weld Metal	245	247	248
12. Weld Metal	228	234	245
13. Weld Metal	231	253	245
14. Weld Metal	240	249	238
15. Weld Metal	239	234	248
16. Weld Metal	238	234	239
17. Weld Metal	236	248	246
18. HAZ (CG)	228	216	226
19. HAZ (CG)	211	226	233
20. HAZ (CG)	209	205	205
21. HAZ (FG)	201	193	202
22. HAZ (FG)	180	196	180
23. HAZ (FG)	182	187	191
24. HAZ (FG)	174	184	180
25. Parent Metal	173	165	160
26. Parent Metal	175	173	172
27. Parent Metal	168	169	163
28. Parent Metal	161	174	176
29. Parent Metal	172	169	180
30. Parent Metal	177	186	174
31. HAZ (FG)	187	187	188
32. HAZ (FG)	197	189	192
33. HAZ (FG)	197	193	206
34. HAZ (FG)	211	222	210
35. HAZ (CG)	223	238	229
36. HAZ (CG)	223	235	236
37. HAZ (CG)	231	232	224
38. Weld Metal	258	275	264
39. Weld Metal	277	273	259
40. Weld Metal	266	276	231
41. HAZ (CG)	234	226	228
42. HAZ (CG)	225	228	231
43. HAZ (CG)	227	217	214
44. HAZ (FG)	197	190	198
45. HAZ (FG)	186	188	193
46. HAZ (FG)	184	189	196
47. HAZ (FG)	189	187	178
48. Parent Metal	171	175	169
49. Parent Metal	178	172	158
50. Parent Metal	176	179	172

TABLE 41

SUMMARY OF WELD-METAL HARDNESS TEST RESULTS

Shielding Gas: $95Ar-5CO_2$

Electrode	Weld Metal Hardness Hv 0.5 kg	
	Subsurface	Root
C-Mn-Si	195 - 268 220	236 - 258 250
LowC-Mn-Si	158 - 228 187	220 - 249 234
C-Mn-Si-Ti	172 - 235 212	222 - 282 248
C-Mn-Ti-B	218 - 255 237	278 - 294 283
C-Mn-Ni	203 - 267 231	253 - 288 273
C-Mn-Ni-Ti	194 - 258 242	219 - 309 273
C-Mn-Mo	266 - 302 284	262 - 313 297
C-Mn-Mo-Ti	224 - 267 244	240 - 282 265

TABLE 41 (cont)

Shielding Gas: $88Ar-10He-2CO_2$

Electrode	Weld Metal Hardness Hv 0.5 kg	
	Subsurface	Root
C-Mn-Si	198 - 239 221	237 - 286 253
C-Mn-Ti-B	211 - 254 241	258 - 287 274

Shielding Gas: $87.5Ar-10He-2CO_2-0.5H_2$

Electrode	Weld Metal Hardness Hv 0.5 kg	
	Subsurface	Root
C-Mn-Si	200 - 255 227	229 - 244 237
C-Mn-Ti-B	228 - 249 241	231 - 277 264

TABLE 42

ALL-WELD-METAL TENSILE PROPERTIES

a) SHIELDING GAS: $95Ar-5CO_2$

Electrode	YS MPa	UTS MPa	Elong. %	RA %
C-Mn-Si	547	666	27	66
	547	667	28	65
LowC-Mn-Si	520	615	25	66
	480	582	28	69
C-Mn-Si-Ti	591	677	28	68
	596	682	28	65
C-Mn-Ti-B	642	707	24	71
	611	681	25	71
C-Mn-Ni	540	664	26	55
	523	643	29	67
C-Mn-Ni-Ti	648	750	25	63
	643	746	25	62
C-Mn-Mo	773	868	23	43
	750	847	24	61
C-Mn-Mo-Ti	682	758	24	71
	649	730	24	67

TABLE 42 (cont)

b) SHIELDING GAS: 88Ar-10He-$2CO_2$

Electrode	YS MPa	UTS MPa	Elong. %	RA %
C-Mn-Si	528	669	29	62
	532	671	29	63
C-Mn-Ti-B	637	731	27	71
	631	727	26	71

c) SHIELDING GAS: 87.5Ar-10He-$2CO_2$-$0.5H_2$

Electrode	YS MPa	UTS MPa	Elong. %	RA %
C-Mn-Si	546	684	26	44
	539	673	25	31
C-Mn-Ti-B	625	735	27	72
	635	742	26	70

TABLE 43

CHARPY IMPACT TEST RESULTS FOR C-Mn-Si/95Ar-5CO_2

Temperature °C	Location	Cv Energy J	Shear Area %
50	Subsurface	120	79
50	"	124	83
50	"	150	86
20	"	90	56
20	"	64	59
20	"	90	74
-30	"	45	10
-30	"	36	10
-30	"	16	5
-45	"	19	10
-45	"	22	10
-45	"	15	10
-60	"	9	5
-60	"	11	5
-60	"	9	5
-45	Root	42	10
-45	"	32	15
-45	"	26	10

TABLE 44

CHARPY IMPACT TEST RESULTS FOR LowC-Mn-Si/95Ar-5CO_2

Temperature °C	Location	Cv Energy J	Shear Area %
20	Subsurface	162	69
20	"	128	67
20	"	172	70
- 5	"	73	50
- 5	"	162	69
- 5	"	140	65
-30	"	100	25
-30	"	41	10
-30	"	64	5
-45	"	49	5
-45	"	79	12
-45	"	29	5
-60	"	48	5
-60	"	9	5
-60	"	18	5
-45	Root	36	16
-45	"	27	10
-45	"	26	11

TABLE 45

CHARPY IMPACT TEST RESULTS FOR C-Mn-Si-Ti/95Ar-5CO_2

Temperature °C	Location	Cv Energy J	Shear Area %
- 5	Subsurface	190	65
- 5	"	190	69
- 5	"	230	82
-30	"	146	56
-30	"	134	56
-30	"	177	69
-45	"	68	31
-45	"	98	36
-45	"	80	31
-60	"	41	15
-60	"	66	15
-60	"	80	10
-75	"	40	30
-75	"	19	16
-75	"	36	30
-45	Root	56	23
-45	"	39	25
-45	"	56	20

TABLE 46

CHARPY IMPACT TEST RESULTS FOR C-Mn-Ti-B/95Ar-5CO_2

Temperature °C	Location	Cv Energy J	Shear Area %
-30	Subsurface	287	100
-30	"	229	78
-30	"	192	75
-45	"	181	56
-45	"	155	52
-45	"	188	62
-60	"	79	40
-60	"	134	36
-60	"	84	33
-75	"	42	43
-75	"	34	44
-75	"	29	44
-90	"	20	20
-90	"	31	30
-90	"	28	20
-45	Root	170	55
-45	"	140	50
-45	"	158	61

TABLE 47

CHARPY IMPACT TEST RESULTS FOR C-Mn-Ni/95Ar-5CO_2

Temperature °C	Location	Cv Energy J	Shear Area %
20	Subsurface	152	95
20	"	122	70
20	"	130	85
- 5	"	100	56
- 5	"	100	67
- 5	"	105	67
-30	"	56	40
-30	"	39	47
-30	"	53	44
-45	"	39	35
-45	"	25	21
-45	"	32	31
-60	"	21	20
-60	"	22	15
-60	"	22	16
-45	Root	29	39
-45	"	32	34
-45	"	30	43

TABLE 48

CHARPY IMPACT TEST RESULTS FOR C-Mn-Ni-Ti/95Ar-5CO_2

Temperature °C	Location	Cv Energy J	Shear Area %
20	Subsurface	192	77
20	"	160	75
20	"	160	80
- 5	"	190	67
- 5	"	138	62
- 5	"	158	63
-30	"	120	50
-30	"	95	47
-30	"	112	36
-45	"	51	21
-45	"	49	11
-45	"	49	17
-60	"	36	5
-60	"	38	15
-60	"	36	5
-45	Root	31	26
-45	"	14	25
-45	"	32	16

TABLE 49

CHARPY IMPACT TEST RESULTS FOR C-Mn-Mo/95Ar-5CO_2

Temperature °C	Location	Cv Energy J	Shear Area %
20	Subsurface	90	66
20	"	98	72
20	"	94	69
- 5	"	62	69
- 5	"	56	47
- 5	"	52	47
-30	"	46	43
-30	"	42	30
-30	"	41	39
-45	"	34	15
-45	"	34	20
-45	"	32	26
-60	"	16	15
-60	"	30	10
-60	"	24	10
-45	Root	32	25
-45	"	35	20
-45	"	41	30

TABLE 50

CHARPY IMPACT TEST RESULTS FOR C-Mn-Mo-Ti/95Ar-5CO_2

Temperature °C	Location	Cv Energy J	Shear Area %
50	Subsurface	182	85
50	"	189	72
50	"	190	88
20	"	118	65
20	"	140	70
20	"	122	59
-30	"	21	5
-30	"	55	11
-30	"	22	20
-45	"	10	5
-45	"	9	5
-45	"	9	5
-60	"	16	5
-60	"	10	5
60	"	6	5
-45	Root	12	5
-45	"	11	10
-45	"	7	5

TABLE 51

CHARPY IMPACT TEST RESULTS FOR C-Mn-Si/88Ar-10He-2CO_2

Temperature °C	Location	Cv Energy J	Shear Area %
20	Subsurface	110	72
20	"	84	70
20	"	111	72
- 5	"	96	50
- 5	"	78	42
- 5	"	75	45
-30	"	19	30
-30	"	38	30
-30	"	43	39
-45	"	38	31
-45	"	30	31
-45	"	12	26
-60	"	14	21
-60	"	14	11
-60	"	15	20
-45	Root	29	17
-45	"	32	30
-45	"	29	25

TABLE 52

CHARPY IMPACT TEST RESULTS FOR C-Mn-Ti-B/88Ar-10He-2CO_2

Temperature °C	Location	Cv Energy J	Shear Area %
20	Subsurface	250	90
20	"	220	86
20	"	252	95
- 5	"	192	72
- 5	"	240	79
- 5	"	180	75
-30	"	80	36
-30	"	70	36
-30	"	31	26
-45	"	33	31
-45	"	83	27
-45	"	26	36
-60	"	20	31
-60	"	25	20
-60	"	24	31
-45	Root	98	58
-45	"	86	53
-45	"	--	--

TABLE 53

CHARPY IMPACT TEST RESULTS FOR C-Mn-Si/87.5Ar-10He-2CO_2-0.5H_2

Temperature °C	Location	Cv Energy J	Shear Area %
20	Subsurface	101	59
20	"	102	59
20	"	82	59
- 5	"	68	56
- 5	"	80	47
- 5	"	70	45
-30	"	39	44
-30	"	48	40
-30	"	44	39
-45	"	29	31
-45	"	22	35
-45	"	30	31
-60	"	12	20
-60	"	25	20
-60	"	19	16
-45	Root	48	39
-45	"	46	39
-45	"	50	34

TABLE 54

CHARPY IMPACT TEST RESULTS FOR C-Mn-Ti-B/87.5Ar-10He-$2CO_2$-$0.5H_2$

Temperature °C	Location	Cv Energy J	Shear Area %
20	Subsurface	194	81
20	"	89	55
20	"	190	72
- 5	"	142	52
- 5	"	94	50
- 5	"	72	55
-30	"	64	40
-30	"	28	45
-30	"	35	40
-45	"	48	44
-45	"	27	35
-45	"	36	50
-60	"	20	26
-60	"	27	26
-60	"	15	21
-45	Root	86	48
-45	"	24	47
-45	"	34	44

TABLE 55

CTOD TEST RESULTS

a) Shielding Gas: $95Ar-5CO_2$

Electrode	CTOD at -45°C mm
C-Mn-Si	0.050, 0.088, 0.056
LowC-Mn-Si	0.038, 0.033, 0.029
C-Mn-Si-Ti	0.060, 0.051, 0.069
C-Mn-Ti-B	0.321*, 0.294*, 0.083
C-Mn-Ni	0.040, 0.037, -
C-Mn-Ni-Ti	0.033, 0.038, 0.052
C-Mn-Mo	0.020, 0.034, 0.039
C-Mn-Mo-Ti	0.040, 0.028, 0.021

Asterisk indicates δ_u: all other values δ_c

TABLE 55 (cont)

b) Shielding Gas: 88Ar-10He-2CO_2

Electrode	CTOD at -45°C mm
C-Mn-Si	0.055, 0.046, 0.036
C-Mn-Ti-B	0.063, 0.066, 0.047

c) Shielding Gas: 87.5Ar-10He-2CO_2-0.5H_2

Electrode	CTOD at -45°C mm
C-Mn-Si	0.161*, 0.124*, 0.137*
C-Mn-Ti-B	0.054, 0.056, 0.050

Asterisk indicates δ_u: all other values δ_c

TABLE 56

CTOD TEST RESULTS

EFFECT OF WELDING PROCEDURE WITH C-Mn-Ti-B/95Ar-5CO_2

Procedure	CTOD at -45°C mm
SMAW full penetration root, PGMAW fills & cap	0.147*, 0.141*, 0.150*
PGMAW full penetration root, PGMAW fills & cap	0.683*, 0.189*, 0.157*
PGMAW full penetration root, low heat input PGMAW fills & cap	0.201*, 0.238*, 0.107

Asterisk indicates δ_u: all other values δ_c

TABLE 57

PROPORTION OF REFINED MICROSTRUCTURE IN NOTCH PLANE OF IMPACT TESTPIECES

SHIELDING GAS: 95Ar-5CO_2

Electrode	Location	% Refined Microstructure
C-Mn-Si	Subsurface	51
	Root	35
LowC-Mn-Si	Subsurface	59
	Root	34
C-Mn-Si-Ti	Subsurface	42
	Root	35
C-Mn-Ti-B	Subsurface	41
	Root	14
C-Mn-Ni	Subsurface	47
	Root	45
C-Mn-Ni-Ti	Subsurface	40
	Root	20
C-Mn-Mo	Subsurface	5
	Root	5
C-Mn-Mo-Ti	Subsurface	12
	Root	13

SHIELDING GAS: 88Ar-10He-2CO_2

C-Mn-Si	Subsurface	21
	Root	29
C-Mn-Ti-B	Subsurface	26
	Root	15

SHIELDING GAS: 87.5Ar-10He-2CO_2-0.5H_2

C-Mn-Si	Subsurface	29
	Root	31
C-Mn-Ti-B	Subsurface	38
	Root	20

TABLE 58

VALUES OF CONSTANTS α AND β DETERMINED FROM FIGURE 46

	100 A	150 A	200 A
$95Ar-5CO_2$			
α, mm A^{-1} s^{-1}	0.38	0.37	0.37
β, A^{-2} s^{-1}	3.96×10^{-5}	5.25×10^{-5}	5.87×10^{-5}
$80Ar-20CO_2$			
α	0.44	0.37	0.35
β	3.54×10^{-5}	5.22×10^{-5}	6.23×10^{-5}
$88Ar-10He-2CO_2$			
α	0.39	0.41	0.34
β	3.75×10^{-5}	4.15×10^{-5}	6.40×10^{-5}
$87.5Ar-10He-2CO_2-0.5H_2$			
α	0.36	0.40	0.34
β	4.77×10^{-5}	3.68×10^{-5}	6.25×10^{-5}

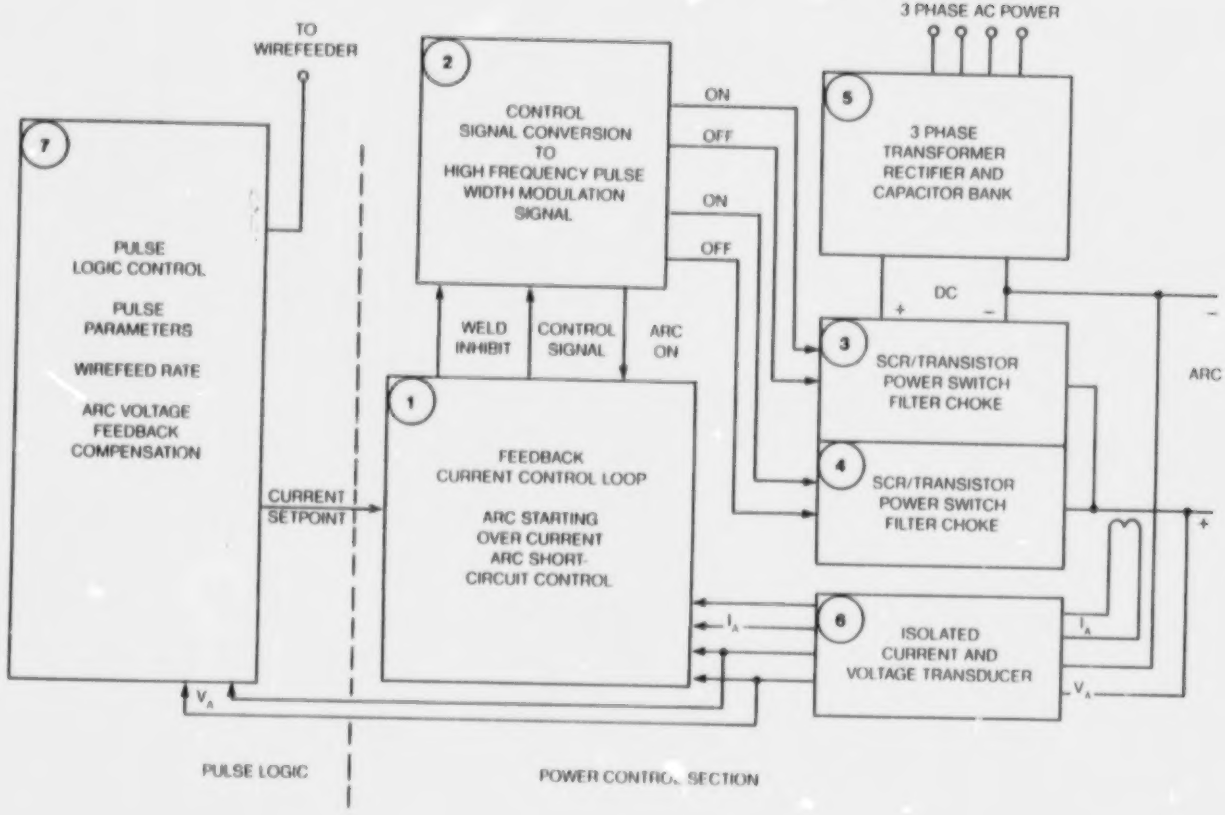
TO WIREFEEDER
3 PHASE AC POWER
7
PULSE LOGIC CONTROL
PULSE PARAMETERS
WIREFEED RATE
ARC VOLTAGE FEEDBACK COMPENSATION
2
CONTROL SIGNAL CONVERSION TO HIGH FREQUENCY PULSE WIDTH MODULATION SIGNAL
ON
OFF
ON
OFF
5
3 PHASE TRANSFORMER RECTIFIER AND CAPACITOR BANK
DC
+
−
WELD INHIBIT
CONTROL SIGNAL
ARC ON
1
FEEDBACK CURRENT CONTROL LOOP
ARC STARTING OVER CURRENT ARC SHORT-CIRCUIT CONTROL
3
SCR/TRANSISTOR POWER SWITCH FILTER CHOKE
4
SCR/TRANSISTOR POWER SWITCH FILTER CHOKE
−
ARC
+
CURRENT SETPOINT
6
ISOLATED CURRENT AND VOLTAGE TRANSDUCER
I_A
I_A
V_A
V_A
PULSE LOGIC
POWER CONTRO. SECTION

Figure 1: GEC M450PS Programmable/Synergic Pulsed GMAW Power Source

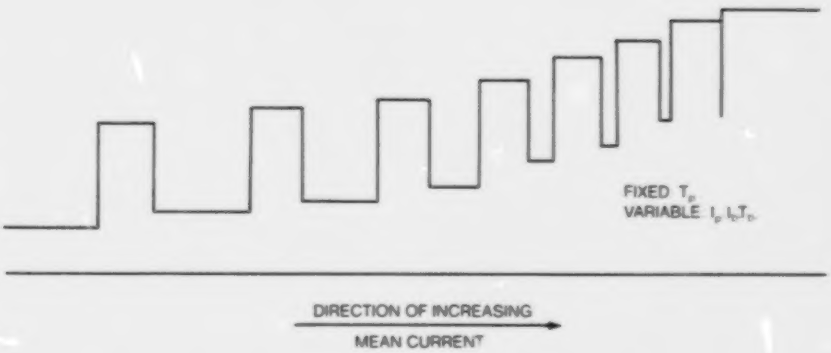
FIXED T_p
VARIABLE I_p I_b T_b
DIRECTION OF INCREASING
MEAN CURRENT

Figure 2: M450PS Original Synergic Waveform

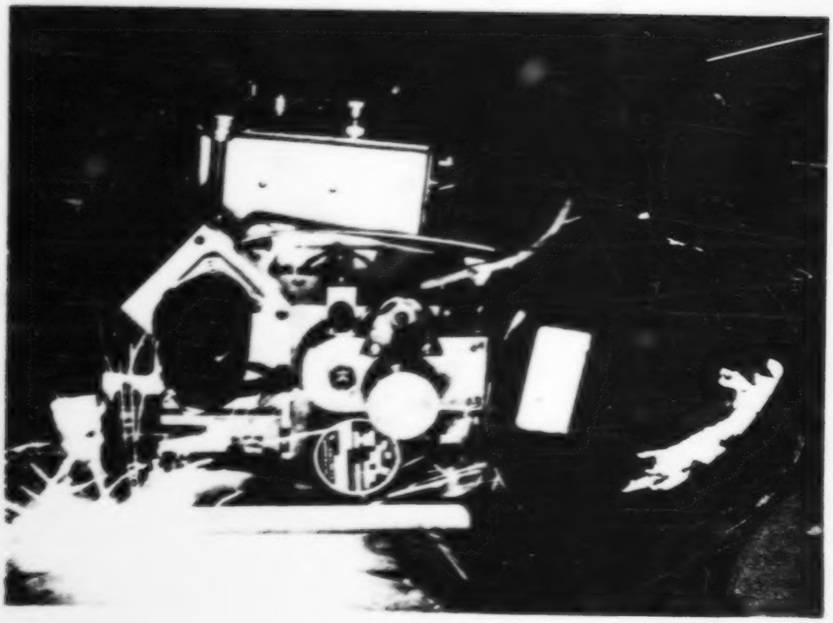

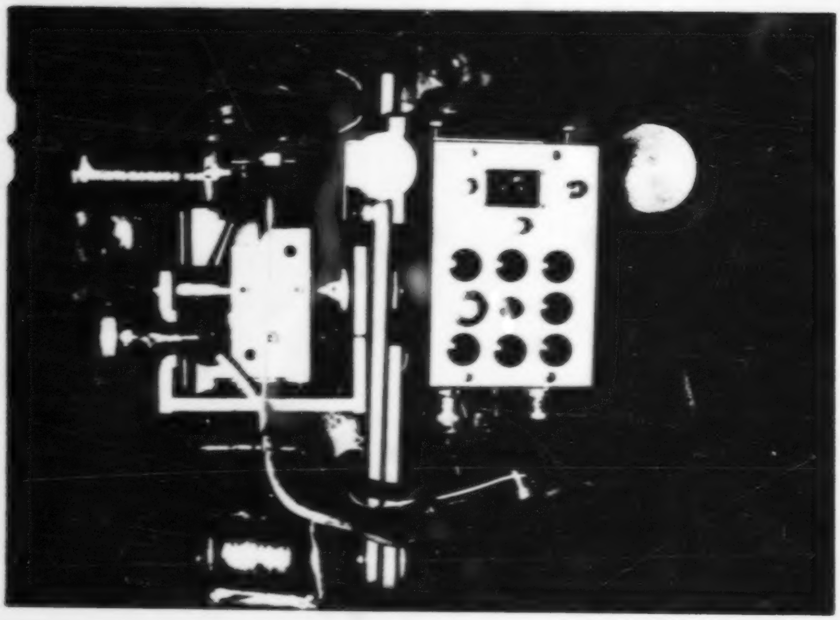

Figure 3: CRC Model M-200 Mechanized Welding System

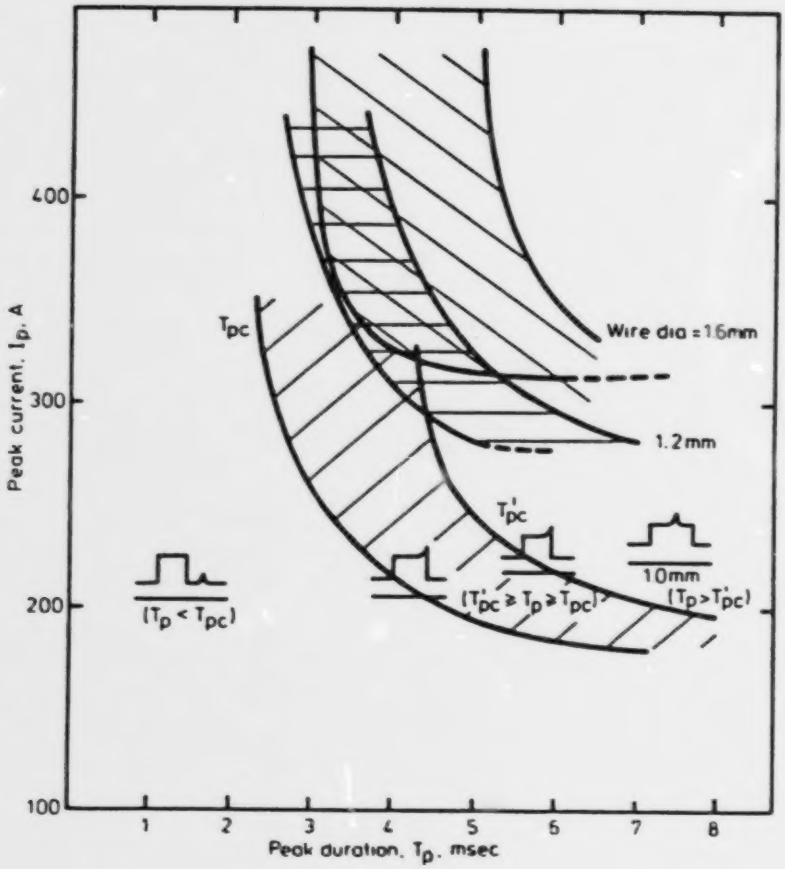

Figure 4: Influence of Peak Parameters on Droplet Detachment for Mild Steel Wire in Argon/5%CO_2 [After Allum (5)]

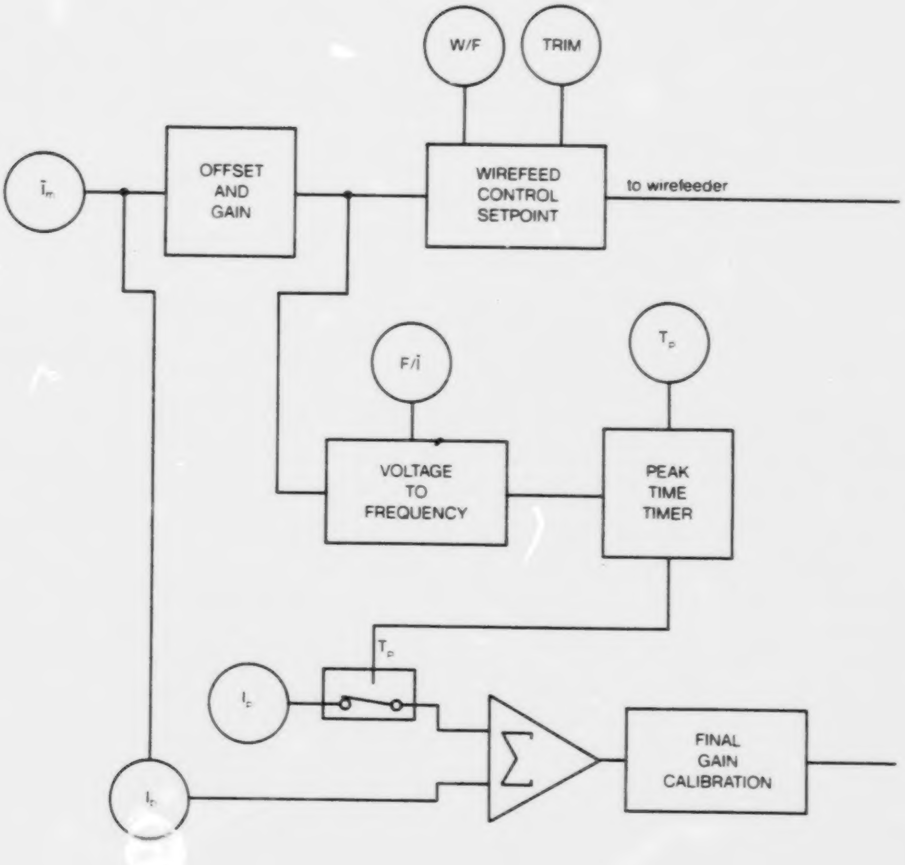
W/F
TRIM
Ī_m
OFFSET AND GAIN
WIREFEED CONTROL SETPOINT
to wirefeeder
F/Ī
T_p
VOLTAGE TO FREQUENCY
PEAK TIME TIMER
T_p
I_p
Σ
FINAL GAIN CALIBRATION
I_b

Figure 5: M450PS Original Synergic Pulse Logic Circuit

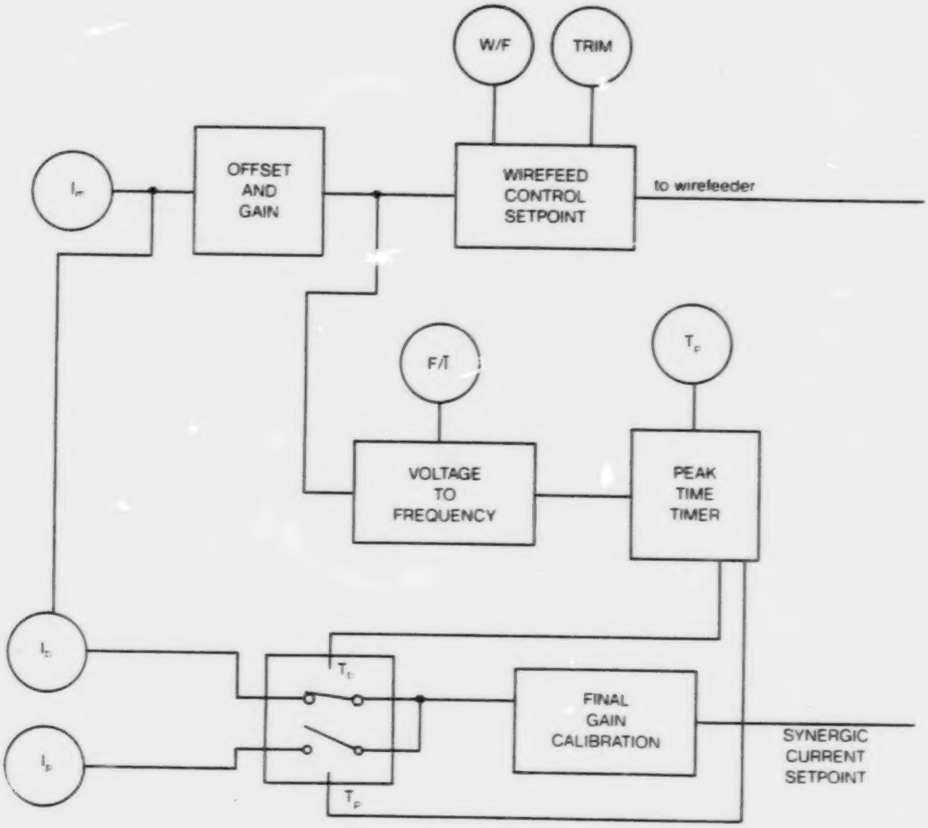
W/F
TRIM
I_m
OFFSET AND GAIN
WIREFEED CONTROL SETPOINT
to wirefeeder
F/T
T_p
VOLTAGE TO FREQUENCY
PEAK TIME TIMER
I_b
T_b
I_p
T_p
FINAL GAIN CALIBRATION
SYNERGIC CURRENT SETPOINT

Figure 6: M450PS Modified Synergic Pulse Logic Circuit

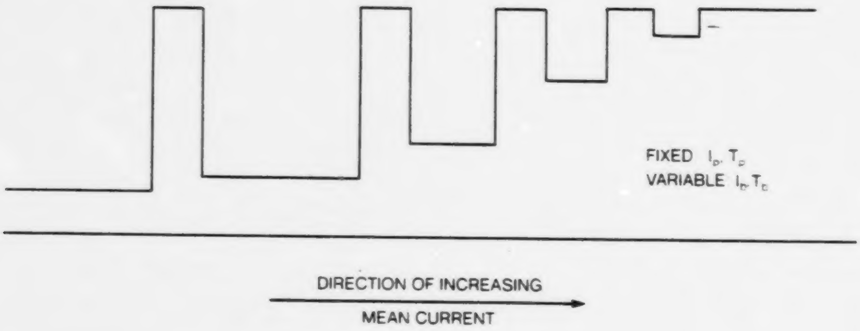
FIXED I_p, T_p
VARIABLE I_b, T_b
DIRECTION OF INCREASING
MEAN CURRENT

Figure 7: M450PS Synergic Waveform as Modified to Maintain One Drop Per Pulse

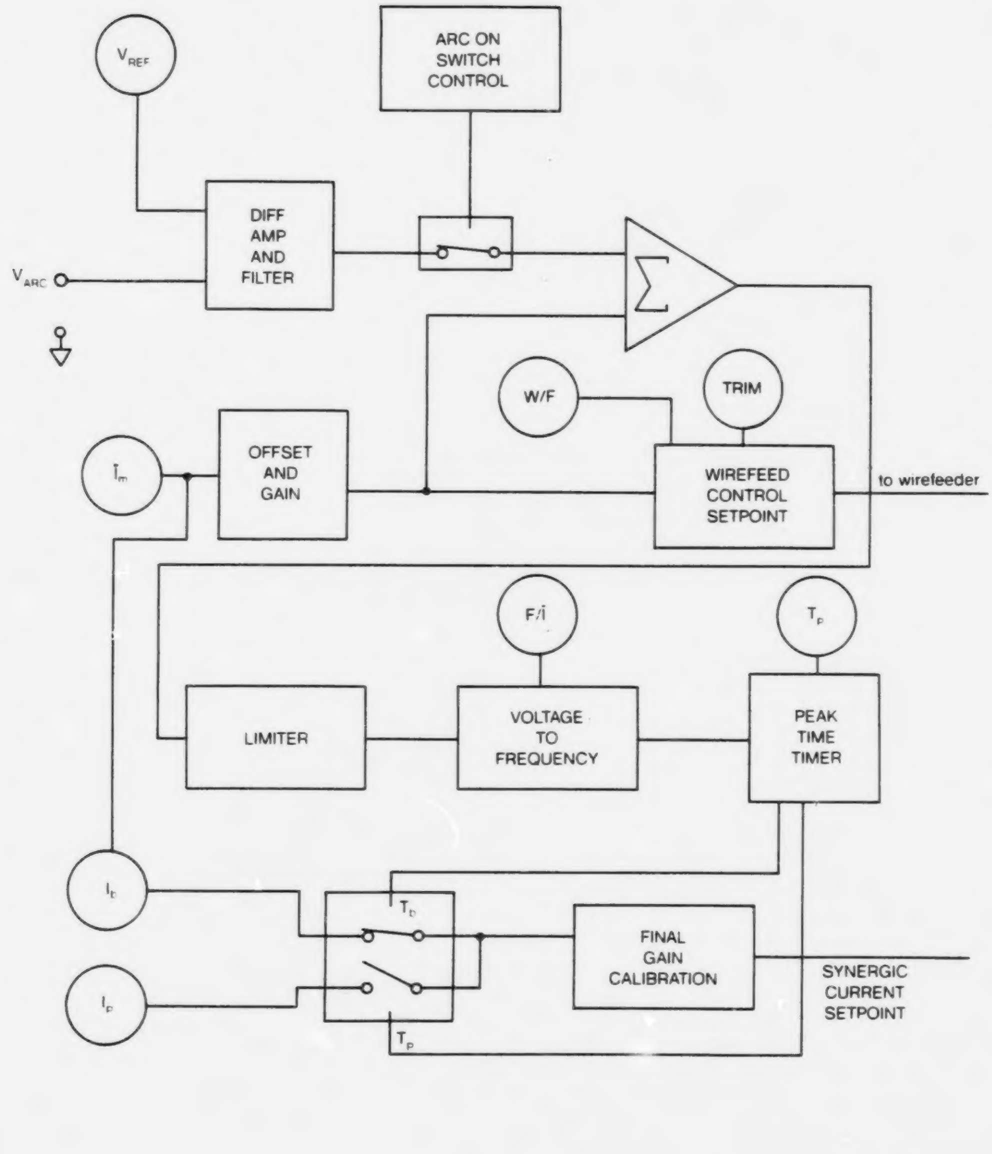

V_{REF}
ARC ON SWITCH CONTROL
DIFF AMP AND FILTER
V_{ARC}
Σ
W/F
TRIM
$\bar{I}_m$
OFFSET AND GAIN
WIREFEED CONTROL SETPOINT
to wirefeeder
F/Ī
T_p
LIMITER
VOLTAGE TO FREQUENCY
PEAK TIME TIMER
I_b
T_b
FINAL GAIN CALIBRATION
I_p
T_p
SYNERGIC CURRENT SETPOINT

Figure 8: M450PS Modified Synergic Pulse Logic Circuit with Arc Voltage Compensation

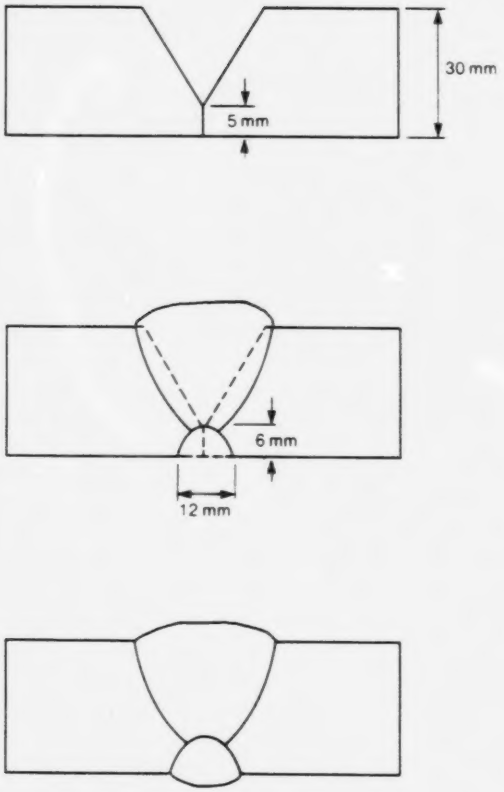
30 mm
5 mm
6 mm
12 mm

Figure 9: Edge Preparation and Backgouge Profile for LT60 Test Panels

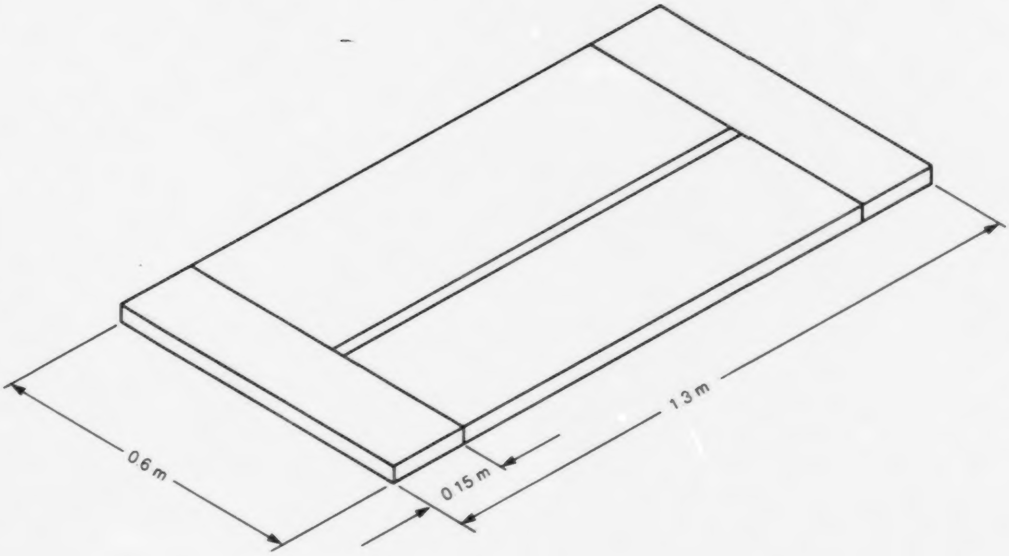
0.6 m
0.15 m
1.3 m

Figure 10: Test Panel Assembly

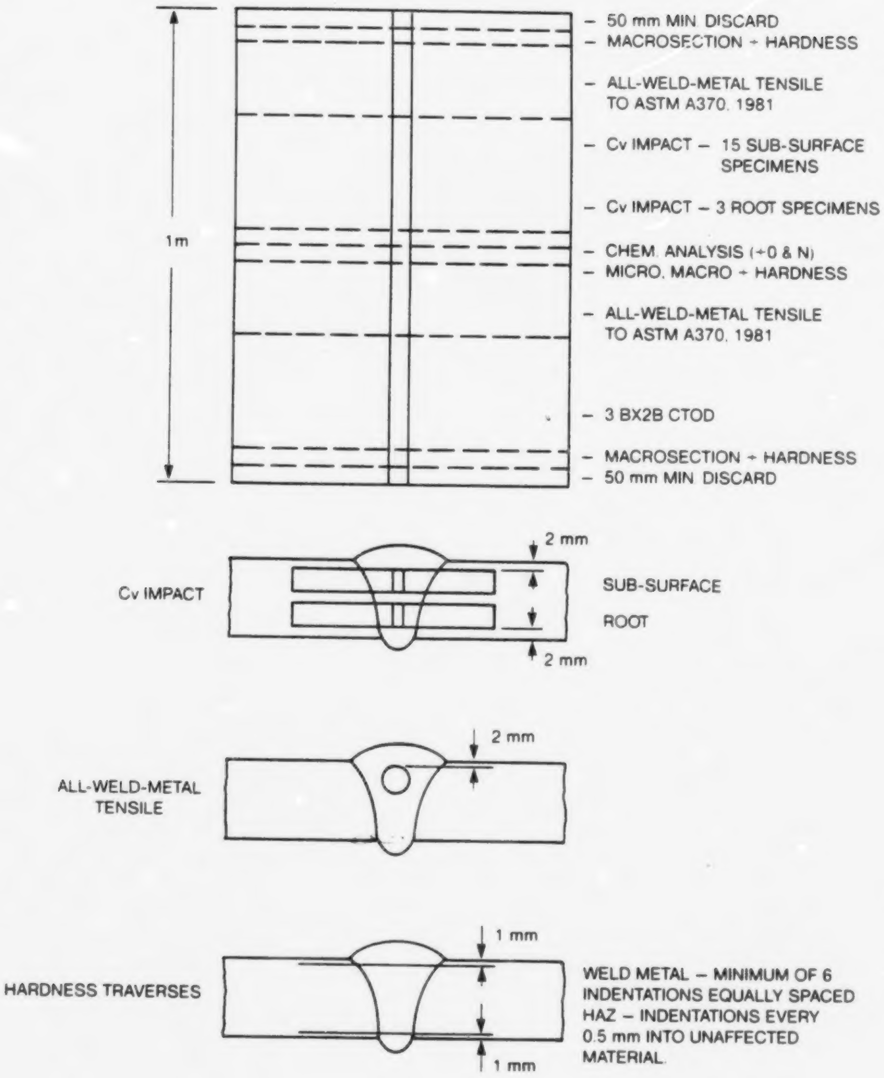
1m
– 50 mm MIN. DISCARD
– MACROSECTION + HARDNESS
– ALL-WELD-METAL TENSILE TO ASTM A370, 1981
– Cv IMPACT – 15 SUB-SURFACE SPECIMENS
– Cv IMPACT – 3 ROOT SPECIMENS
– CHEM. ANALYSIS (+O & N)
– MICRO, MACRO + HARDNESS
– ALL-WELD-METAL TENSILE TO ASTM A370, 1981
– 3 BX2B CTOD
– MACROSECTION + HARDNESS
– 50 mm MIN. DISCARD
Cv IMPACT
2 mm
SUB-SURFACE
ROOT
2 mm
ALL-WELD-METAL TENSILE
2 mm
HARDNESS TRAVERSES
1 mm
1 mm
WELD METAL – MINIMUM OF 6 INDENTATIONS EQUALLY SPACED
HAZ – INDENTATIONS EVERY 0.5 mm INTO UNAFFECTED MATERIAL.

Figure 11: Mechanical Test Specimen Locations

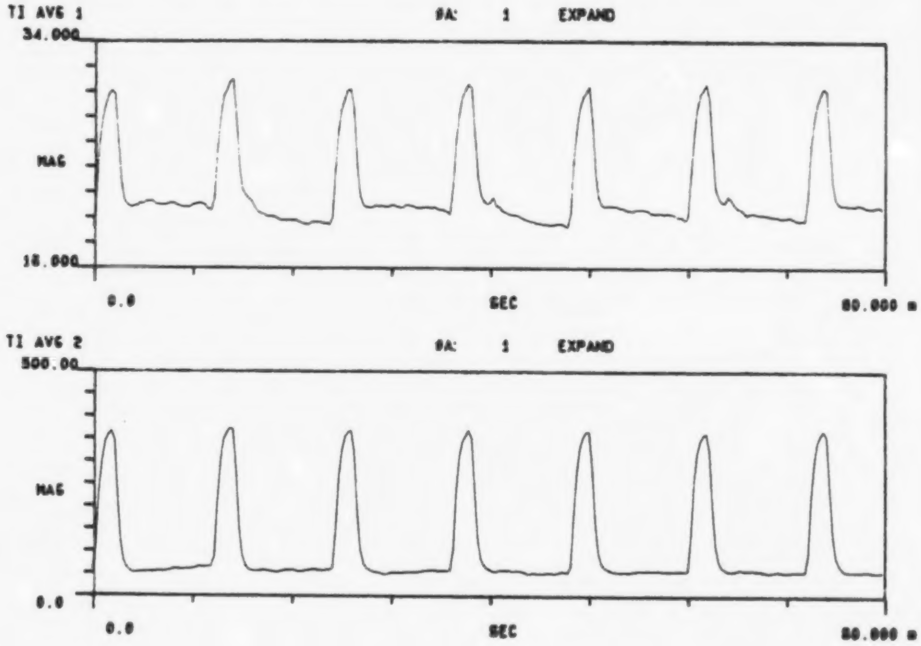

a) Tp = 2 ms

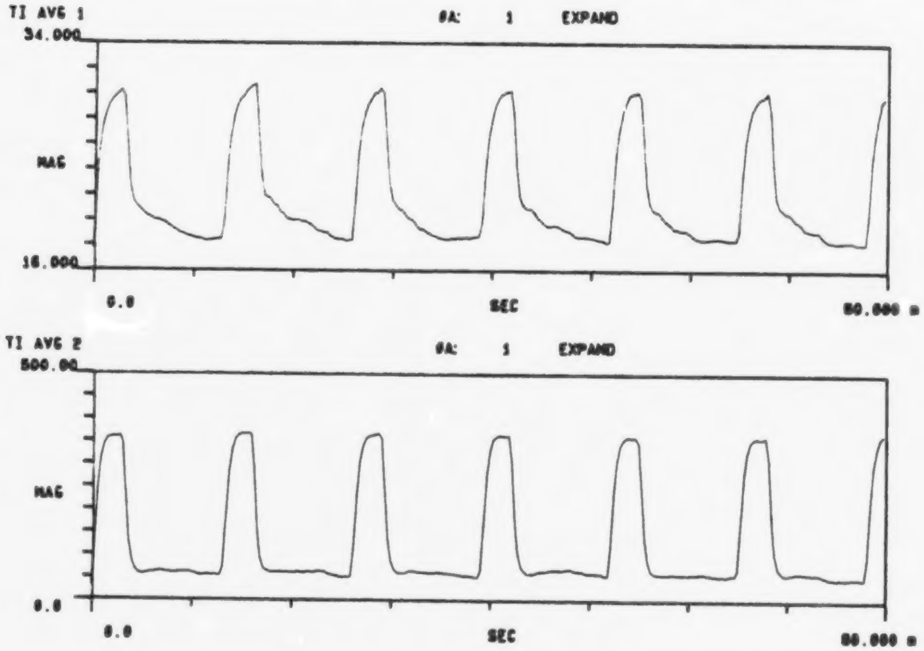

b) Tp = 3 ms

Figure 12: Typical Current and Voltage Traces: C-Mn-Mo Wire in 95Ar-5CO$_2$ Shielding Gas at 350 A Peak Current

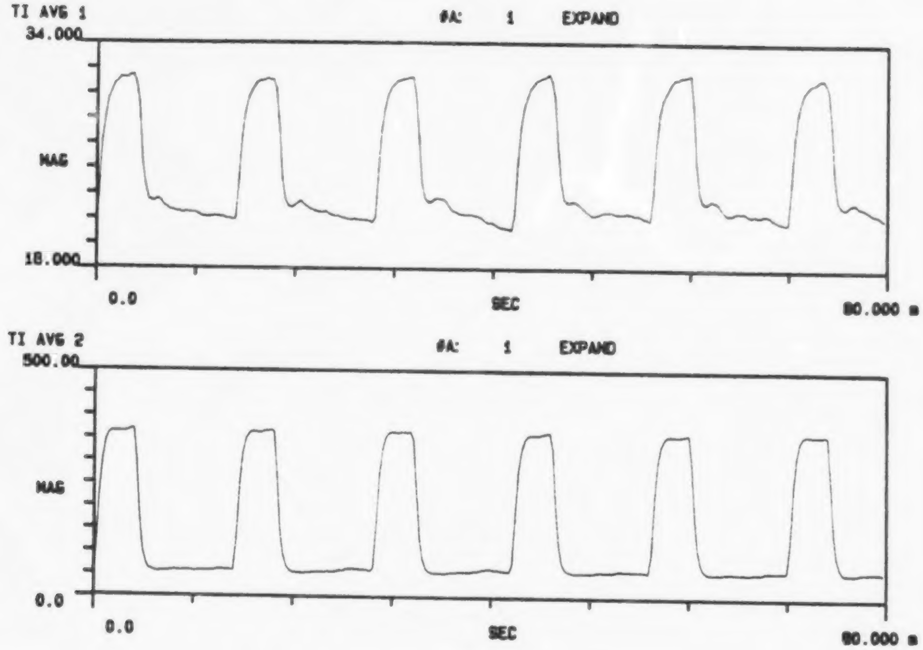

c) Tp = 4 ms

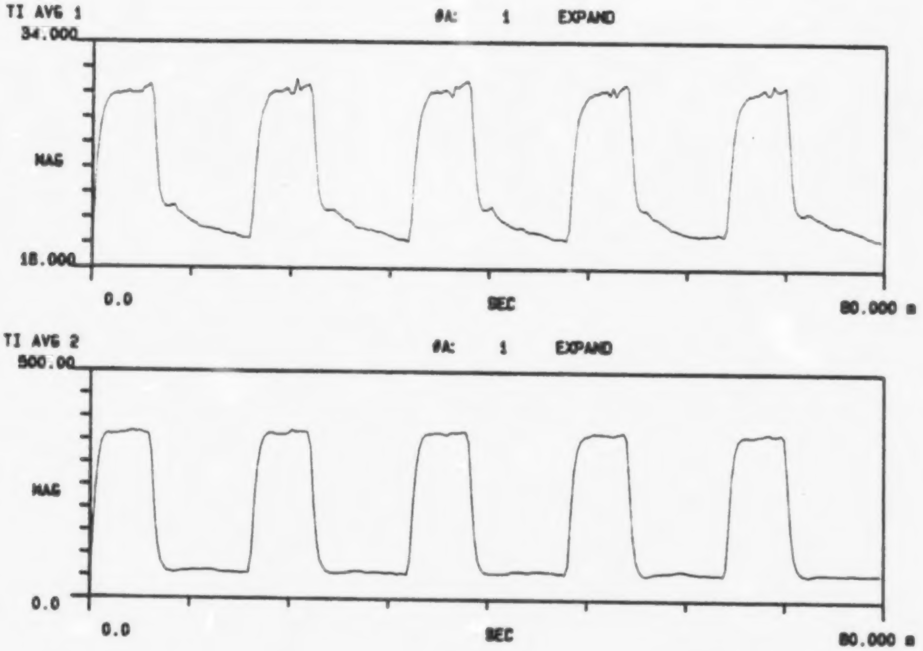

d) Tp = 6 ms

Figure 12 (cont)

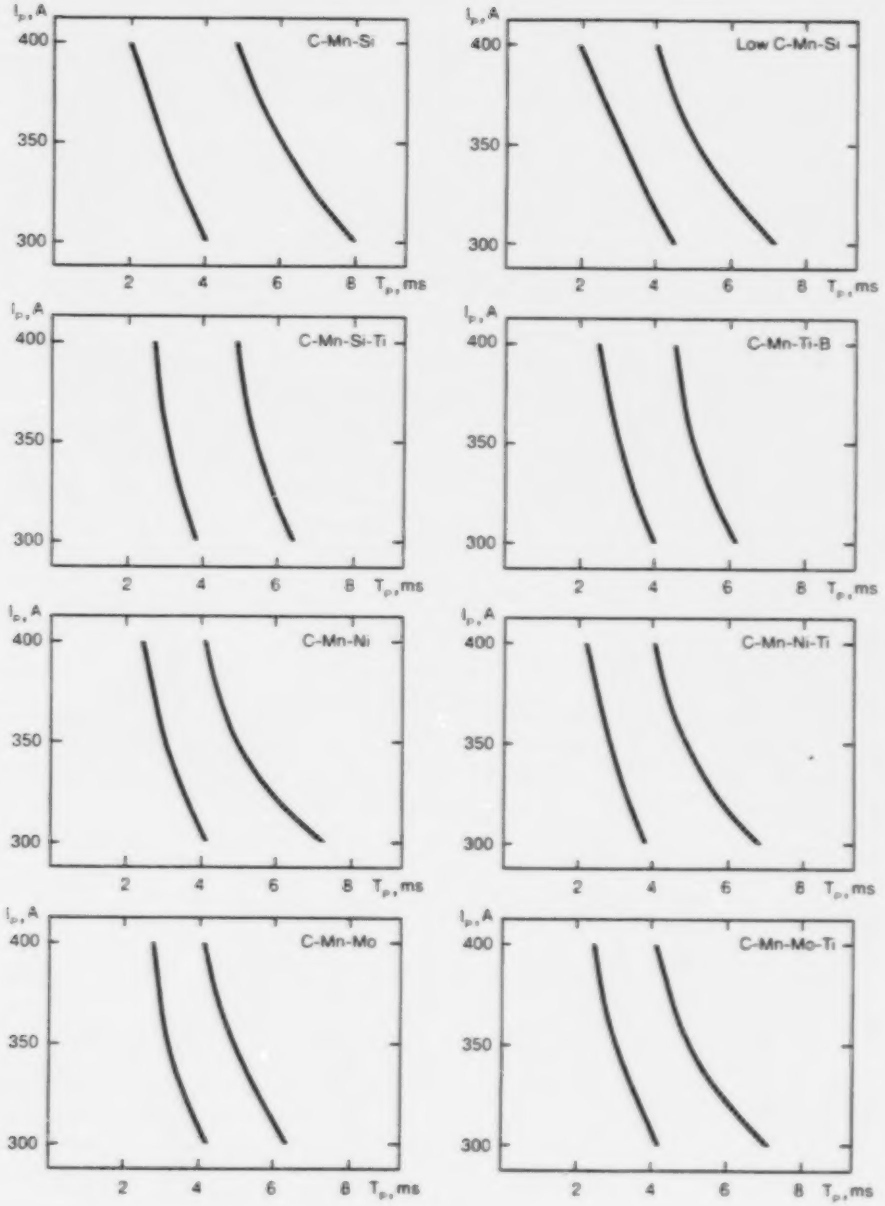

Figure 13: Zones for Stable Operation in 95Ar-5CO_2 Shielding Gas

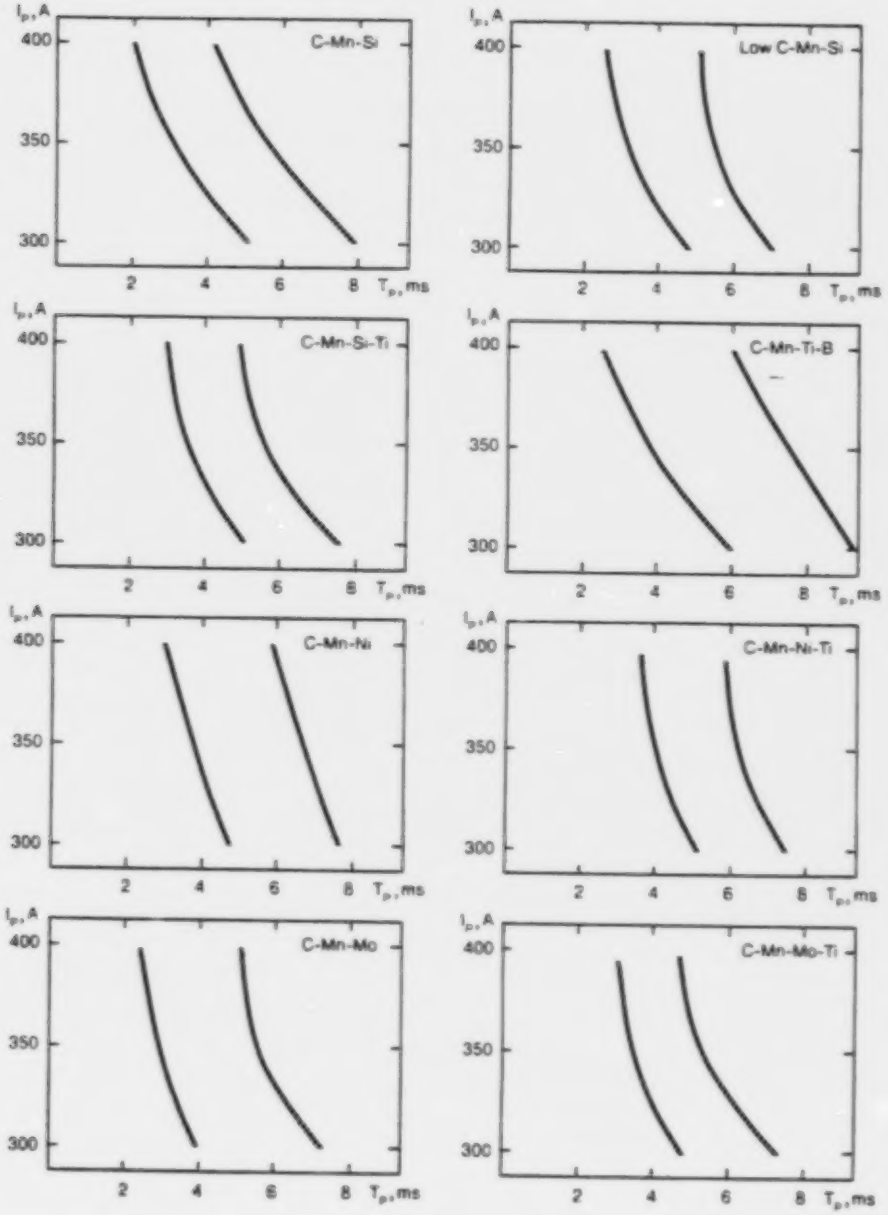

Figure 14: Zones for Stable Operation in 80Ar-20CO$_2$ Shielding Gas

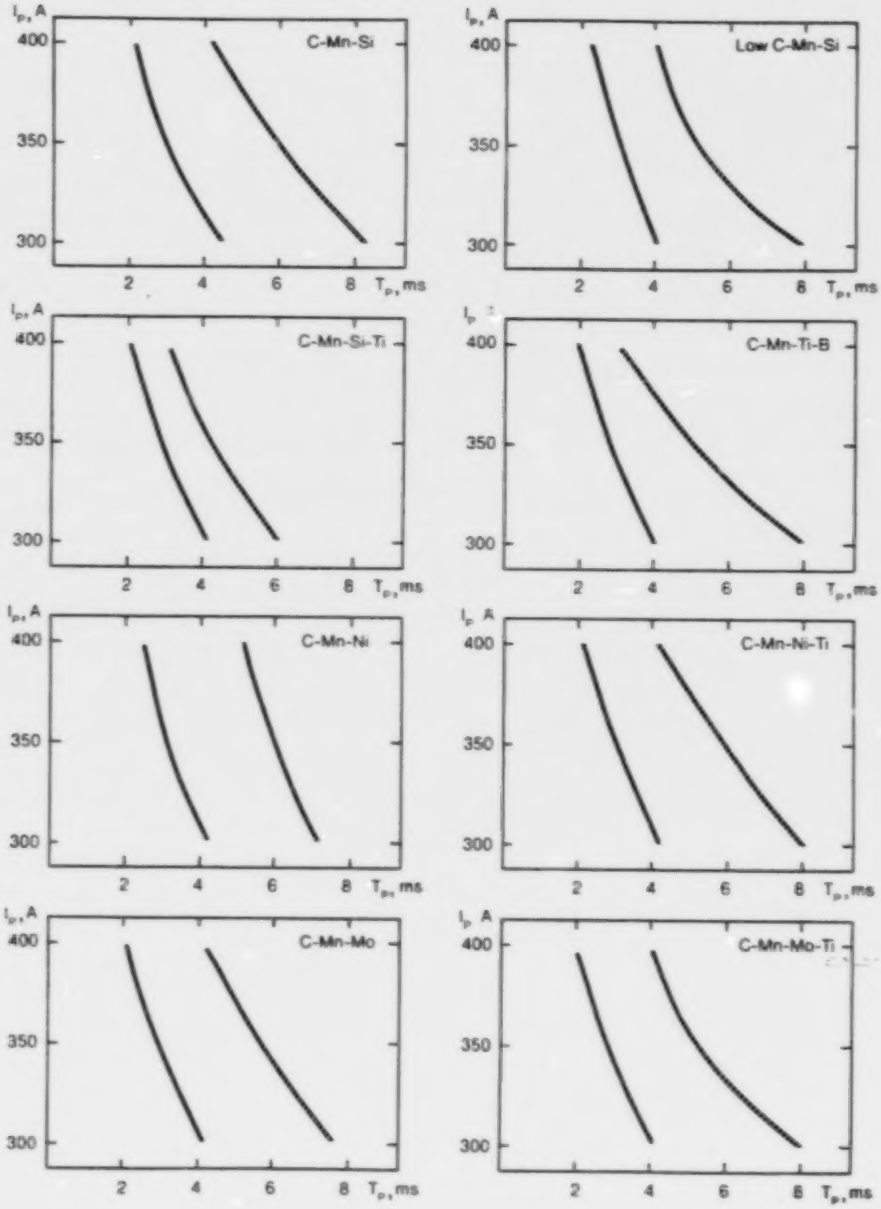

Figure 15: Zones for Stable Operation in 88Ar-10He-2CO_2 Shielding Gas

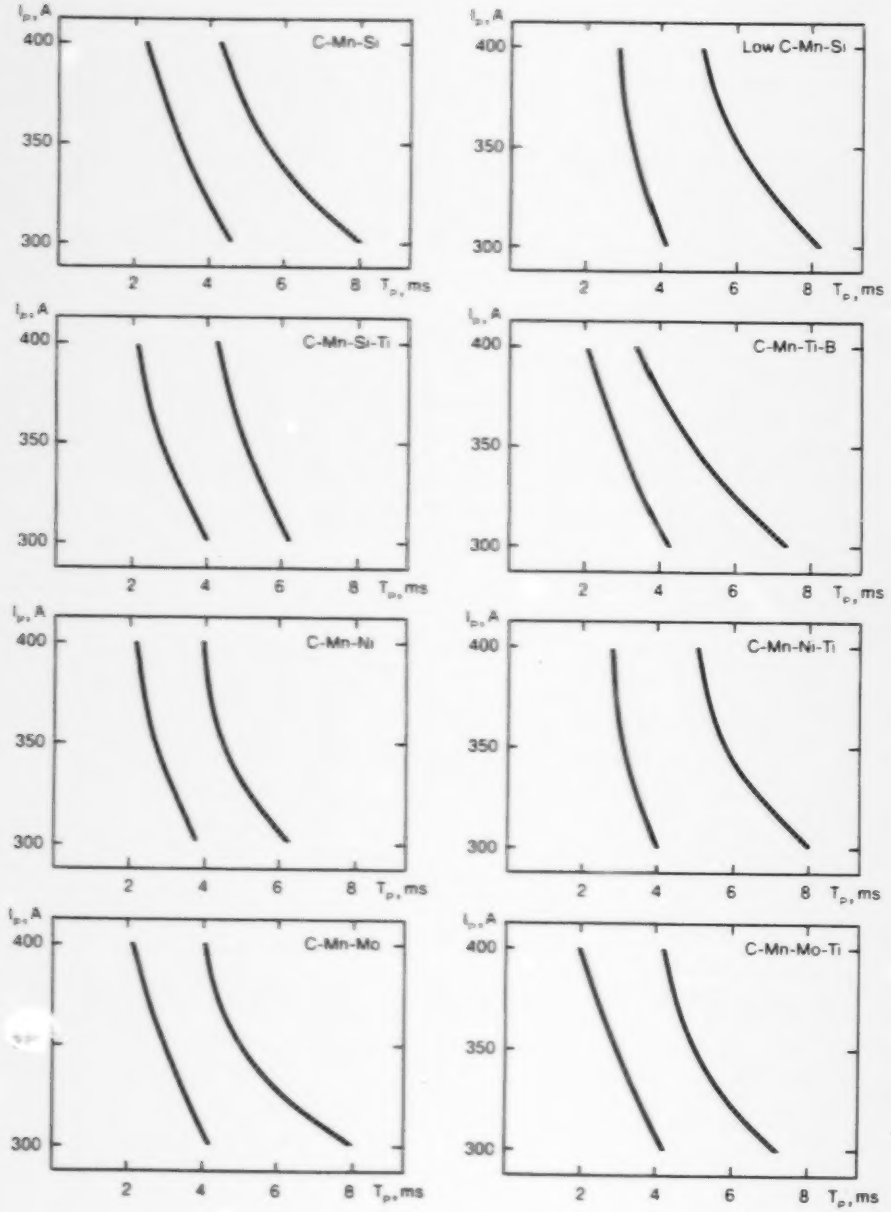

Figure 16: Zones for Stable Operation in 87.5Ar-10He-$2CO_2$-$0.5H_2$ Shielding Gas

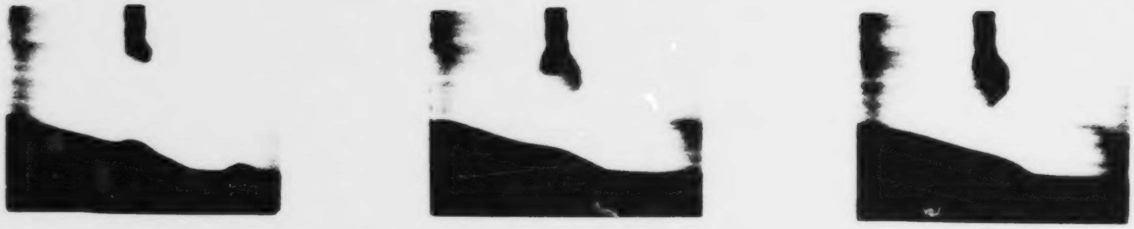

a. Tp = 2 ms

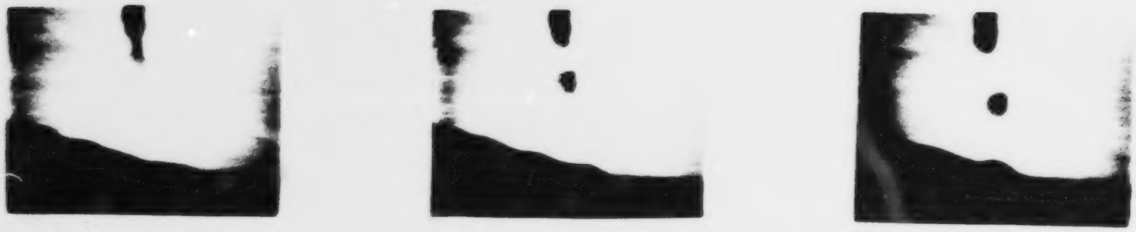

b. Tp = 3 ms

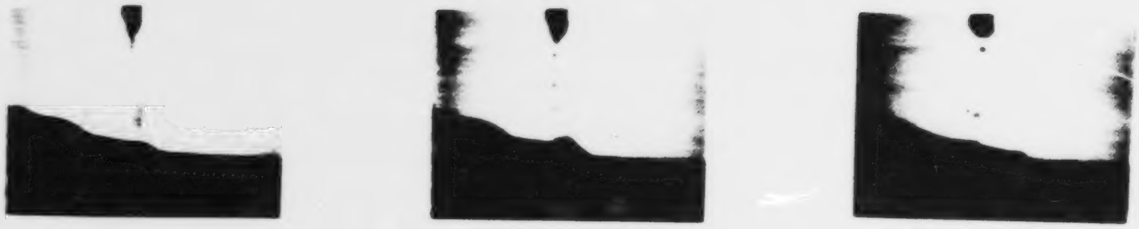

c. Tp = 4 ms

Figure 17: The Effect of Peak Duration on Drop Detachment Phenomena: C-Mn-Mo Wire in 95Ar-5CO_2 Shielding Gas at 350 A Peak Current

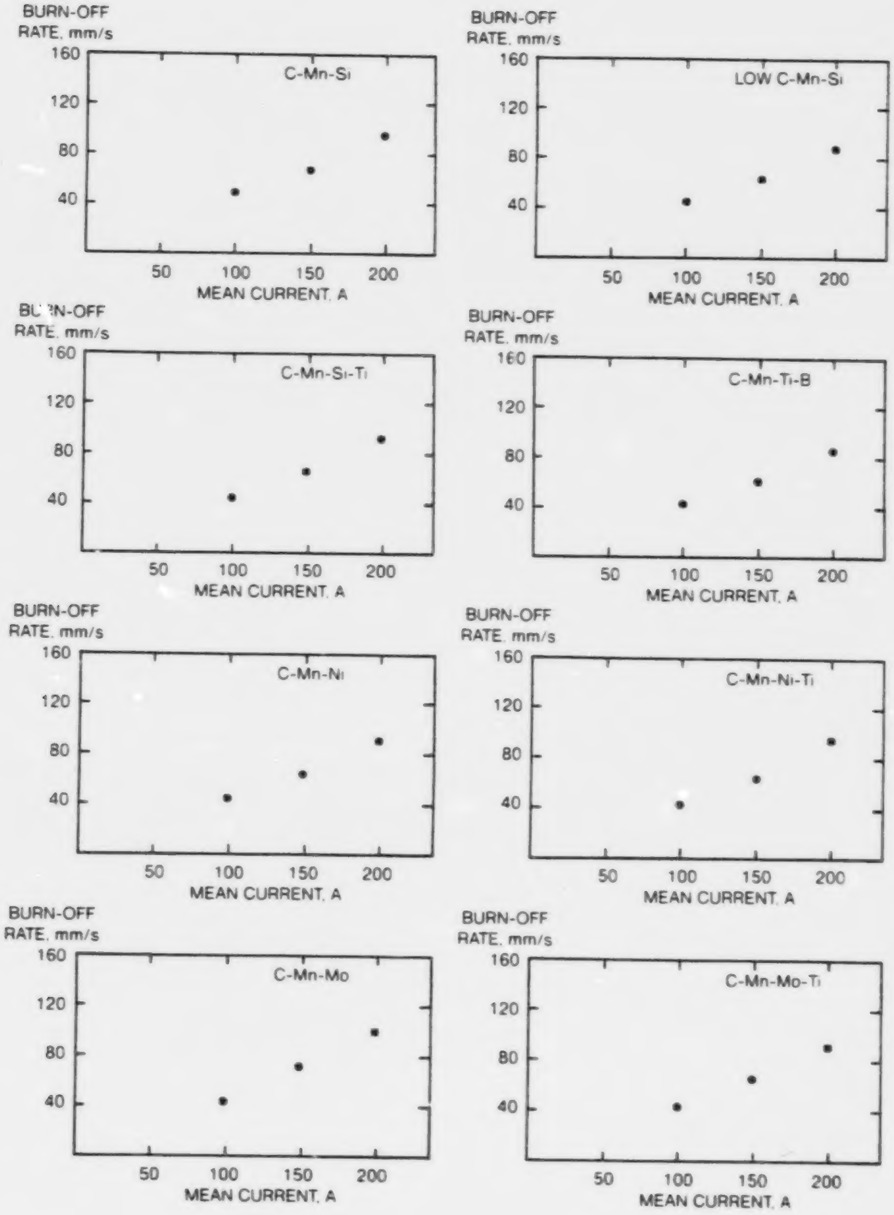

Figure 18: Burn-off Characteristics in 95Ar-5CO$_2$ Shielding Gas Mixture - Effect of Wire Composition

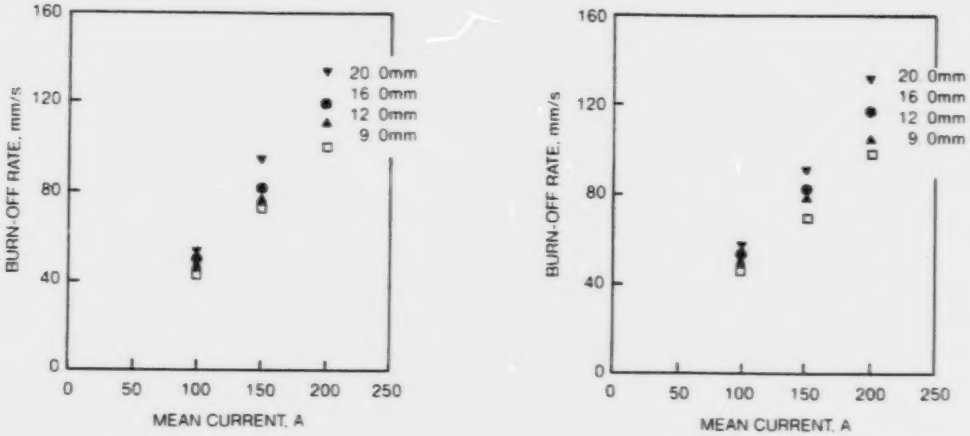

a 95Ar-5CO_2

b 80Ar-20CO_2

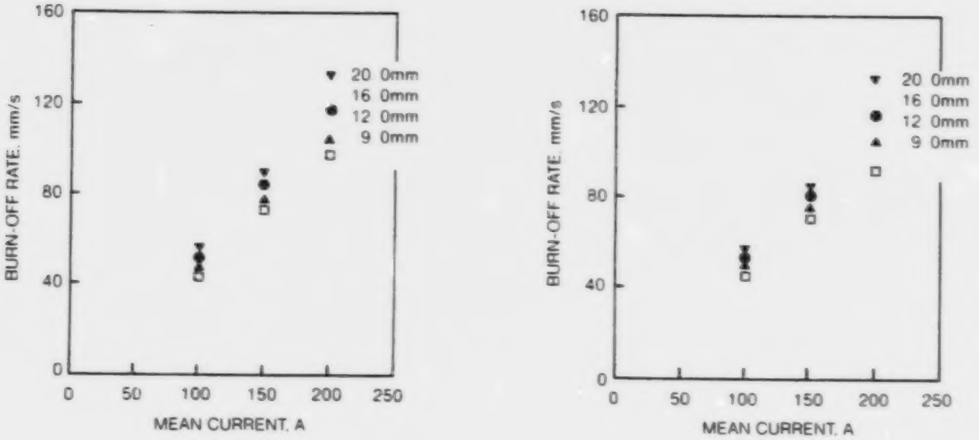

c 88Ar-10He-2CO_2

d 87.5 Ar-10He-2CO_2-0.5H_2

Figure 19: Burn-Off Characteristics of C-Mn-Mo Wire: Effect of Shielding Gas Composition

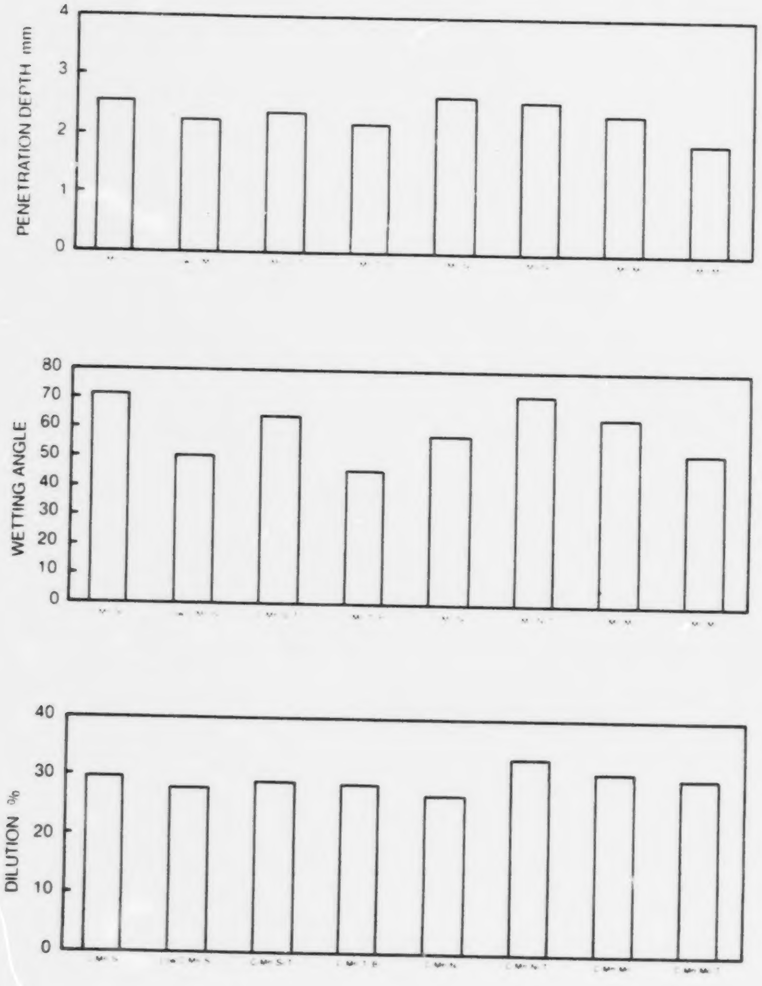

Figure 20: Effect of Wire Chemistry on Fusion Characteristics in 95Ar-5CO_2 Shielding Gas at 150 A Mean Current

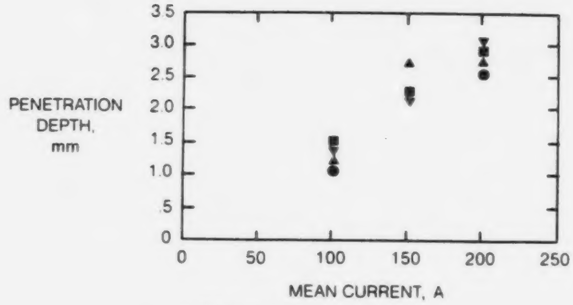

a. PENETRATION

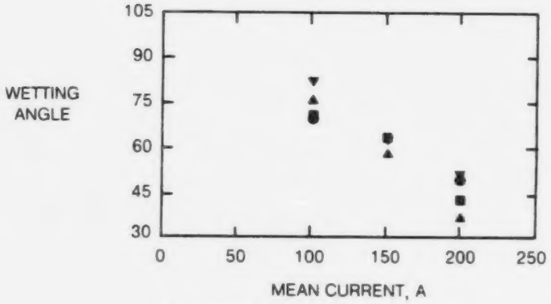

b. WETTING ANGLE

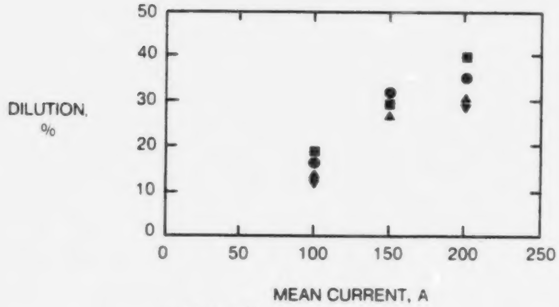

c. DILUTION

▼ Low C-Mn-Si
■ C-Mn-Si-Ti
▲ C-Mn-Ni
● C-Mn-Mo

Figure 21: Effect of Mean Current on Fusion Characteristics: C-Mn-Si, C-Mn-Ti, C-Mn-Ni and C-Mo-Mo Wires in 95Ar-5CO_2 Shielding Gas

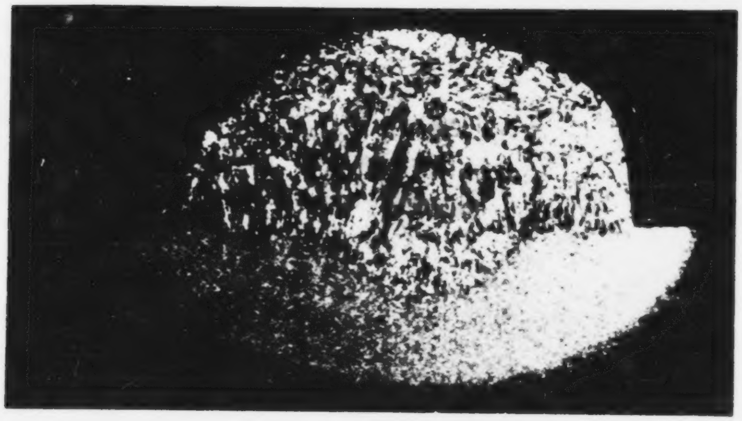

a. 100 A Mean Current

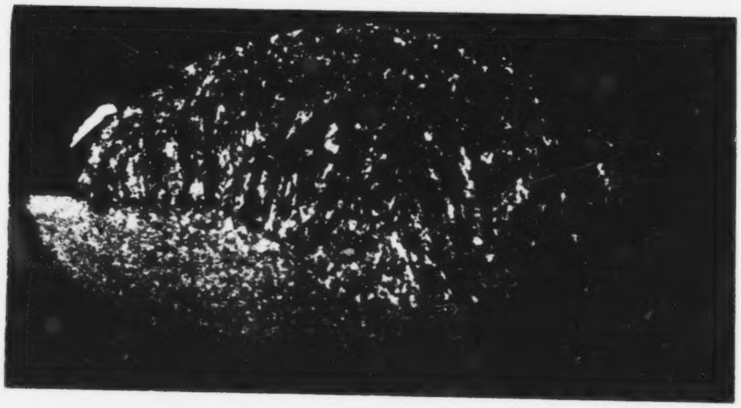

b. 150 A Mean Current

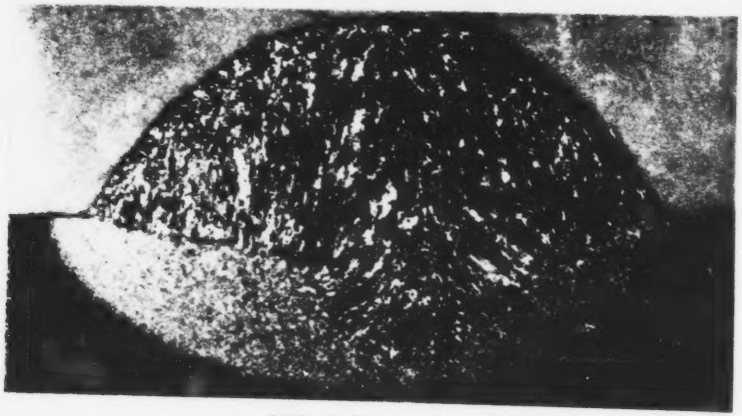

c. 200 A Mean Current

Figure 22: The Effect of Mean Current on Fusion Characteristics: C-Mn-Mo Wire in 95Ar-5CO_2 Shielding Gas

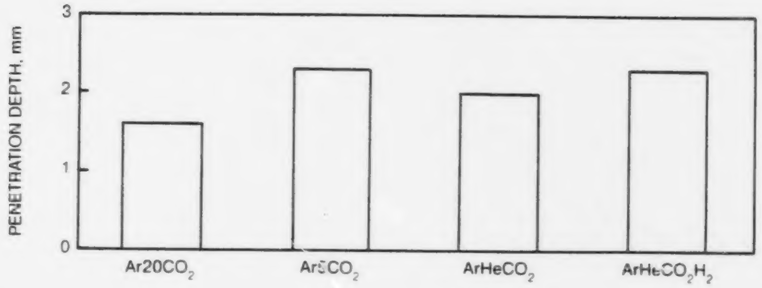

a. PENETRATION

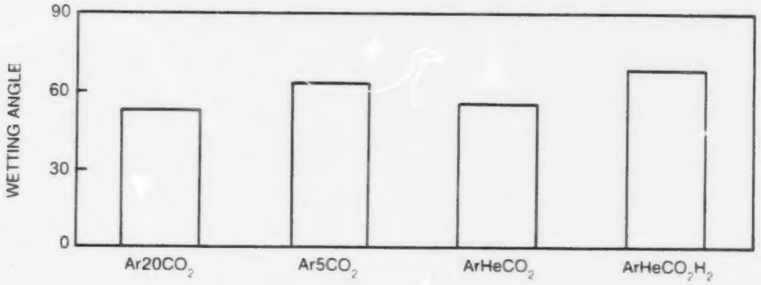

b. WETTING ANGLE

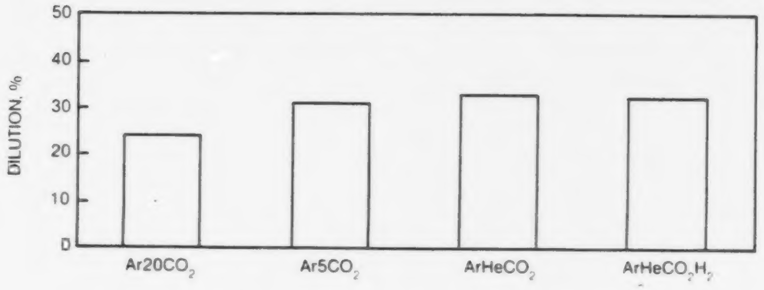

c. DILUTION

Figure 23: Influence of Shielding Gas on Fusion Characteristics for C-Mn-Mo Wire at 150 A Mean Current

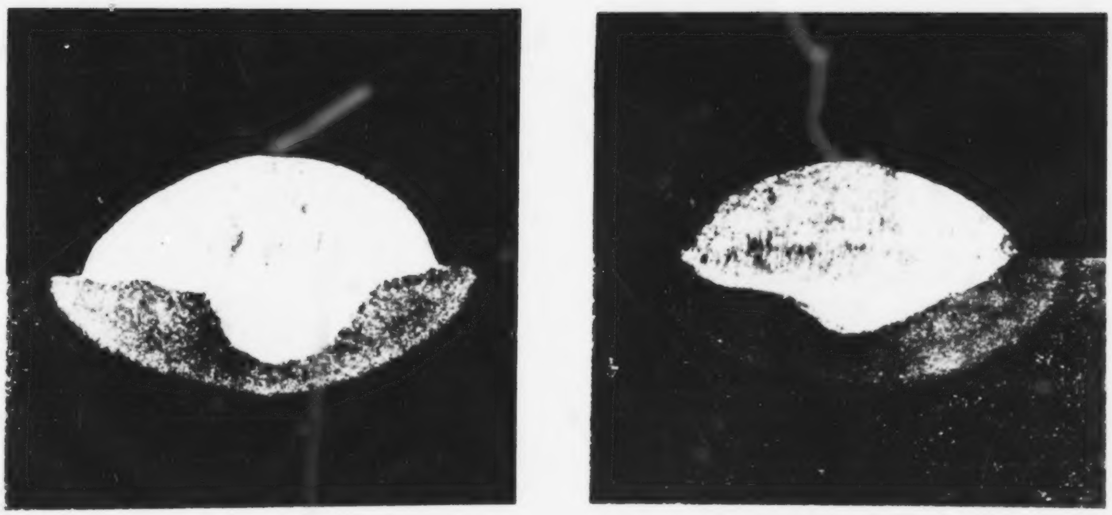

a. $95Ar-5CO_2$

b. $80Ar-20CO_2$

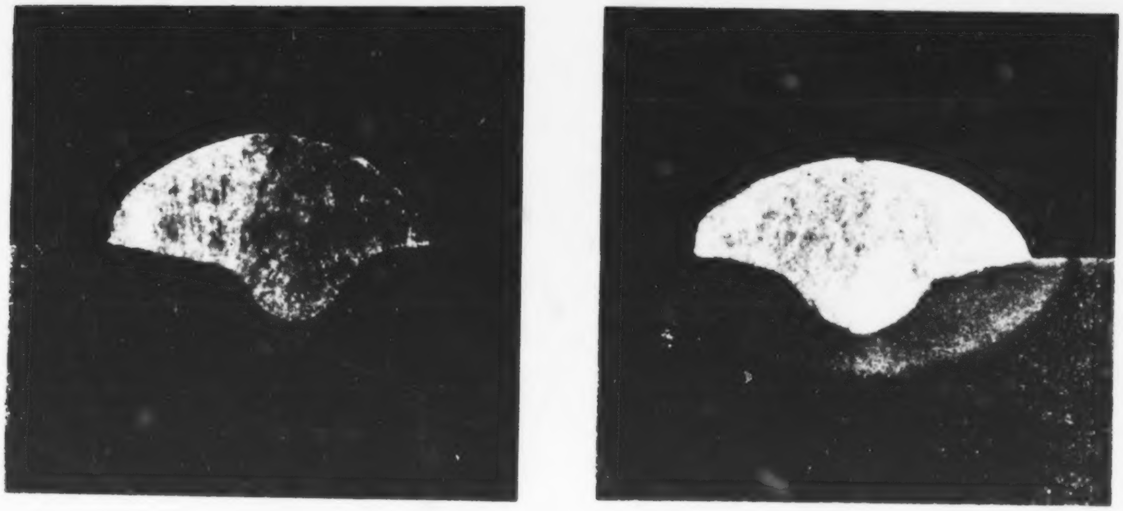

c. $88Ar-10He-2CO_2$

d. $87.5Ar-10He-2CO_2-0.5H_2$

Figure 24: The Influence of Shielding Gas Composition on Fusion Characteristics at 150 A Mean Current

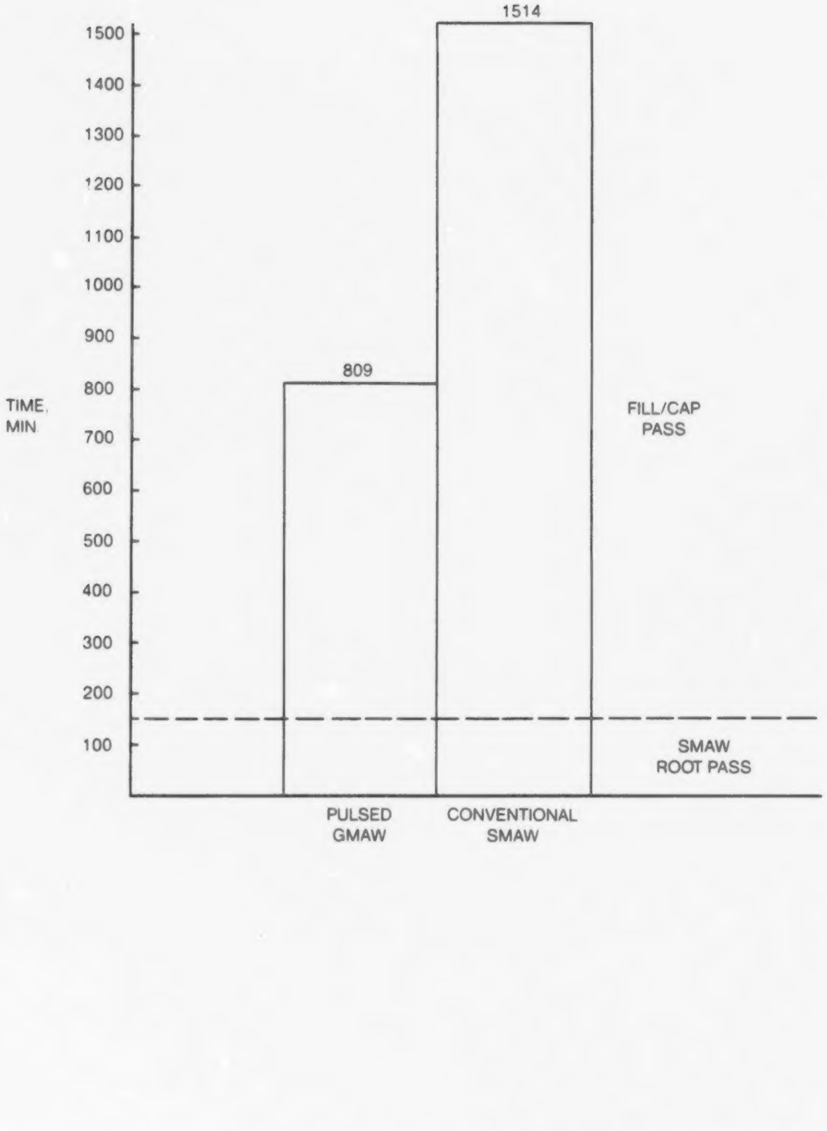

Figure 25: Joint Completion Times for Girth Welds in 1067 mm O.D., 30 mm W.T. Pipe

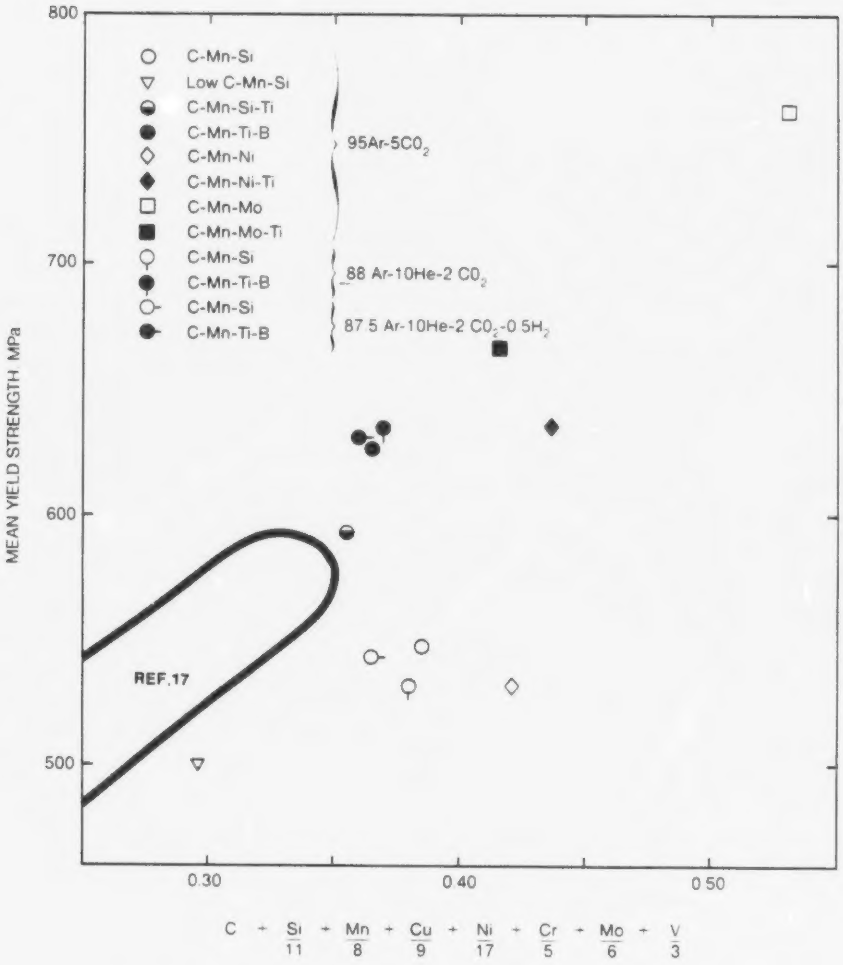

Figure 26: Variation of Weld Metal Yield Strength with Chemical Composition

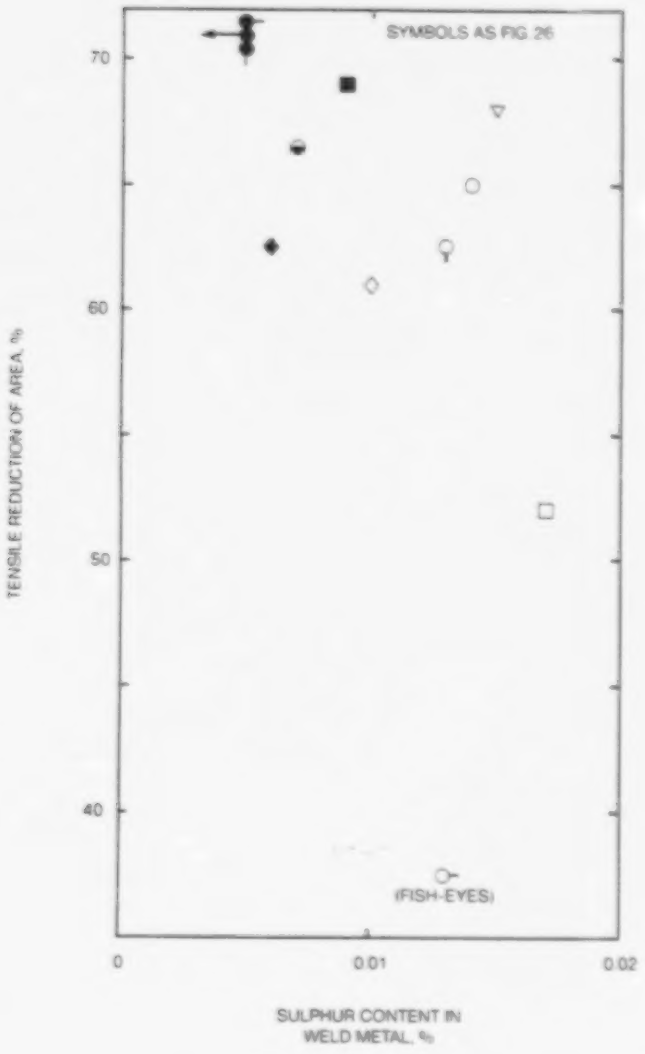

Figure 27: Variation of Weld-Metal Tensile Ductility with Sulphur Content

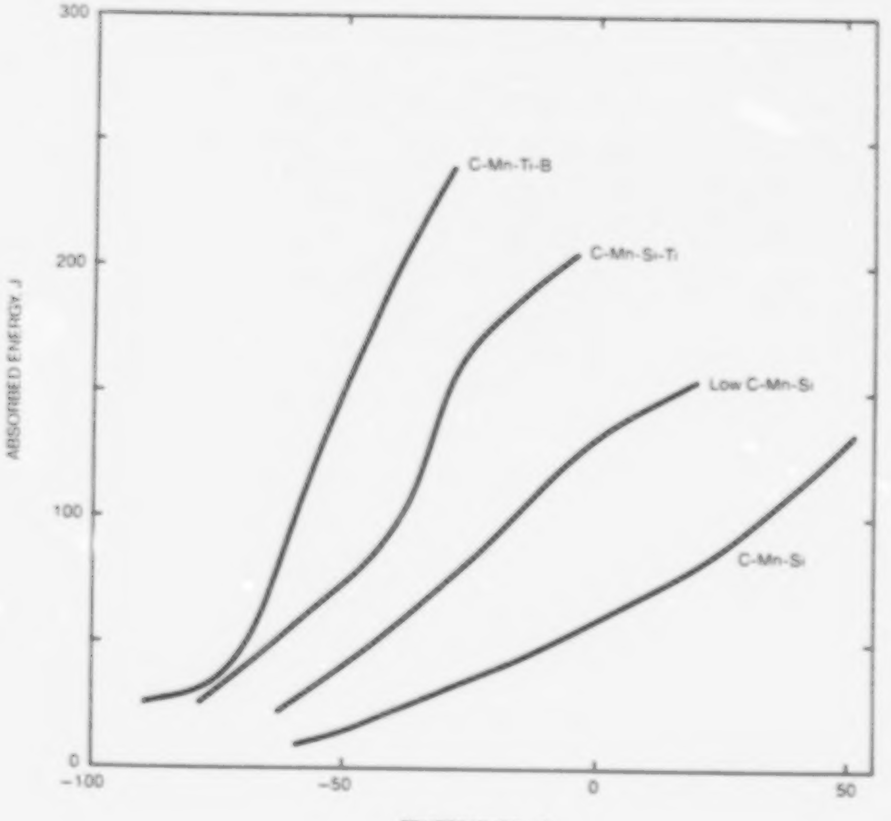

Figure 28: Charpy Impact Transition Curves for C-Mn-Si, LowC-Mn-Si, C-Mn-Si-Ti and C-Mn-Ti-B Welds Made Under 95Ar-5CO_2

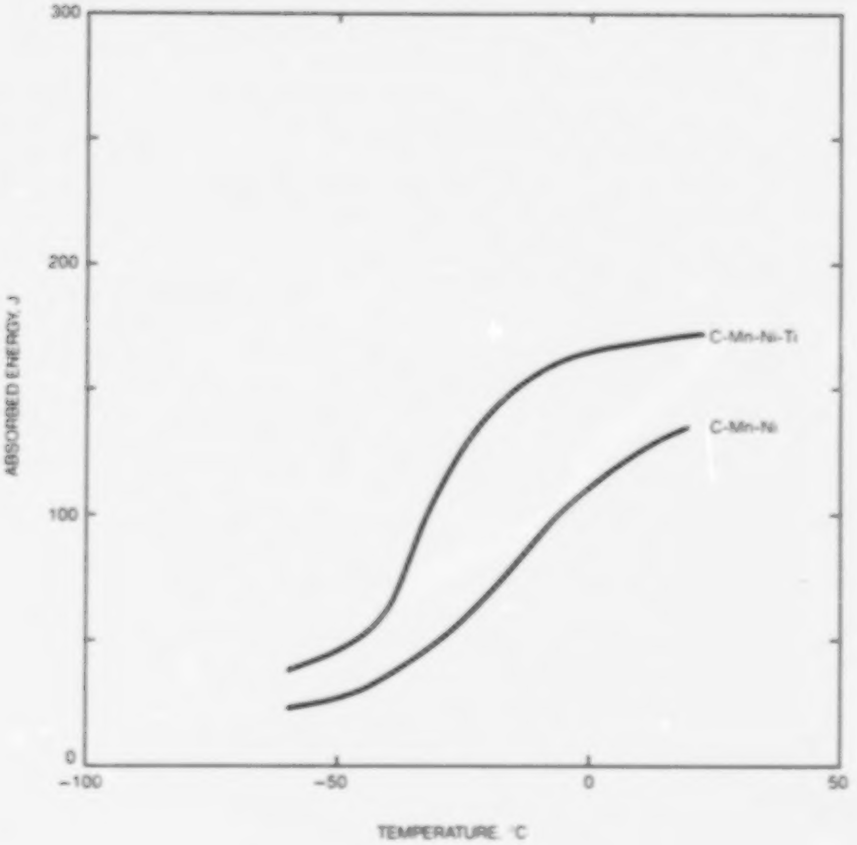

Figure 29: Charpy Impact Transition Curves for C-Mn-Ni and C-Mn-Ni-Ti Welds Made Under 95Ar-5CO_2

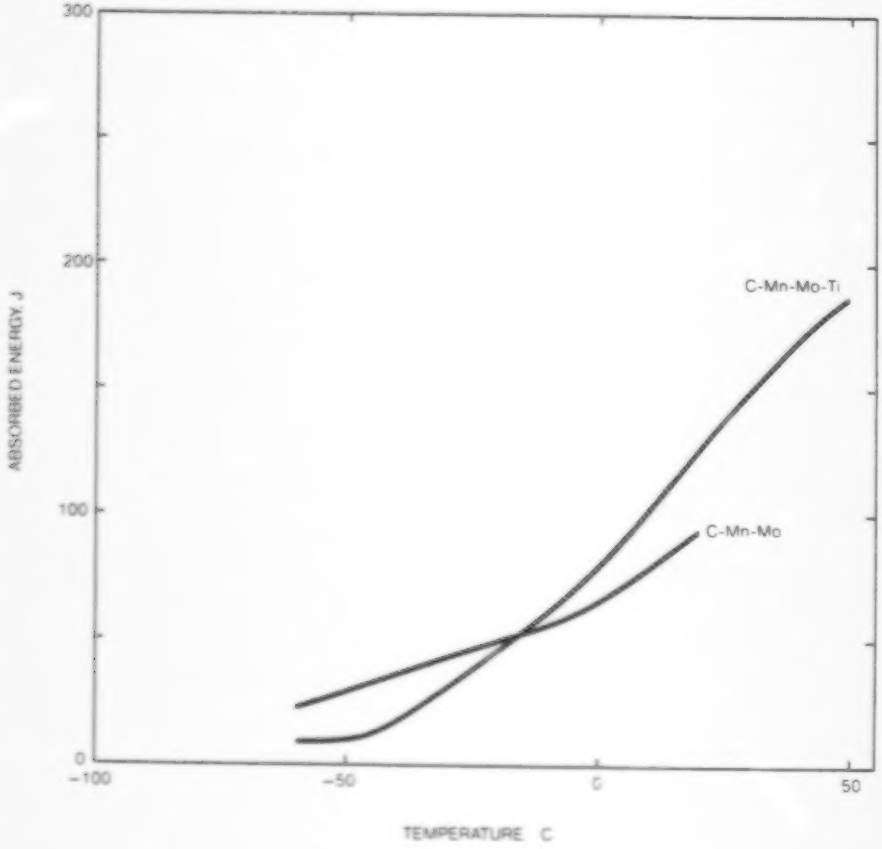

Figure 30: Charpy Impact Transition Curves for C-Mn-Mo and C-Mn-Mo-Ti Welds Made Under 95Ar-5CO_2

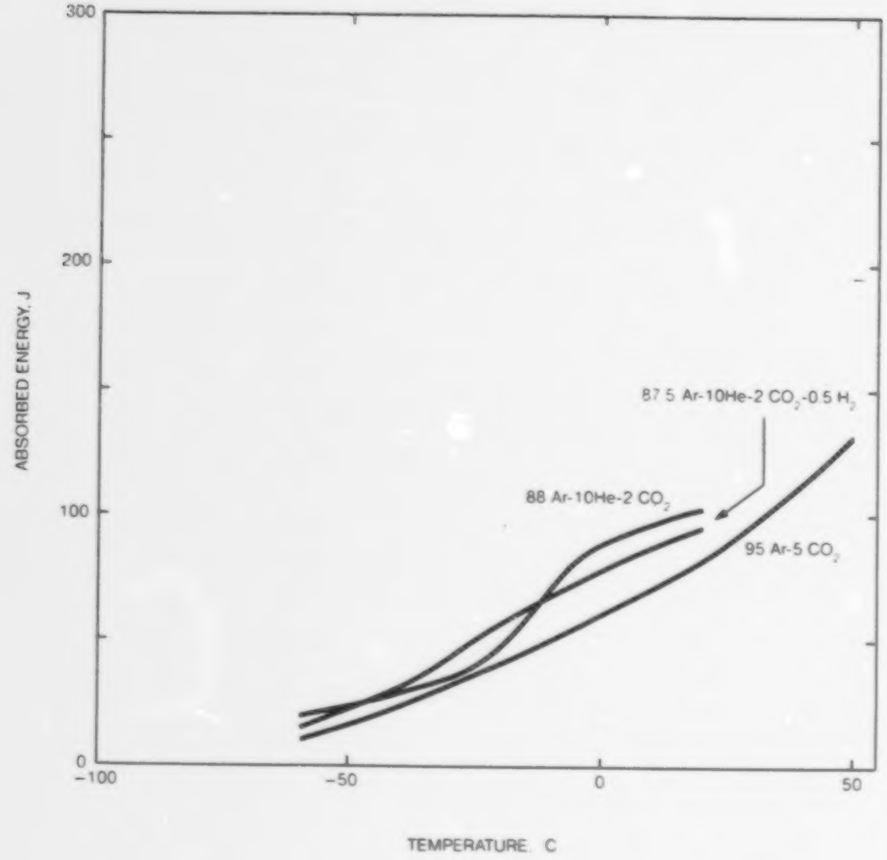

Figure 31: Charpy Impact Transition Curves for C-Mn-Si Welds Made Under Different Gases

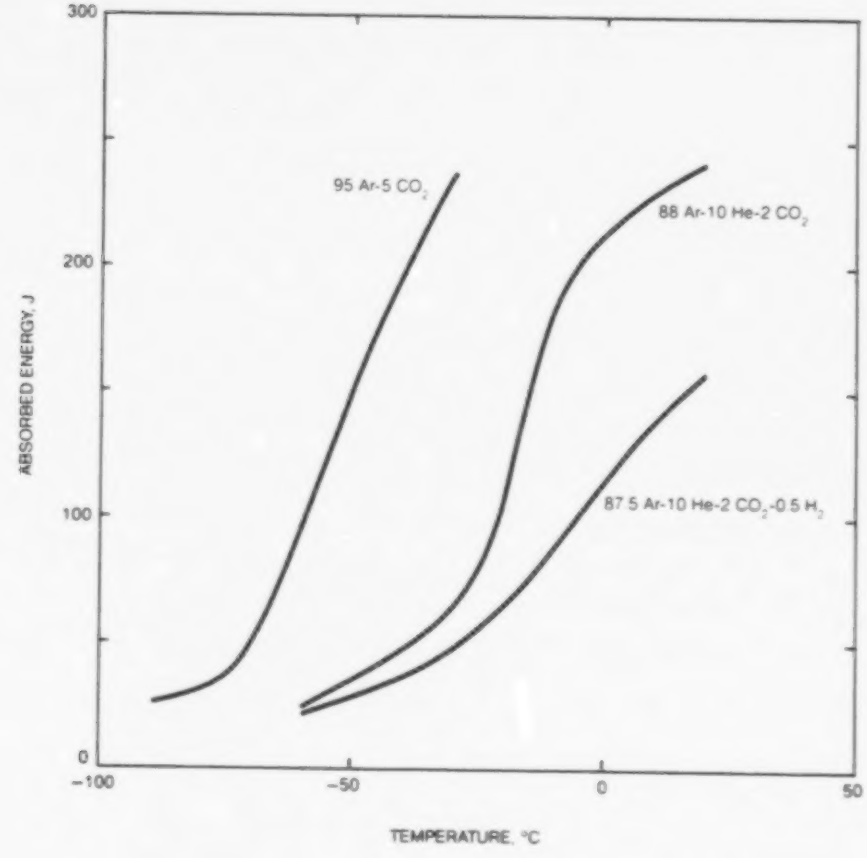

Figure 32: Charpy Impact Transition Curves for C-Mn-Ti-B Welds Made Under Different Gases

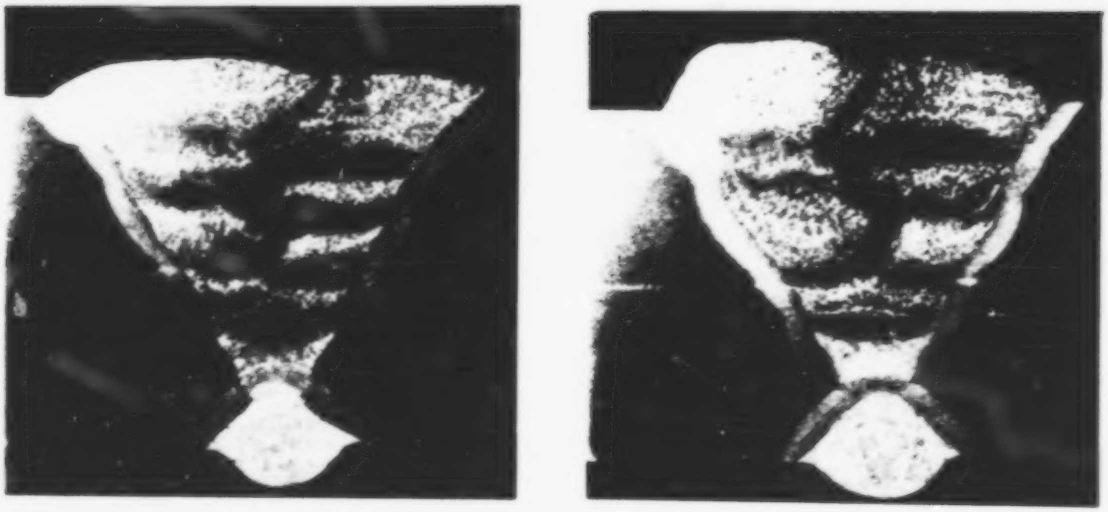

a. C-Mn-Si/95Ar-5CO_2

b. LowC-Mn-Si/95Ar-5CO_2

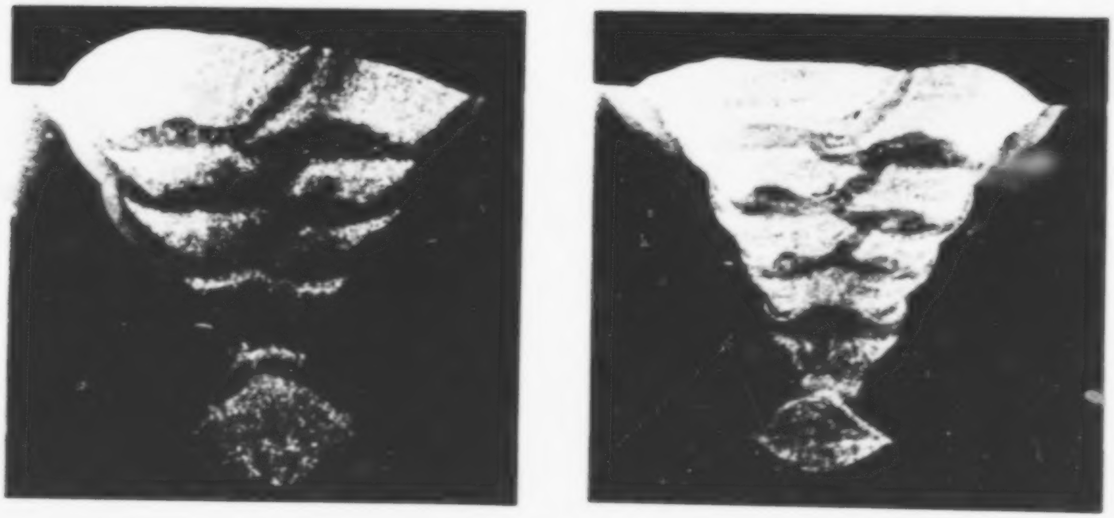

c. C-Mn-Si-Ti/95Ar-5CO_2

d. C-Mn-Ti-B/95Ar-5CO_2

Figure 33: Macrosections of Welds Made in Lloyds LT60 Test Panels

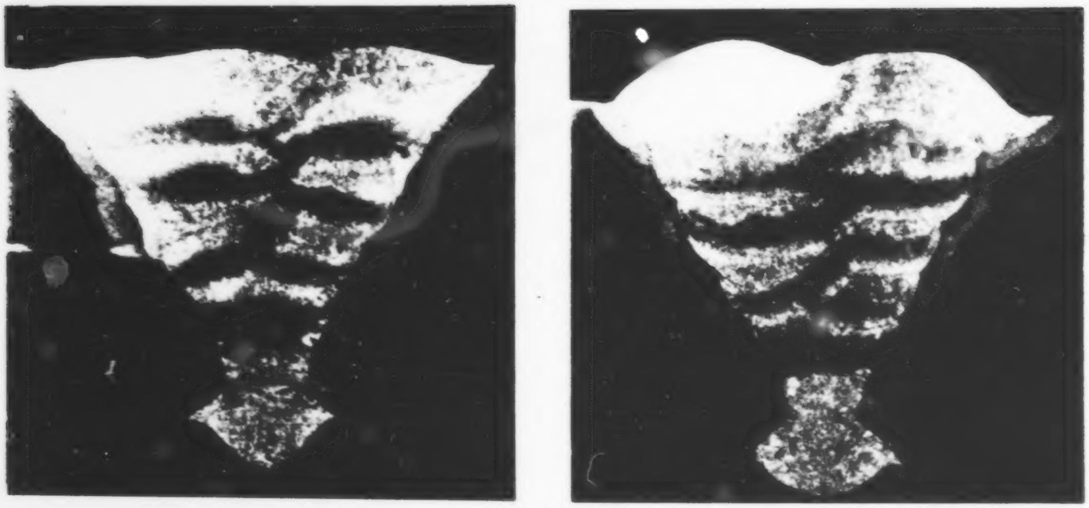

e. C-Mn-Ni/95Ar-5CO_2 f. C-Mn-Ni-Ti/95Ar-5CO_2

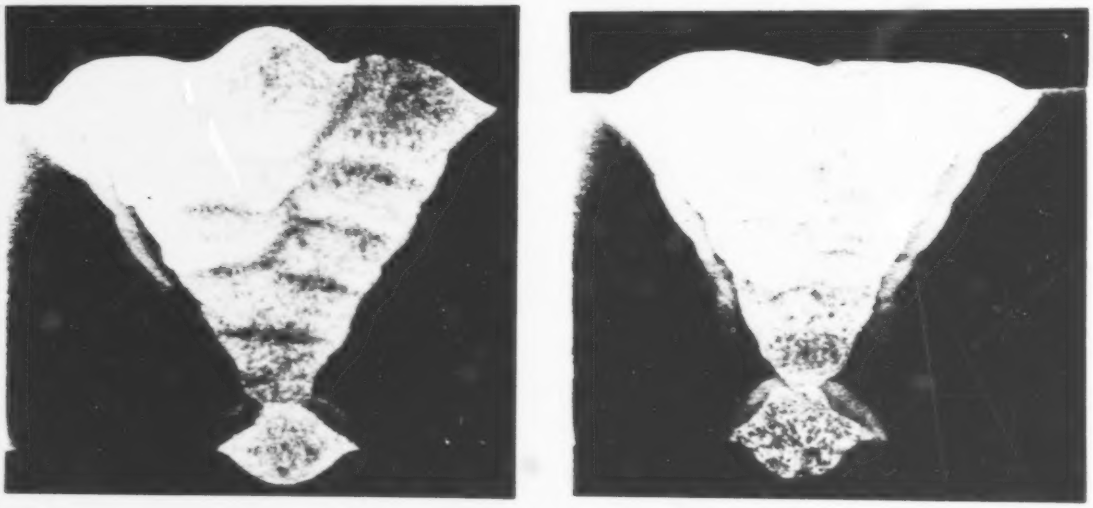

g. C-Mn-Mo/95Ar-5CO_2 h. C-Mn-Mo-Ti/95Ar-5CO_2

Figure 33 (cont)

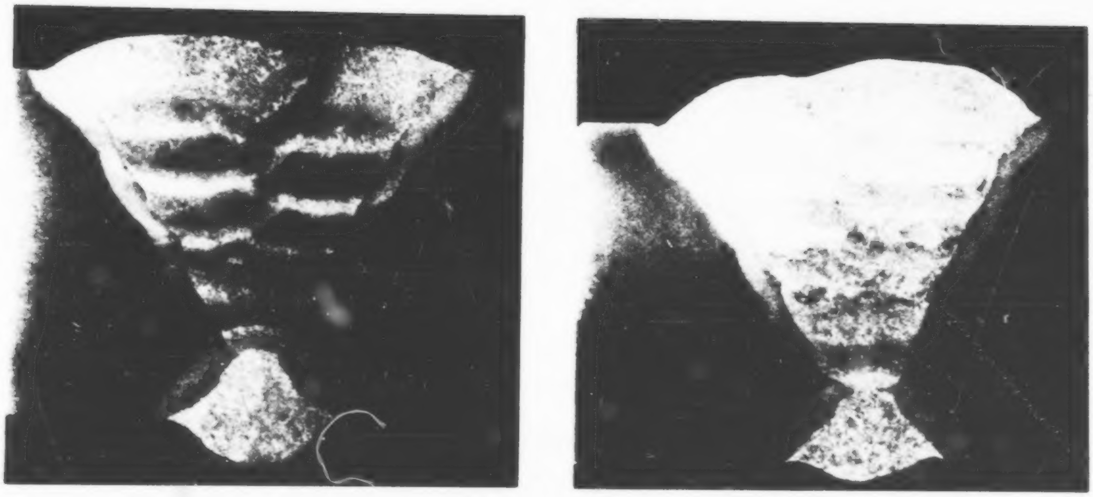

i. C-Mn-Si/88Ar-10He-$2CO_2$ j. C-Mn-Ti-B/88Ar-10He-$2CO_2$

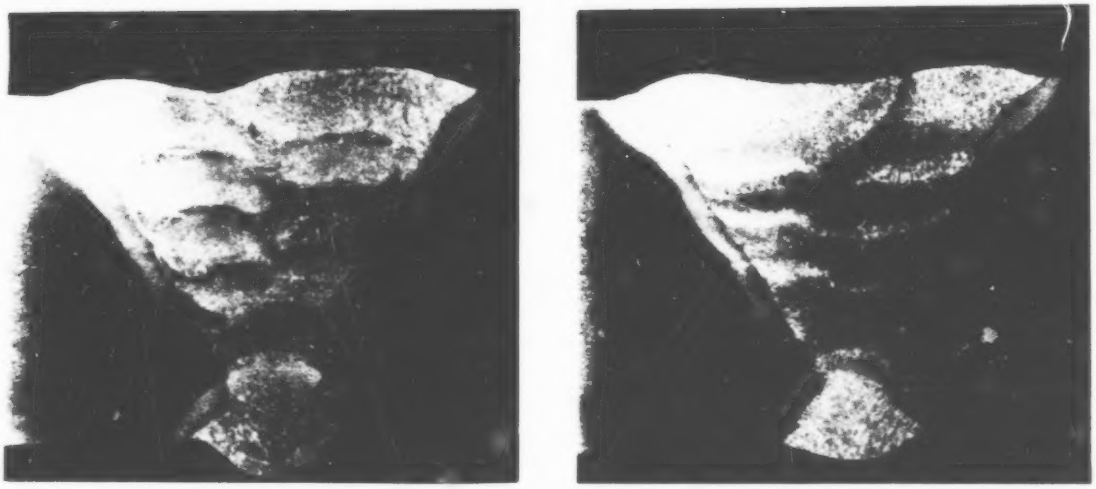

k. C-Mn-Si/87.5Ar-10He-$2CO_2$-$0.5H_2$ l. C-Mn-Ti-B/87.5Ar-10He-$2CO_2$-$0.5H_2$

Figure 33 (cont)

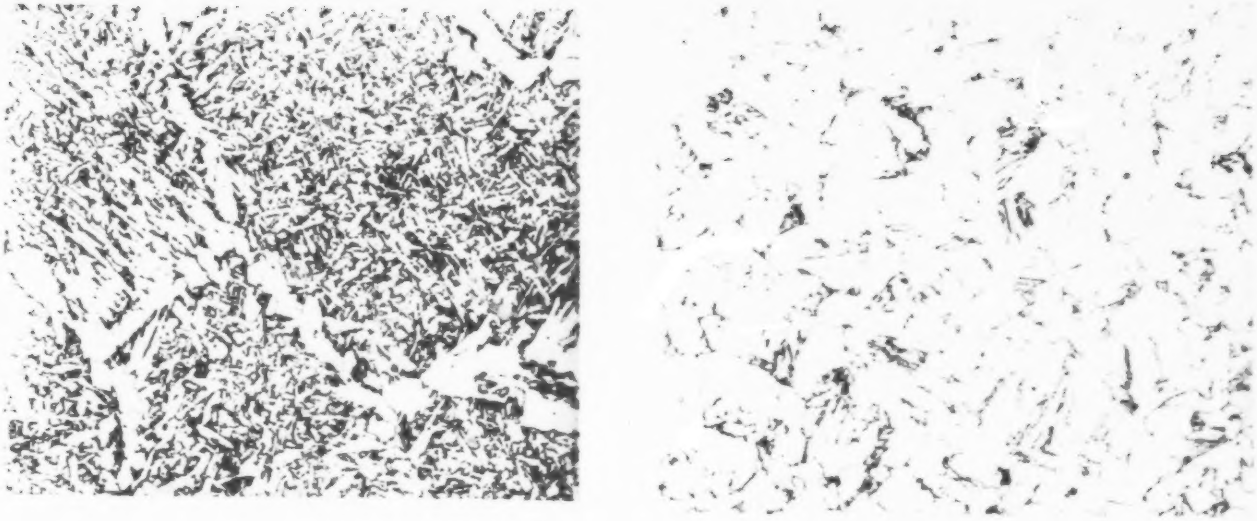

a. Subsurface, as-deposited

b. Subsurface, refined

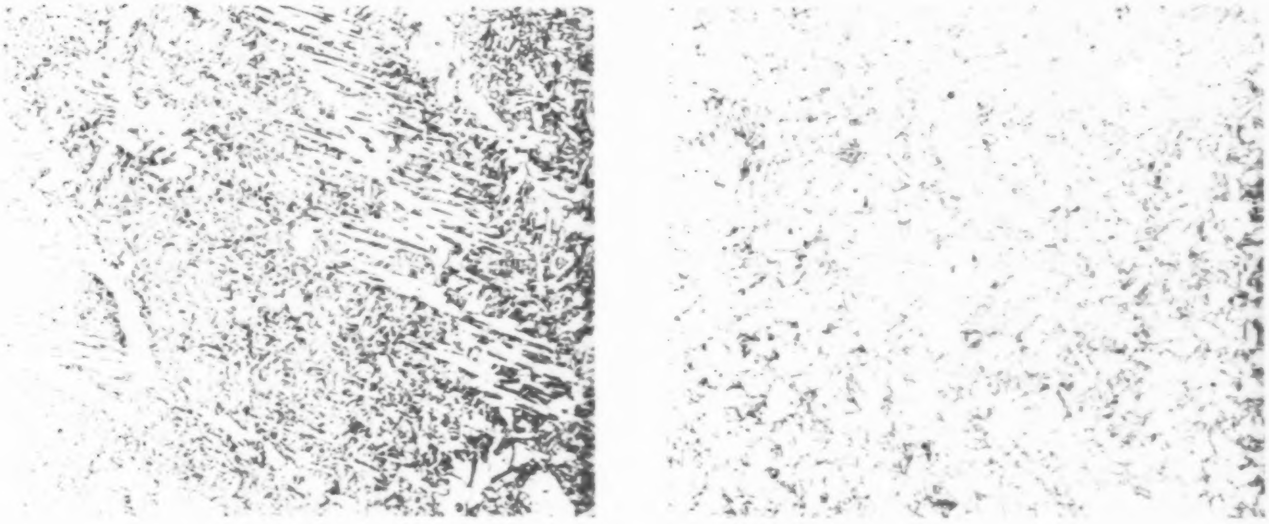

c. Root, as-deposited

d. Root, refined

Figure 34: Typical Microstructural Features: C-Mn-Si/95Ar-5CO_2

a. Subsurface, as-deposited

b. Subsurface, refined

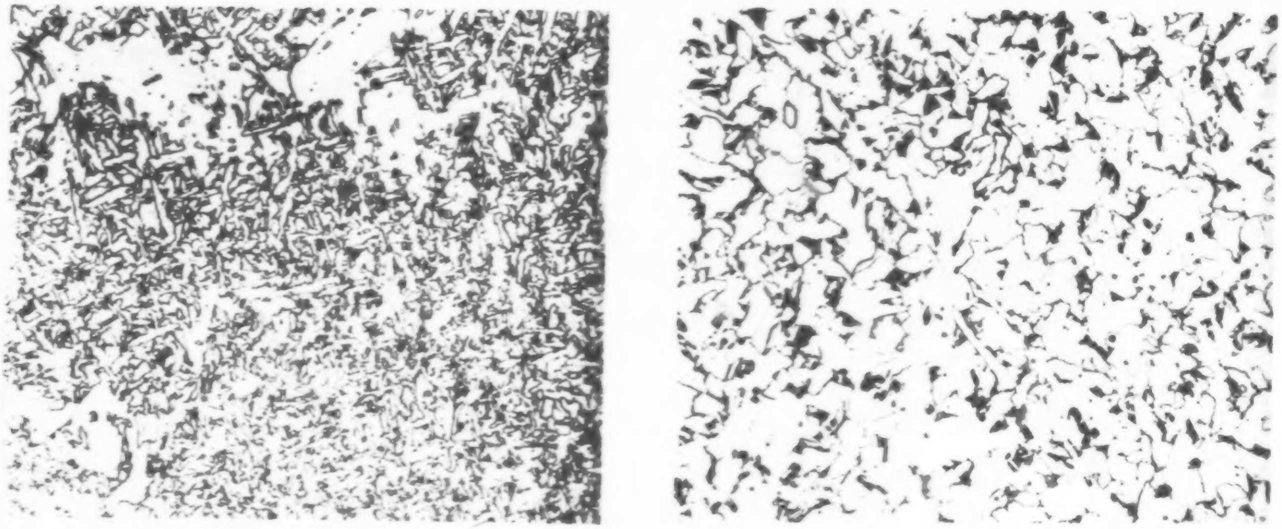

c. Root, as-deposited

d. Root, refined

Figure 35: Typical Microstructural Features: LowC-Mn-Si/95Ar-5CO_2

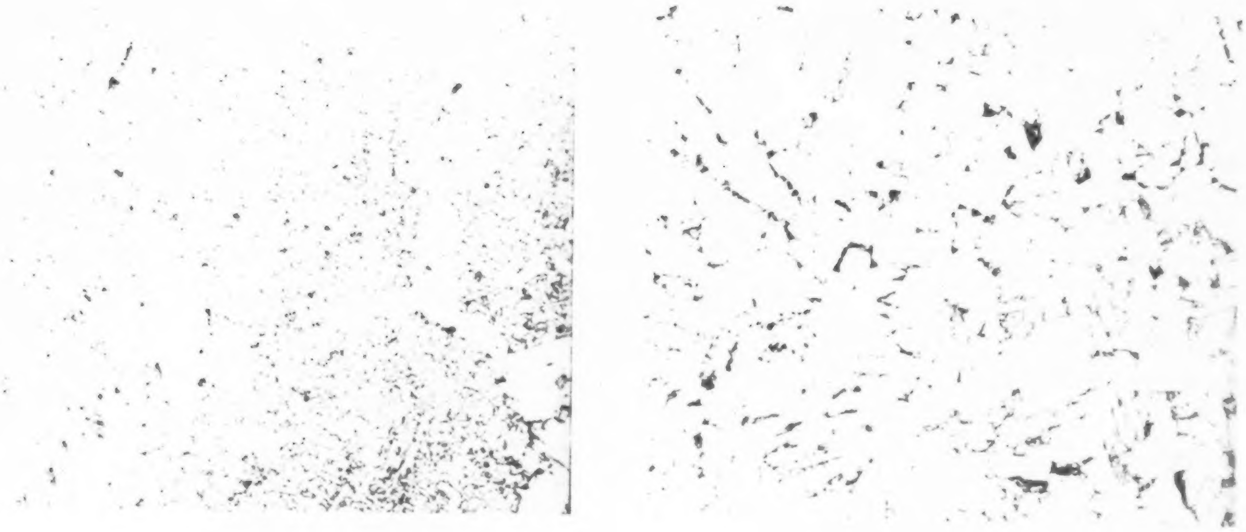

a. Subsurface, as-deposited

b. Subsurface, refined

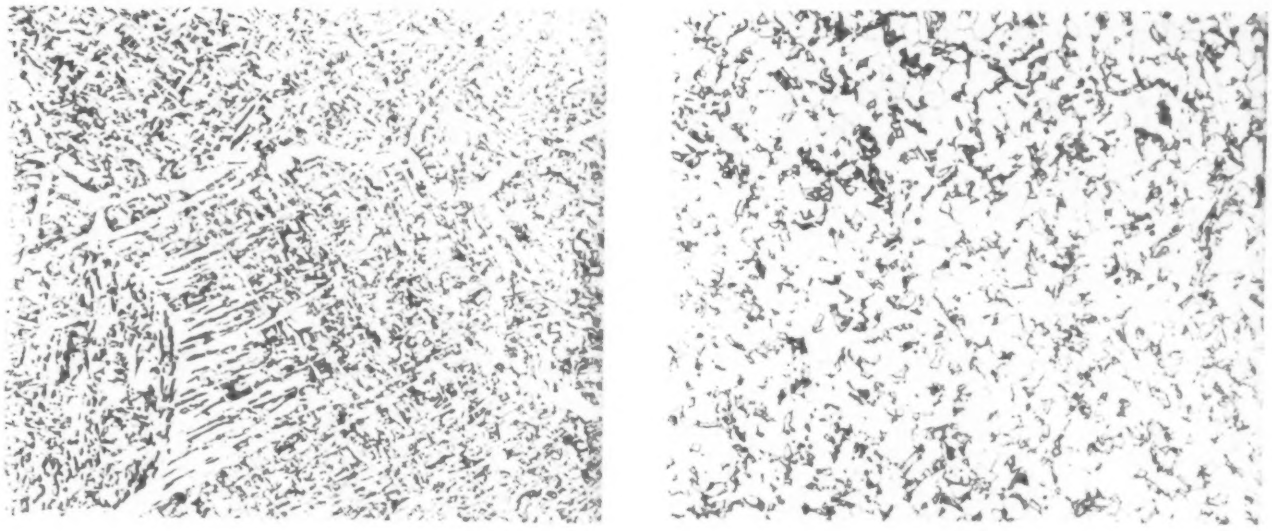

c. Root, as-deposited

d. Root, refined

Figure 36: Typical Microstructural Features: C-Mn-Si-Ti/95Ar-5CO_2

a. Subsurface, as-deposited

b. Subsurface, refined

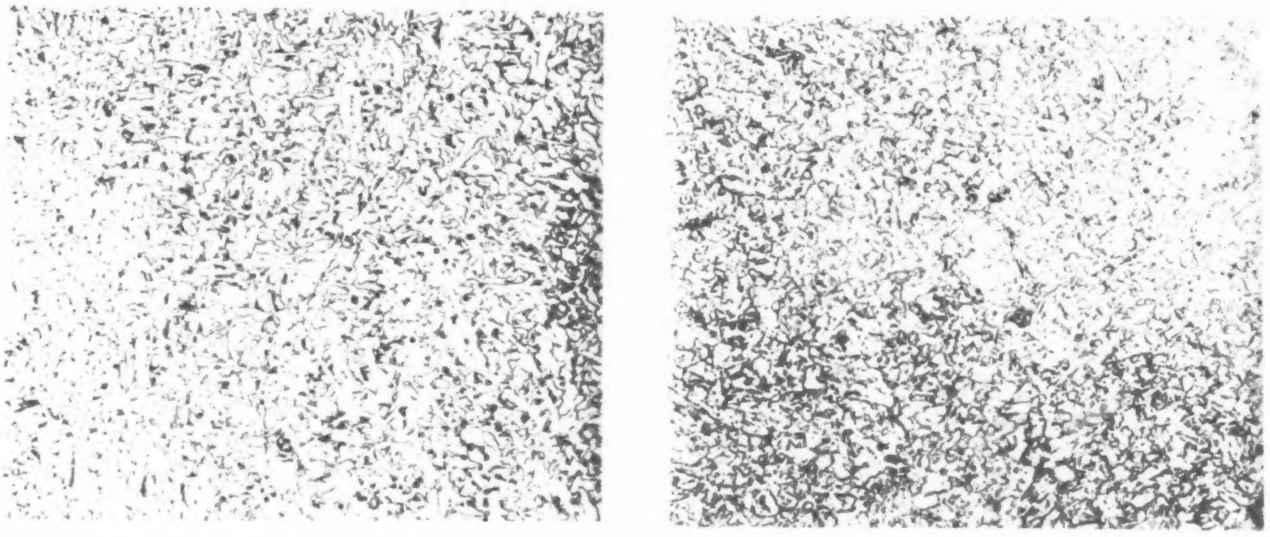

c. Root, as-deposited

d. Root, refined

Figure 37: Typical Microstructural Features: C-Mn-Ti-B/95Ar-5CO_2

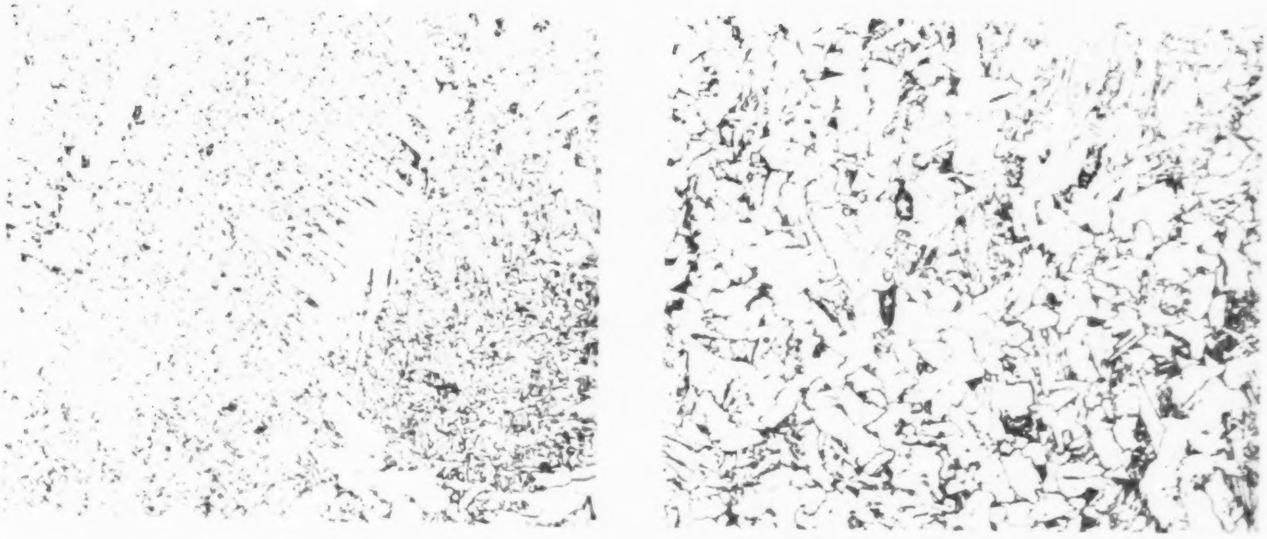

a. Subsurface, as-deposited

b. Subsurface, refined

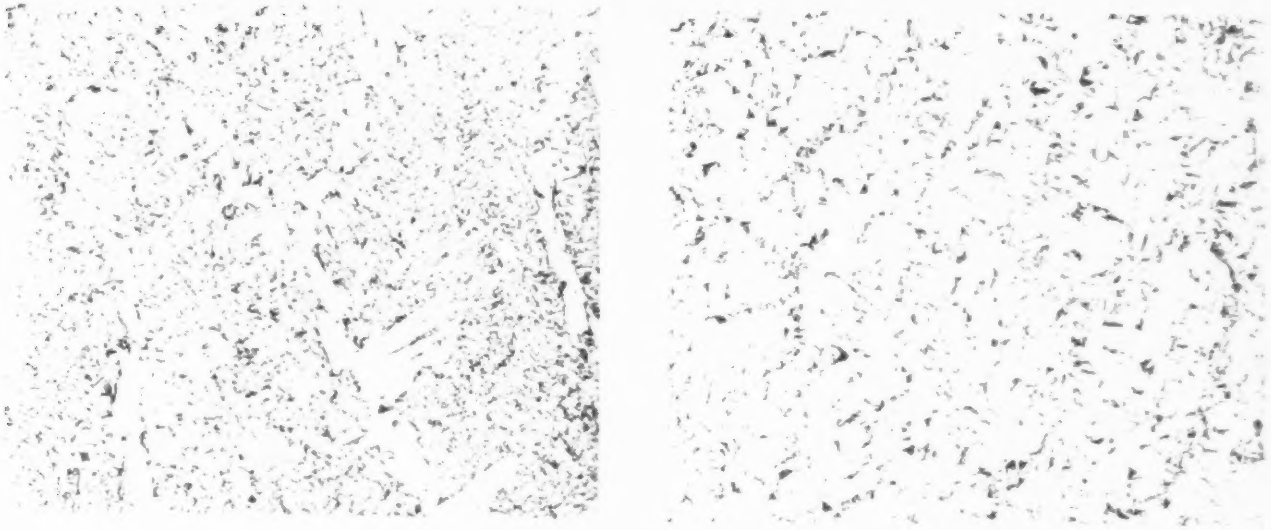

c. Root, as-deposited

d. Root, refined

Figure 38: Typical Microstructural Features: C-Mn-Ni/95Ar-5CO_2

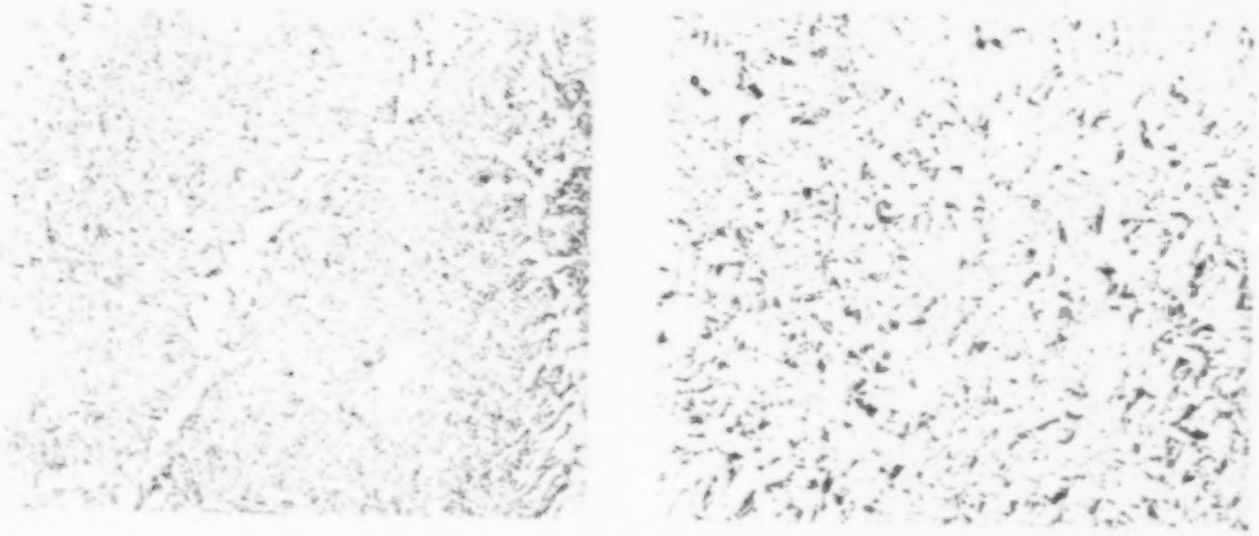

a. Subsurface, as-deposited

b. Subsurface, refined

c. Root, as-deposited

d. Root, refined

Figure 39: Typical Microstructural Features: C-Mn-Ni-Ti/95Ar-5CO_2

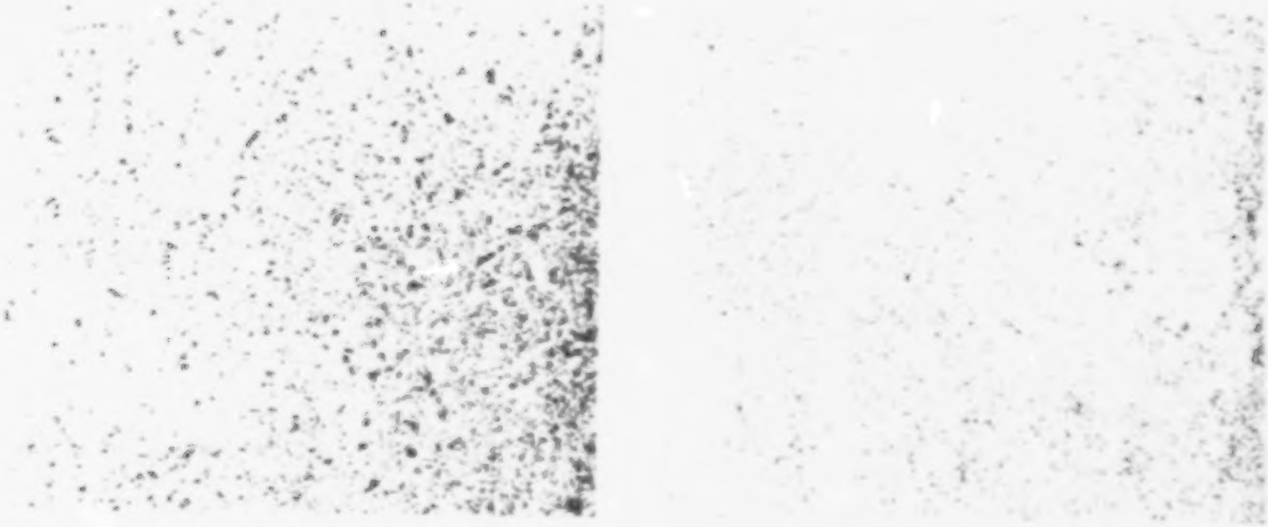

a. Subsurface, as-deposited

b. Subsurface, refined

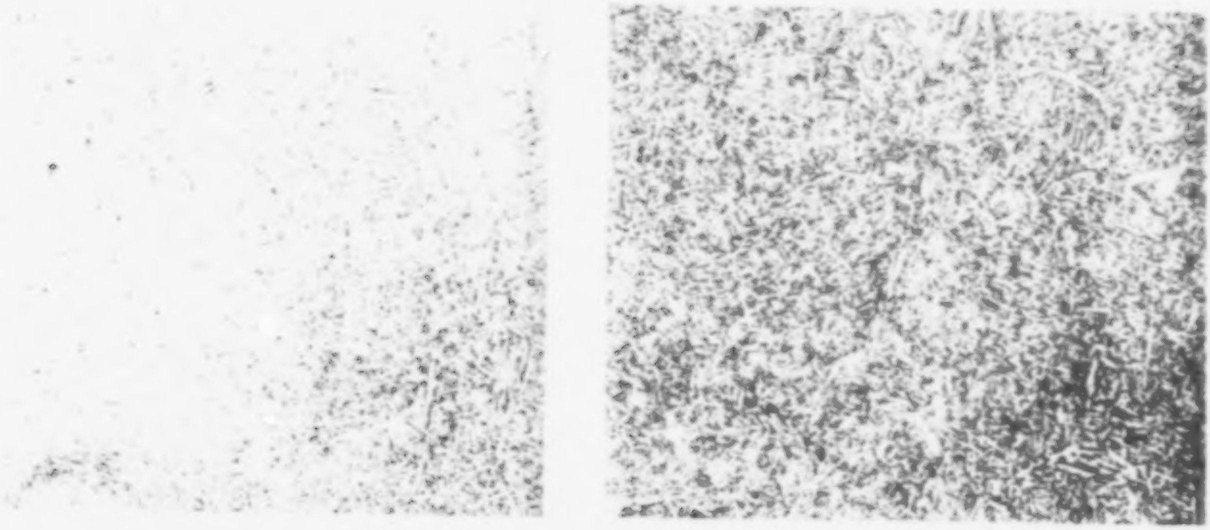

c. Root, as-deposited

d. Root, refined

Figure 40: Typical Microstructural Features: C-Mn-Mo/95Ar-5CO_2

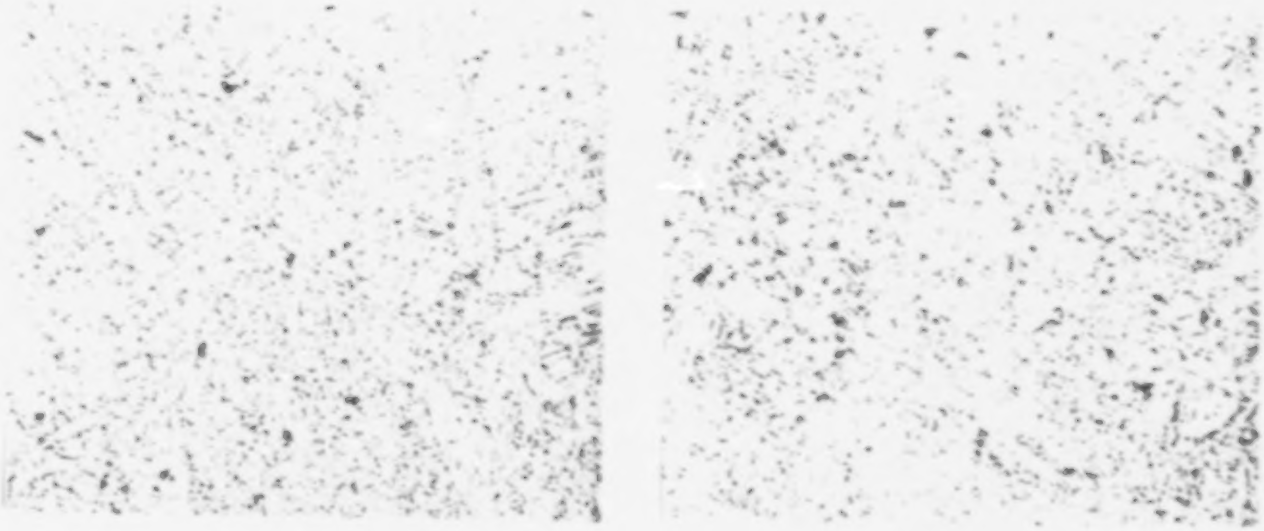

a. Subsurface, as-deposited b. Subsurface, refined

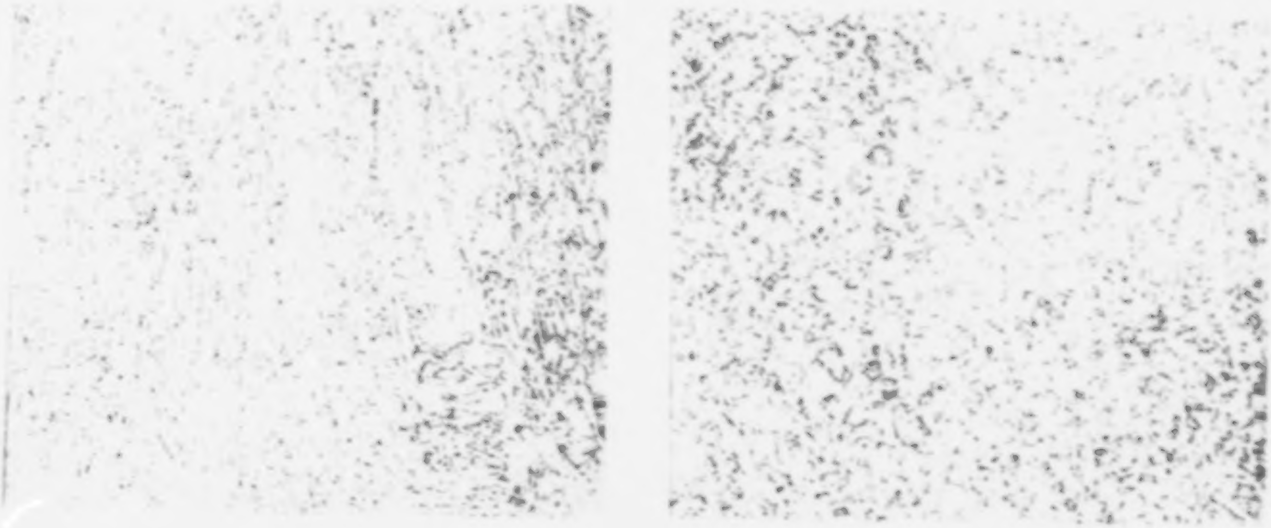

c. Root, as-deposited d. Root, refined

Figure 41: Typical Microstructural Features: C-Mn-Mo-Ti/95Ar-5CO_2

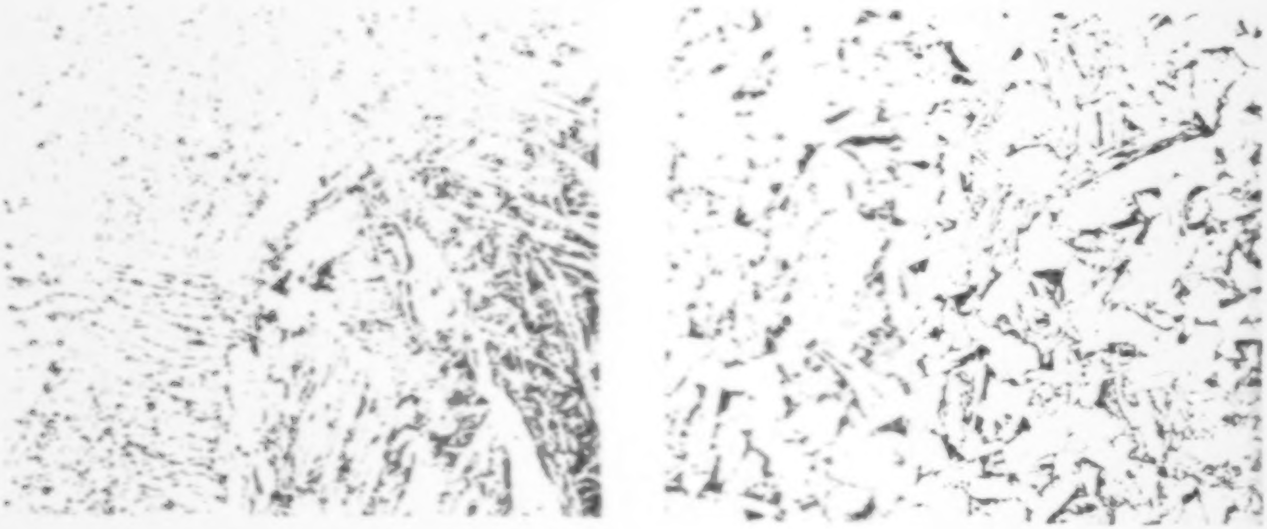

a. Subsurface, as-deposited

b. Subsurface, refined

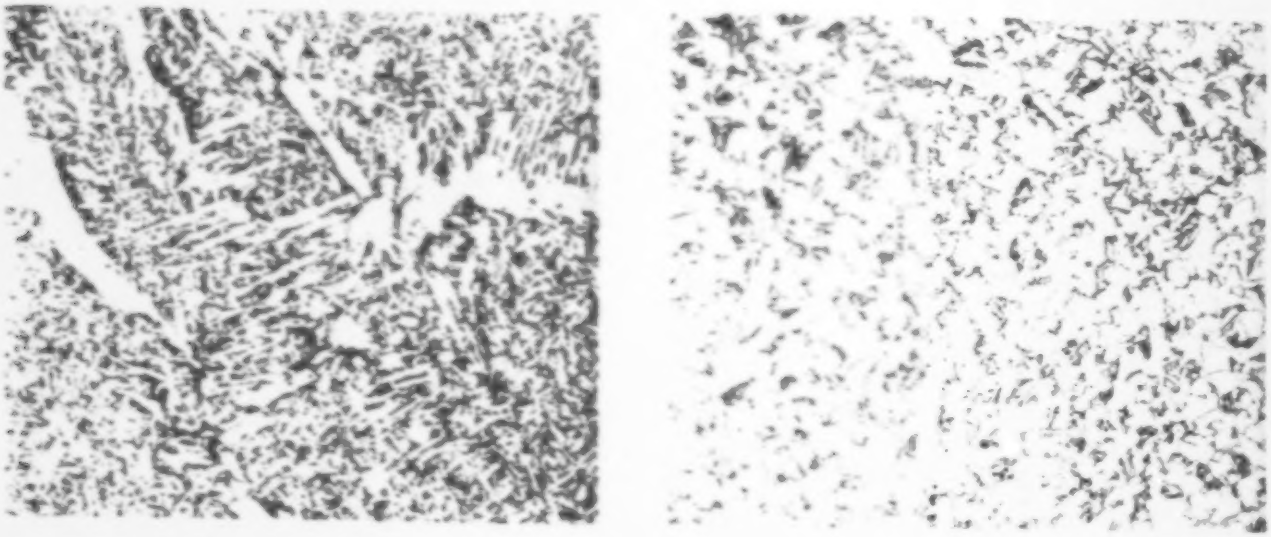

c. Root, as-deposited

d. Root, refined

Figure 42: Typical Microstructural Features: C-Mn-Si/88Ar-10He-$2CO_2$

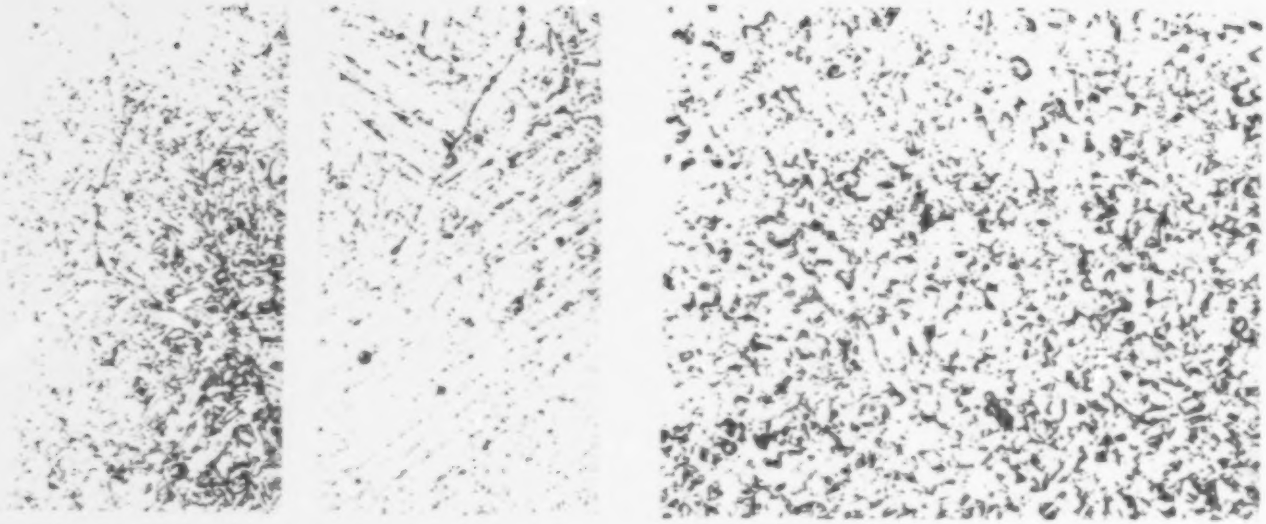

a. Subsurface, as-deposited

b. Subsurface, refined

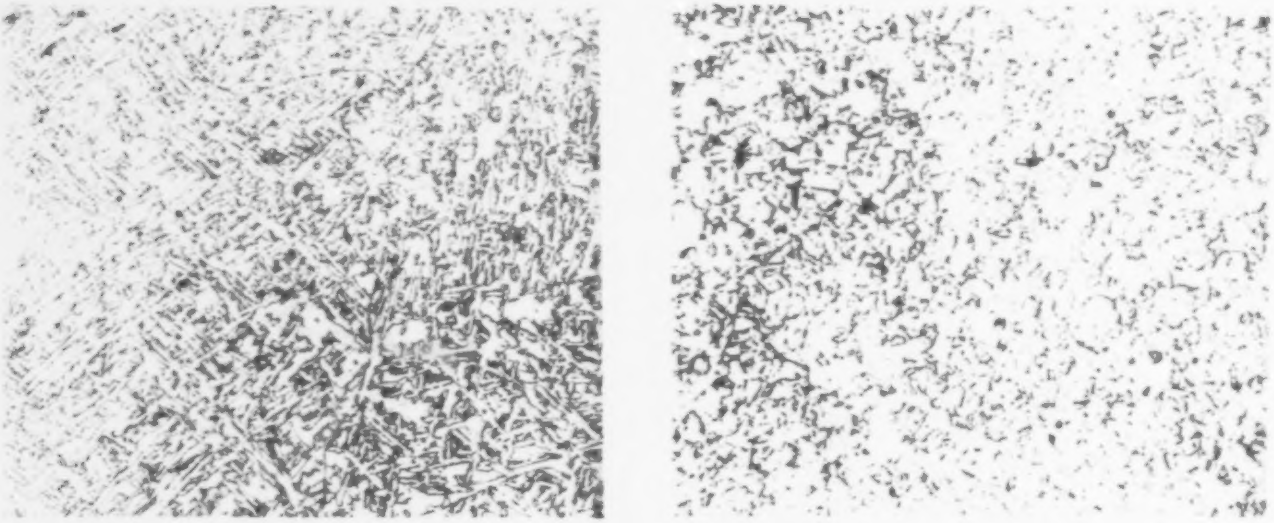

c. Root, as-deposited

d. Root, refined

Figure 43: Typical Microstructural Features: C-Mn-Ti-B/88Ar-10He-$2CO_2$

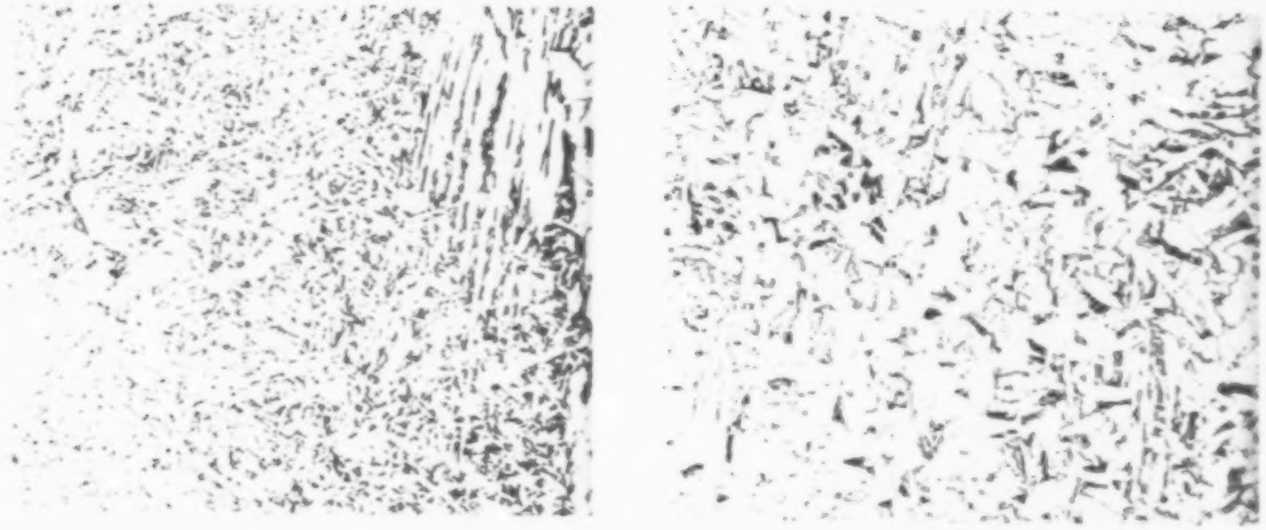

a. Subsurface, as-deposited

b. Subsurface, refined

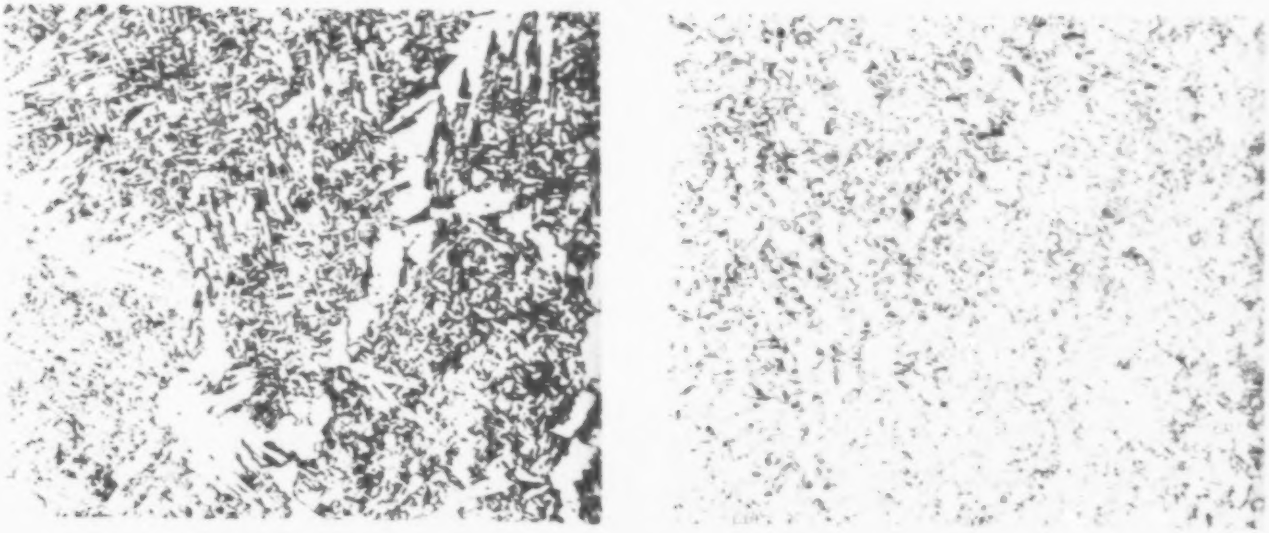

c. Root, as-deposited

d. Root, refined

Figure 44: Typical Microstructural Features: C-Mn-Si/87.5Ar-10He-2CO_2-0.5H_2

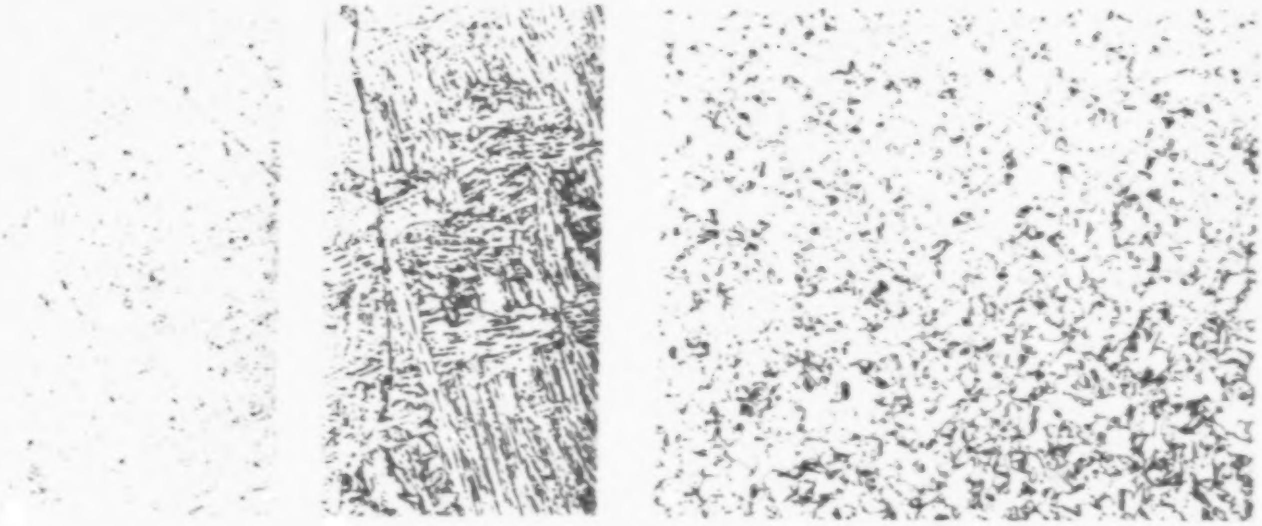

a. Subsurface, as-deposited

b. Subsurface, refined

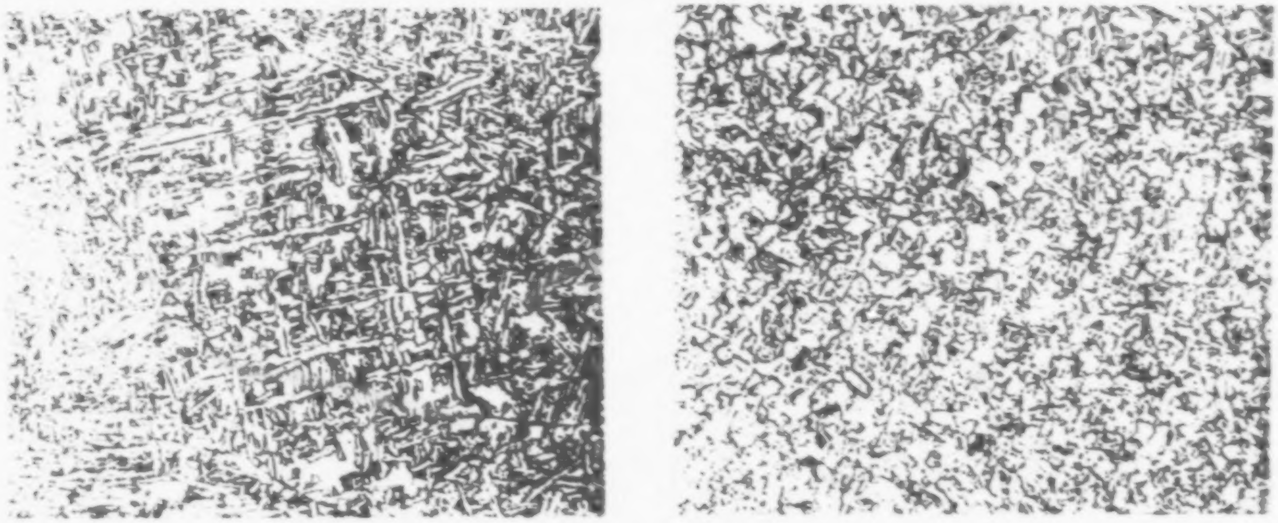

c. Root, as-deposited

d. Root, refined

Figure 45: Typical Microstructural Features: C-Mn-Ti-B/87.5Ar-10He-2CO_2-0.5H_2

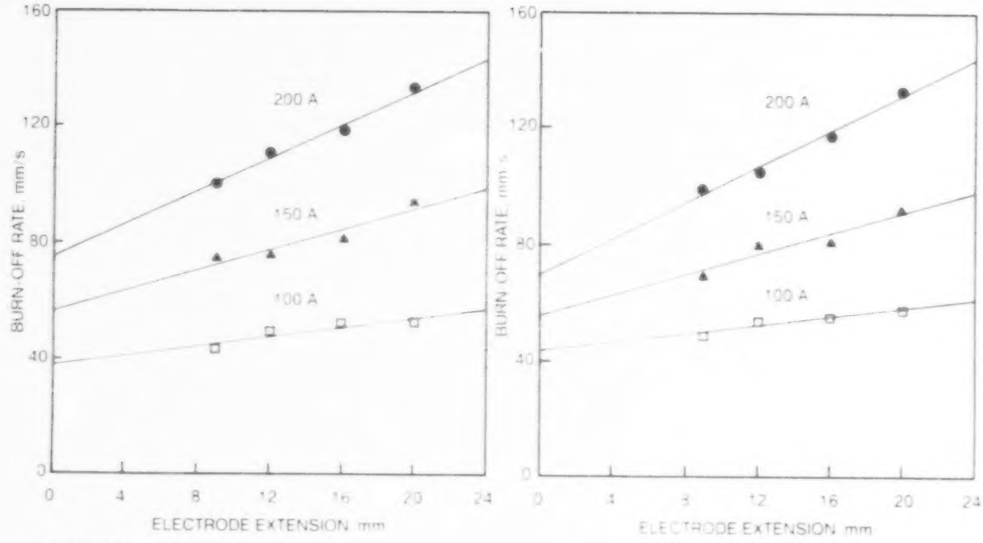

a 95Ar-5CO$_2$

b 80Ar-20CO$_2$

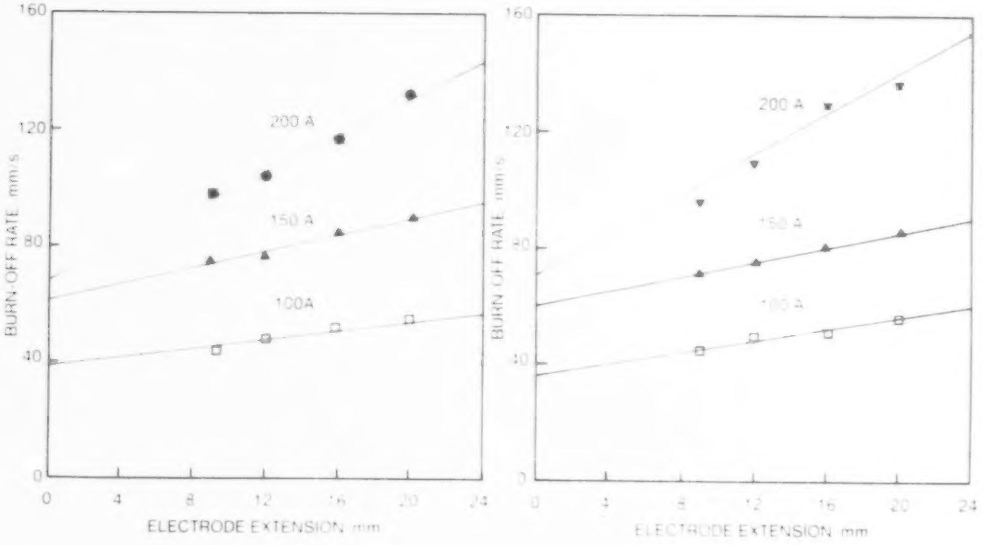

c 88Ar-10He-2CO$_2$

d 87.5Ar-10He-2CO$_2$-0.5H$_2$

Figure 46: Effect of Electrode Extension on Burn-Off Rate for C-Mn-Mo Wire

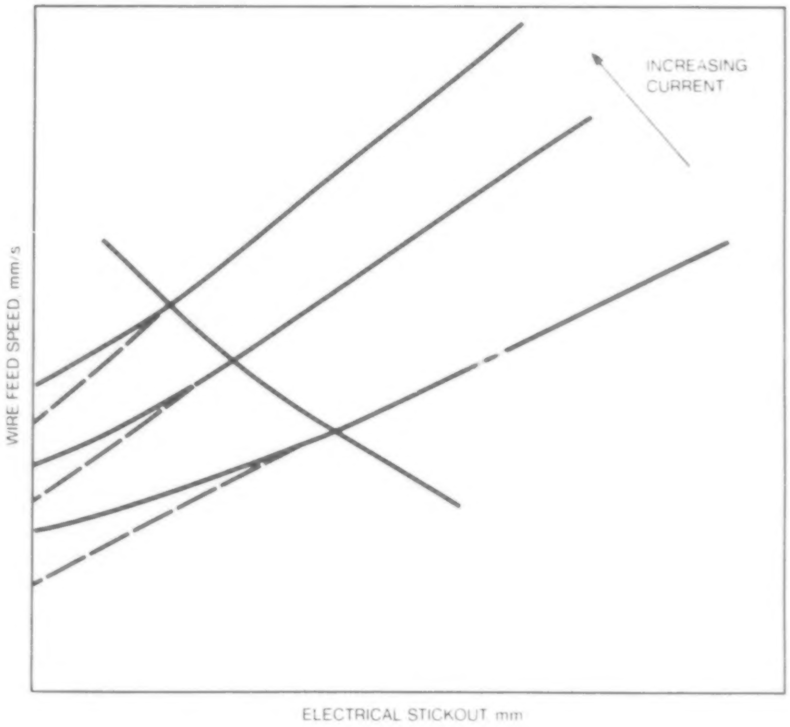

Figure 47: Wire Speed as a Function of Electrode Extension and Current for DC Welding (schematic) after Halmoy (21)